Including the inertia to a 1D model

A study on energy radiation in railway tracks

Bilal Ouchene

Delft University of Technology

TU Delft

Including the inertia to a 1D model

A study on energy radiation in railway tracks

by

Bilal Ouchene

to obtain the degree of Master of Science
at the Delft University of Technology,
to be defended publicly on Tuesday April 7, 2021 at 13:00.

Student number:	4480333	
Thesis committee:	Dr. ir. K.N. van Dalen (chair),	Dynamics of Solids and Structures
	Prof. dr. ir. A.V. Metrikine,	Dynamics of Solids and Structures
	Ir. A.B. Faragau,	Dynamics of Solids and Structures
	Ir. J.S. Hoving,	Offshore Engineering

TU Delft

Acknowledgements

بسم الله الرحمن الرحيم

In the name of Allah, the most gracious, the most merciful.

This thesis is the final report of the study 'Including the inertia to a 1D model: a study on energy radiation in railway tracks' which I carried out as MSc-graduation candidate in order to finish my studies at the faculty of Civil Engineering and Geosciences, at Delft University of Technology. The period in which I performed this study has been one filled with commitment, hard work, interest, aversion, setbacks and accomplishments. Along the way I have encountered different complications that tempted me to just finish the job and get it over with. I am happy to say that I did not take the easy way out and it has shown me once again that hard work makes that what is hard easy. I am content with the results and hope that it may be beneficial to others.

It would be arrogant to say that this would be possible by myself and should therefore show gratitude. I firstly show gratitude to Allah, the one who blessed me with sight, hearing, ability to think and everything else I have. It is also he who blessed me with my family, friends, teachers and colleagues. All of these people have either helped me or shown their support throughout this project.

Of all people, I thank my mother first and foremost. She is the one who brought me to my first day of school when I was a child and she, if God permits, is the first one that I will surprise with my graduation. I could not wish for someone more supportive than my mother. I would also like to tank my father, sisters and brother for their compassion and support.

I have been lucky to share my time at the university with great friends. We have helped each other out immensely over the years. I recall the many study sessions that we had, especially those that lasted longer than twenty four hours which oddly seemed to happen a lot during the weeks of examinations. I thank you all for the great memories.

A supervisor that I need to thank is Andrei Faragau. I have heard stories of other supervisors who tend to disappear when students start facing difficulties in their research. I can surely state that you are not one of those, rather the opposite. If I did not contact you for a while you showed initiative by contacting me, you were not reluctant to help out when needed and kept me sharp. Andrei, thank you for everything. And now the chairman, Karel van Dalen. I am now finishing my master's at the Dynamics of Solids and Structures section but I also did my bachelor thesis at the same section. I remember that I knocked on Karel's door without having an appointment and boldly asked whether there was a thesis subject for me to do. He answered by saying that there was no room left for any additional graduation students at the moment. I responded by saying that he should make an exception and that if he would give me the opportunity I would not disappoint. The project was finished successfully and afterwards Karel mentioned that he respected the 'Amsterdamse bravoure'. I am now finishing my master thesis, once again under the supervision of Karel. Thank you for both opportunities. And now, Andrei Metrikine. Your lectures have been really educational and well put together. But more important, you almost always made time for me when I had a question or wanted to discuss something. Whether this was during the lecture breaks, on the hallway or when I knocked on the door of your office in the evening with a question about the assignments. Thank you for everything.

Bilal Ouchene
Amsterdam, March 2021

Contents

Abstract

Areas of railways with considerable variation of track properties encountered near structures such as bridges and tunnels are referred to as transition zones. Degradation rates at these transition zones are higher compared to the remaining railways. These high degradation rates result in high maintenance expenses. In order to come up with solutions that reduce this degradation and thus also the expenses it is needed to have an understanding of the underlying mechanisms in the railway tracks. This is done by formulating a mathematical model of the railway track which can then be analyzed. Researchers have been using different models for this purpose.

The choice is often made to model the railway track an elastically supported beam. This elastic foundation represents the supporting structure of the railway tracks and its stiffness is based on static load cases. This 1D model is often used due to its relative simplicity compared to other more complicated multidimensional models. This model has been thoroughly analyzed and it has turned out to have an important constraint which is its inability to result in a critical velocity that makes sense for railway tracks. The critical velocity of a railway track is that velocity at which waves travel near the surface of the subsoil of the supporting structure. A vehicle that moves with a velocity close to the critical velocity of the railway track causes a strong amplification of the response. Another important constraint of this model is the fact that there is no possibility to directly adjust the stiffness properties of the different components of which the railway track exists individually.

It is opted in this thesis to adjust the previously mentioned 1D model by the addition of a distributed mass and an extra elastic layer. The upper elastic layer represents the pads and the lower elastic layer represents the remaining of the supporting structure. The idea behind the addition of the distributed mass is to include the activated mass of the supporting structure by the moving load. This is done in order to take the dynamical behavior of the supporting structure into account and thus obtain realistic critical velocities. The idea behind the addition of an elastic layer is that it enables to adjust the stiffness of the pads individually. By using this model one can thus modify the stiffness of the pads at transition zones and study whether it is possible to decrease the degradation which is the initial goal of all studies on transition zones.

In this thesis the adjusted model is analyzed thoroughly for different physical phenomena. Such analyses cannot be found in the literature, to the best of the authors knowledge. The system response has been investigated for a uniformly moving load of a constant magnitude. This has been done for homogeneous properties of the elastic layers and for an abrupt jump in the stiffness of the lower layer. Attention has been given to both the displacement fields of the rails and energy propagation in the system. Also a numerical model has been formulated for other load cases and stiffness properties. In order to simulate infinite system behavior non-reflective boundary conditions have been derived and applied to the numerical model. It has been found that indeed a far more realistic critical velocity can be obtained by making use of the adjusted model. It has furthermore turned out that the system response at a transition zone are very similar for both models for the same ratio of load velocity to the critical velocity. The adjusted model has been investigated extensively in this thesis and it can thus be used as a reference work for future researchers that wish to apply the model. The research that should be performed next in the authors view is to investigate the possibility of reducing the degradation at transition zones by adjusting the stiffness of the pads.

1 Introduction

1.1. Background

The world has been getting smaller at a rapid pace over the last decades due to the development of digital transport structures. Inhabitants of different parts of the world are nowadays in direct connection which each other through these structures. This connection enables new types of relationships between the inhabitants of these different parts such as friendships, business relationships and other types. These relationships however demand physical transport structures in which fast and efficient transport of people and objects is possible. Railroads play an integral role in fulfilling this task. Because of their importance it is thus needed to maintain the railroads such that efficiency is secured. This maintenance comes with expenses which need to be kept as low as possible. It has been shown that the degradation rates at areas of railways with considerable variation of track properties encountered near structures such as bridges and tunnels are higher compared to the remaining railway [26]. These areas are referred to as transition zones. It may be possible to come up with solutions that reduce these degradation rates when the underlying degradation mechanisms at transition zones are understood.

The vehicles moving on the rails exert forces on the rails which causes the rails and the supporting structure to exert dynamic behaviour. The forces exerted by a moving vehicle insert energy in the railway track which is radiated away from the vehicle through waves propagating in the track. The railway track is therefore interpreted as a field in which waves travel. The physical world shows that waves occur in all kinds of different fields. Examples of such fields are stress fields, strain fields, electrical fields, magnetic fields and many others. Due to the large frequency of occurrence in physical processes waves have been investigated by renowned scientists of the past and present. Two types of waves that have been investigated extensively and have shown to exhibit great similarities are mechanical and electromagnetic waves.

Waves of the electromagnetic field, carrying electromagnetic radiant energy, are referred to as electromagnetic radiation. Two types of important electromagnetic radiation are transition radiation which has been demonstrated theoretically by Vitaly Ginzburg and Ilya Frank [10] and Vavilov-Cherenkov radiation which has been detected by Pavel Cherenkov under the supervision of Sergey Vavilov [5]. Transition radiation is emitted when a source moves uniformly through inhomogeneous media, such as a boundary between two different media. Vavilov-Cherenkov radiation is emitted when a source moves uniformly through a dielectric medium with a velocity greater than the velocity of propagation of light in that medium. The principle of Vavilov-Cherenkov and transition radiation can also be observed in mechanical systems. An example of Vavilov-Cherenkov radiation in mechanics is a supersonic aircraft which travels faster than the speed of sound causing the formation of a shock front. An example of transition radiation in mechanics is a train which passes a bridge.

An analogy can be made between a source moving in a dielectric medium and a vehicle moving on a rail. The force exerted by the vehicle is therefore seen as the source and the rail with the supporting structure as the medium. This analogy begs the question whether the two previously mentioned types of radiation occurring in dielectric media also occur in railway systems. This occurrence of Vavilov-Cherenkov and transition radiation has indeed been confirmed to occur in rail systems. The wave mechanics research group of the university of technology Delft has had its fair share in the research of these phenomena in rails and other mechanical systems. Transition radiation has been discussed in detail for a number of mechanical systems in 1995 by Metrikine [27], Wolfert [30] completed his doctoral work with a report in which he discussed both transition and Vavilov-Cherenkov radiation in railways and other members of the group have also contributed to the study of mechanical waves in railways. Transition radiation has also been studied extensively by other researchers. Examples of such studies are that of Castro Jorge [13], Dimitrovova [8], Germonpre [9], Lei [17], Paixao [20], Varandas [25] and that of Sadri [22]. There is however enough room for research left due to physical properties of the subsoil which in general shows a strong inhomogeneous behaviour.

1.2. Problem statement

As mentioned previously maintenance is required more frequently at transition zones due to the high degradation rates. This may occur due to several reasons of which one is the occurrence of transition radiation. It is thus required to obtain a good insight in the way transition radiation occurs in such a system in order to work towards a solution for this problem on the long run.

A multitude of models of the vehicle interacting with the railway and supporting structure have been developed over the years. Early on researchers have been using 1D models because of their apparent simplicity. The supporting structure is often represented by a Winkler[1] foundation in these 1D models. Examples of studies in which such 1D models are used are a study of Vesnitiskii and Metrikine [27] which gives an in-depth overview of transition radiation in mechanics , a study of Dipanjan Basu [3] in which a load moves on a Winkler foundation that accounts for resistance due to both the compressive and shear strains in the soil and a study of Faragau [1] in which a load moves on an Euler-Bernoulli beam supported by a non-linear Kelvin foundation. Later on people have studied models in which the subsoil is represented as a half-space or as a continuum of finite-depth. Examples of such studies are a study of Kaynia[15] in which he investigated defects and inhomogeneities in railway tracks by modeling the subsoil as a multidimensional continuum , a study of van Dalen [16] in which transition radiation is studied of a system in which a load moves over the interference of two elastic layers and a study of Dieterman and Metrikine [7] in which a load moves over an Euler-Bernoulli beam which is supported by a linear elastic medium. The latter study had the interesting result that the elastic half space can be replaced by equivalent frequency dependent springs. These types of modeling in which the subsoil is interpreted as a continuum has the possibility to take more properties of the soil into account but they result into complex calculations. The Winkler foundation is therefore a more attractive alternative from an engineering point of view due to its relative simplicity. Over the years it has been shown that application of the Winkler foundation is justifiable and does not necessary lead to large errors in comparison to the methods in which the subsoil is interpreted as a continuum for static load cases [2]. For moving loads, which is obviously a dynamic load, this is not the case. One of the main problems is that the obtained minimum velocity of wave propagation based on a Winkler foundation is way higher than the measured velocity at which surface waves travel.

1.3. Novelties

The problem statement raises the question whether it is possible to make adjustments to the Winkler foundation in order to lower the obtained minimum velocity of wave propagation. The stiffness in a default Winkler foundation is based on purely static behaviour, neglecting the inertia of the supporting structure. It is therefore opted in this thesis to add a secondary beam without bending stiffness to the Winkler foundation in order to take the inertia into account. This secondary beam is an additional distributed mass which represents the activated mass of the supporting structure by the moving load and is from now on referred to as the inertia beam. The activated mass could also be represented by increasing the mass density of the Euler-Bernoulli beam. This has already been done in the literature and will also lead to a reduction of the minimum velocity of wave propagation. However, our choice has the added benefit that one can, for example, tune the springs between the two beams to represent the rail pads. This provides more versatility to the model by which one can investigate different configurations in order to reduce transition radiation. Thorough analyses on the steady state behaviour, critical velocities and transition radiation have been performed in this thesis for the adjusted model. According to the authors knowledge these analyses can not be found in the literature on such a profound level.

[1] In the case that viscous damping is included the foundation is called a Kelvin foundation

1.4. Research questions

Next to changing the minimum velocity of wave propagation, also referred to as the critical velocity, the modification to the default Winkler supported Euler-Bernoulli model will most probably also lead to other changes in the results. It is thus expected that the adjustments will also lead to differences in the transition radiation behaviour and the vehicle-structure interaction. In line with the above the following research questions are posed:

- Does the incorporation of the inertia of the supported structure in the form of an additional inertia beam lead to a more realistic value of the critical velocity?
- How do the steady state displacement fields of the system with and without additional inertia beam compare to each other?
- How does the transition radiation energy predicted by the model with and without additional inertia beam compare to each other?
- How do the transient displacement fields of a vehicle passing by a transition zone based on the model with and without additional inertia beam compare to each other?

1.5. Objectives

In order to answer the research questions the following objectives have been set:

- Investigate the influence of the addition of the inertia beam on the the critical velocity.
- Investigate the influence of the addition of the inertia beam on the transition radiation phenomenon.
- Formulate an efficient model of a transition zone that interacts with a vehicle.
- Compare the results of the transient displacement field for a uniformly moving load of constant magnitude for the inertia included and excluded model.

1.6. Outline

In this chapter an introduction to this thesis was provided. In Chapter 2 the inertia-excluded and included models are formulated. The system parameters are set and the equations of motions are derived. The way mechanical energy propagates and is distributed over the different components in the models is also considered. Moreover, uniqueness proofs for both models are presented.

In Chapter 3 the steady state displacement fields due to a uniformly moving load of constant magnitude for both models are determined. These displacement fields are determined by making use of both a geometrical method and Fourier transformations. These methods lead to equivalent solutions which is in line with the uniqueness proofs of Chapter 2. The geometrical method is used to provide the reader with the physical meaning behind the different steps in obtaining the steady state solutions. Special attention is paid to the dispersion curves, the kinematic invariant, group velocity, phase velocity and the critical velocity. The differences between the eigenfield and Vavilov-Cherenkov displacement field are pointed out for the inertia-excluded system. It is also investigated whether these displacement fields can be distinguished for the inertia-included model. The transform method is presented as a more direct mathematical approach to obtain the steady state displacement fields.

In chapter 4 the transition radiation due to an abrupt jump in the stiffness properties for both models are studied. The term free field is introduced to the reader as a homogeneous solution that is added to the eigenfield in order to satisfy the interface conditions at the transition. Afterward, the spectral density functions are determined based on the free field for both models.

In chapter 5 a numerical model for a transition zone is formulated. The finite element method is applied for the spatial discretization and the Newmark-beta method for the time discretization. The possibility for non constant system paramters is also included. This chapter finishes with the derivation of non-reflective boundary conditions. These are used to simulate infinite system behaviour by a finite model.

In Chapter 6 different results are shown and discussed from which the research questions can be answered. This leads to the conclusion provided in Chapter 7.

2

Model properties

2.1. Model definition

A railway track consists of rails, fasteners, pads, sleepers, ballast and the underlying subgrade. Each of the components rests on the following component according to the order mentioned in the previous sentence, except for the fasteners obviously. These fasteners are used to fix the rails to the sleepers.

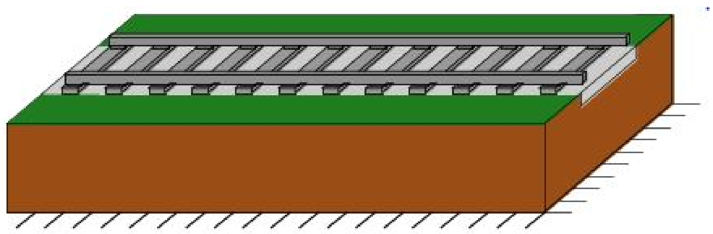

Figure 2.1: A three dimensional view of a railway track.

In this thesis the railway track is subdivided into two categories which are the rails and the supporting structure, consisting of the remaining components of the railway tack. The supporting structure will be described by two models. Before defining these two models a good physical interpretation of the railway track is needed. A schematic view of a cross-section of the railway track is therefore shown.

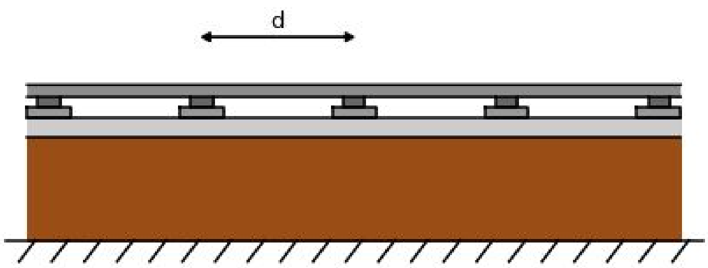

Figure 2.2: A cross-section of a railway track.

From Figure 2.2 it can be observed that the response of the supporting structure due to deflection of the rail is exerted through the pads. This response exists of reaction stresses at the interfaces between the pads and the rails. The pads are located at a distance d from each other. This implies that the rail is periodically supported with period d. This idea has been elaborated in a study done by Metrikine [28]. In that study the rail was modeled by an infinitely long Euler-Bernoulli beam, the pads were modeled as spring-dashpot elements, the sleepers were assumed to behave rigidly and the ballast together with the underlying subgrade were modeled by a visco-elastic continuum. Other important studies on the behaviour of the periodic structure are that of Mead [19], Hoang [11], Jezequel [12] and that of Barbosa [6].

This thesis aims, as elaborated in the Introduction section, to investigate the possibility of obtaining a more realistic critical velocity by making use of a modified version of the classical Winkler foundation. The first of the two models is therefore a default system, consisting of a beam resting on a Winkler foundation, and serves as a means of comparison with the other model. This model is from now on referred to as the inertia-excluded model due to the fact that the inertia of the supporting structure is neglected.

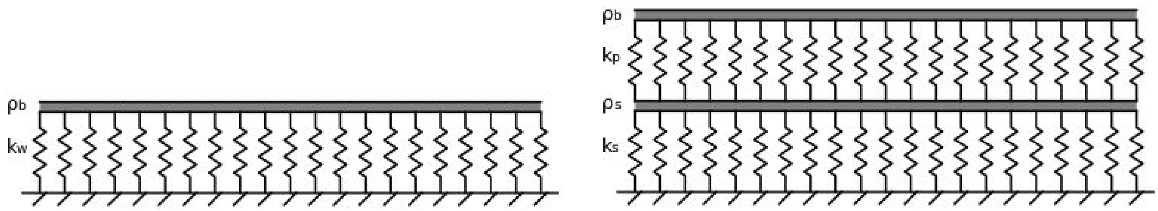

Figure 2.3: The inertia-excluded system (left) and the inertia-included system (right)

In the second model the inertia of the supporting structure is taken into account by adding an inertia beam without bending stiffness to the system. At the end of the previous page a study [28] was mentioned in which the pads were modeled as spring-dashpot elements which were located at discrete distance d from each other. Assuming the supporting structure as a system of such discrete springs is widely used. In the thesis of Rodrigues [21] one can find a summary of this method and general parametric values of these elements for multiple cases. In this thesis the effect of the pads is taken into account by an elastic layer between the Euler-Bernoulli beam and the inertia beam. This upper elastic layer has a distributed stiffness k_p which is obtained by dividing the stiffness of the discrete spring K_p obtained from the mentioned study by d. The sleepers are assumed to be rigid and their only contribution to the system is their mass. This mass is also distributed by division over d and forms only a part of the density ρ_s of the inertia beam. This is because the part of activated inertia by the moving load of the ballast and subgrade also need to be taken into account by the inertia beam. At first sight it is not clear how to integrate these effects and determine ρ_s but at least for now there is a lower bound due to the mass of the sleepers. Remaining for the parameters of the supporting structure is the distributed stiffness k_s of the lower elastic layer. This stiffness is also obtained by division of the discrete spring stiffness K_s by d. The spring K_d is the serial equivalent spring of K_{ba}, representing the ballast, and K_{su}, representing the subgrade.

It is demanded that both the inertia-excluded and included system at least show the same behaviour for static problems, in which the inertia beam can be neglected. The elastic layers in the second model then form a serial system and the equation

$$\frac{1}{k_w} = \frac{1}{k_p} + \frac{1}{k_s} \tag{2.1}$$

should hold. Equation (2.1) can be solved for k_w. All parameters of the supporting structure for both models have been discussed. The rail itself is modeled by an infinite Euler-Bernoulli beam in both models. The mass density ρ_b and bending stiffness EI correspond to that of the UIC60 rail and are obtained from the reader of the course CT3041 [4], given at the University of Technology Delft.

Parameter	Symbol	Value	Unit
Bending stiffness	EI	6.42·10^6	Nm^2
Mass density rail	ρ_b	60.34	kg/m
Mass density inertia beam	ρ_s	> 245	kg/m
Winkler stiffness	k_w	7 .65·10^6	N/m^2
Upper layer stiffness	k_p	208.33·10^6	N/m^2
Lower layer stiffness	k_s	7.94·10^6	N/m^2
Pad-to-pad distance	d	0.60	m

Table 2.1: Numerical values of the parameters of the the supporting structure and rail.

2.2. Equations of motion

2.2.1. Equation of motion for the inertia-excluded model

The Euler-Bernoulli beam theory is one of the cornerstones of structural engineering. The kinematic and constitutive equations of this theory are mentioned in the following:

- The plane rotation to the neutral axis is defined by $\phi(x,t) = -\frac{\partial w(x,t)}{\partial x}$
- The curvature of the beam is defined by $\kappa(x,t) = \frac{\partial \phi(x,t)}{\partial x}$
- The moment and the curvature are related through the relation $M(x,t) = EI\kappa(x,t)$

The equation of motion for the Euler-Bernoulli beam resting on a Kelvin foundation will be derived by making use of the displacement method. To do this a small beam piece of length Δx is obvserved.

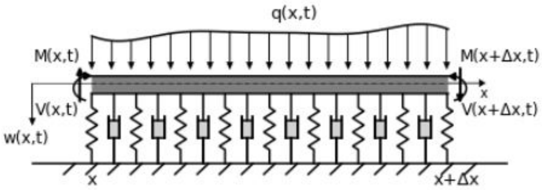

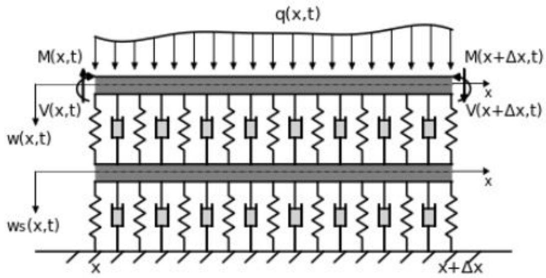

Figure 2.4: A piece of railway track for the inertia-excluded system (left) and the inertia-included system (right).

Applying Newton's second law for the transverse displacement on this piece of the beam leads to

$$\rho_b \Delta x \frac{\partial^2 w(\zeta,t)}{\partial t^2} = V(x+\Delta x,t) - V(x,t) + \int_x^{x+\Delta x} \left(-k_w w(\tilde{x},t) - c_w \frac{\partial w(\tilde{x},t)}{\partial t} + q(\tilde{x},t) \right) d\tilde{x} \quad \text{with } \zeta \in (x, x+\Delta x), \tag{2.2}$$

in which V denotes the shear force in the beam and q the distributed load on the beam. Dividing this expression by Δx and taking the limit $\Delta x \to 0$ yields the following expression for the time derivative of momentum per unite length

$$\rho_b \frac{\partial^2 w(x,t)}{\partial t^2} = \frac{\partial V(x,t)}{\partial x} - k_w w(x,t) - c_w \frac{\partial w(x,t)}{\partial t} + q(x,t). \tag{2.3}$$

Applying the second law of Newton to the rotational degree of freedom[1] and using the kinematic and constitutive equation results in the final expression which is also the equation of motion for an Euler-Bernoulli beam resting on a Kelvin foundation

$$\rho_b \frac{\partial^2 w(x,t)}{\partial t^2} + EI \frac{\partial^4 w(x,t)}{\partial x^4} + c_w \frac{\partial w(x,t)}{\partial t} + k_w w(x,t) = q(x,t). \tag{2.4}$$

2.2.2. Equations of motion for the inertia-included model

The equation of motion for the inertia-included model are also derived by making use of the displacement method. The equation of motion now exists of a set of two equations, one for the Euler-Bernoulli beam and the other for the inertia-beam. The first equation is almost identical to that of equation (2.4) except for the fact that the deformation of the upper visco-elastic layer is now also dependent on the deflection w_s of the inertia beam. The derivation of the second equation is similar to the first one. However no internal forces are present in the inertia beam due to the absence of any bending stiffness. The equations of motion for the inertia-included model thus read

$$\begin{aligned} \rho_b \frac{\partial^2 w}{\partial t^2} + EI \frac{\partial^4 w}{\partial x^4} + c_p \frac{\partial w(x,t)}{\partial t} + k_p w - c_p \frac{\partial w_s(x,t)}{\partial t} - k_p w_s &= q(x,t) \\ \rho_s \frac{\partial^2 w_s}{\partial t^2} + \left(c_p + c_s\right) \frac{\partial w_s(x,t)}{\partial t} + \left(k_p + k_s\right) w_s - c_p \frac{\partial w(x,t)}{\partial t} - k_p w &= 0. \end{aligned} \tag{2.5}$$

[1]The rotational moment of inertia is neglected in the Euler-Bernoulli beam theory.

2.3. Energy considerations

2.3.1. Inertia-excluded model

In order to determine the way energy is transmitted in the railway track it is needed to obtain a mathematical expression that describes the way mechanical energy is distributed along the beam as a function of time. The kinetic energy of a particle is obtained by multiplying the time derivative of its momentum with its velocity and integrating over time. This principle will now be applied to the beam. Note that in the case of the beam an integration over the beam length is also needed because the the equation of motion exists of the time derivative of the momentum per unit length. Multiplying equation (2.2) by the beam velocity, integrating over time and space and rearranging terms leads to

$$\left[\int_{x_a}^{x_b}\left\{\frac{1}{2}\rho_b\left(\frac{\partial w}{\partial t}\right)^2+\frac{1}{2}k_w w^2+\frac{1}{2}M\kappa\right\}dx\right]_{t=t_i}^{t=t}=\int_{t_i}^{t}\left\{\left[M\frac{\partial\phi}{\partial t}+V\frac{\partial w}{\partial t}\right]_{x=x_a}^{x=x_b}\right\}dt+\int_{t_i}^{t}\int_{x_a}^{x_b}\left\{q\frac{\partial w}{\partial t}-c_w\left(\frac{\partial w}{\partial t}\right)^2\right\}dxdt. \tag{2.6}$$

This expression shows the relation between the different energy components in the system. It shows that the increase of total mechanical energy in the system between two time instance equals the work done by the distributed load and the forces at the beam boundaries minus the dissipated energy. Mechanical energy is the summation of the kinetic and potential energy. These energy components are respectively denoted by $E(t)$, $K(t)$ and $P(t)$. From equation (2.6) it can be concluded that the potential energy exists of the potential energy due to deformation of the Winkler foundation and potential energy due to bending strains in the beam. Because the total mechanical energy in the system is an integral over the length of the beam it can be concluded that the integrand shows the way the mechanical energy is distributed over the beam. These energy distributions are called energy density functions in the rest of this thesis and have the following definitions:

- The kinetic energy density: $\eta_K(x,t)=\frac{1}{2}\rho_b\left(\frac{\partial w}{\partial t}\right)^2$
- The potential energy density: $\eta_P(x,t)=\frac{1}{2}k_w w^2+\frac{1}{2}M\kappa$
- The mechanical energy density: $\eta(x,t)=\eta_K(x,t)+\eta_P(x,t)$

In the above different energy components in the railway track have been elaborated. A specific interest of the thesis lays in the way energy 'flows' in the system. This flow can be obtained by studying the time derivative of equation (2.6) which reads

$$\frac{dE(t)}{dt}=\left[M\frac{\partial\phi}{\partial t}+V\frac{\partial w}{\partial t}\right]_{x=x_a}^{x=x_b}+\int_{x_a}^{x_b}\left\{q\frac{\partial w}{\partial t}-c_w\left(\frac{\partial w}{\partial t}\right)^2\right\}dx. \tag{2.7}$$

The first term of the right hand side of equation (2.7) is the inflow of energy per unit time at the boundaries of the system. It can thus be concluded that the outflow of the energy at a certain cross section is defined by

$$S^{(n)}(x,t)=(-1)^{n-1}\left(M\frac{\partial\phi}{\partial t}+V\frac{\partial w}{\partial t}\right), \tag{2.8}$$

in which $n=2$ for a cross-section of which the outward normal vector is in the direction of the positive x-direction and $n=1$ for a cross-section of which the outward normal vector is in the direction of the negative x-direction. When the displacement field is known the energy flow in the system can be determined which will be especially useful when investigating transition radiation.

2.3.2. Inertia-included model

It is once again needed to find mathematical expressions that describe the way mechanical energy is distributed but now for the inertia-included system. This is done in a similar way as in the previous subsection. The system is now coupled as can be seen from (2.5) and two different types of mass particles can be distinguished, that of the Euler-Bernoulli beam and that of the mass beam which represents the inertia of the soil. Each equation is multiplied by the velocity of its respective mass particle, integrated over time and space after which the two resulting expressions are added to each other, leading to

$$
\begin{gathered}
\left[\int_{x_a}^{x_b}\left\{\frac{1}{2}\rho_b\left(\frac{\partial w}{\partial t}\right)^2+\frac{1}{2}EI\kappa^2+\frac{1}{2}k_p(w_s-w)^2+\frac{1}{2}\rho_s\left(\frac{\partial w_s}{\partial t}\right)^2+\frac{1}{2}k_s w_s^2\right\}dx\right]_{t=t_i}^{t=t}= \\
\int_{t_i}^{t}\left\{\left[M\frac{\partial \phi}{\partial t}+V\frac{\partial w}{\partial t}\right]_{x_a}^{x_b}\right\}dt+\int_{t_i}^{t}\int_{x_a}^{x_b}\left\{q\frac{\partial w}{\partial t}-c_p\left(\frac{\partial w_s}{\partial t}-\frac{\partial w}{\partial t}\right)^2-c_s\left(\frac{\partial w_s}{\partial t}\right)^2\right\}dxdt.
\end{gathered}
\tag{2.9}
$$

It is once again observed that the total mechanical energy in the system between two time instances equals the work done by the distributed load and the forces at the beam boundaries minus the dissipated energy. This is in line with the physical expectation. The expressions for the energy components are however slightly different due to the addition of the inertia beam and the visco-elastic layer. Note that the displacement field of the inertia beam has no contribution to the boundary term which can be explained by the absence of internal forces in the inertia beam. For the energy distributions functions the following definitions hold:

- The kinetic energy density: $\eta_K(x,t)=\frac{1}{2}\rho_b\left(\frac{\partial w}{\partial t}\right)^2+\frac{1}{2}\rho_s\left(\frac{\partial w_s}{\partial t}\right)^2$
- The potential energy density: $\eta_P(x,t)=\frac{1}{2}k_w w^2+\frac{1}{2}M\kappa+\frac{1}{2}k_p(w_s-w)^2+\frac{1}{2}k_s w_s^2$
- The mechanical energy density: $\eta(x,t)=\eta_K(x,t)+\eta_P(x,t)$

Differentiation of equation (2.9) to time leads to the time derivative of the mechanical energy in the system

$$
\frac{dE(t)}{dt}=\left[M\frac{\partial \phi}{\partial t}+V\frac{\partial w}{\partial t}\right]_{x=x_a}^{x=x_b}+\int_{x_a}^{x_b}\left\{q\frac{\partial w}{\partial t}-c_p\left(\frac{\partial w_s}{\partial t}-\frac{\partial w}{\partial t}\right)^2-c_s\left(\frac{\partial w_s}{\partial t}\right)^2\right\}dx, \tag{2.10}
$$

from which the flux of the energy at a certain cross section can be determined, yielding

$$
S^{(n)}(x,t)=(-1)^{n-1}\left(M\frac{\partial \phi}{\partial t}+V\frac{\partial w}{\partial t}\right). \tag{2.11}
$$

Note that this expression is equivalent to that of inertia-excluded system and has already been explained by the absence of of internal forces in the inertia beam.

2.4. Uniqueness

From a physical point of view it is expected that one specific mechanical system that has one specific set of system properties and one specific set of initial condition and is submitted to one specific load should behave in one specific way. The physical problems are however modelled under certain assumptions and then transferred into mathematical problems. Attempts can then be made to find the solutions for these mathematical problems with different methods. There arises a problem when there are solutions found through different methods because then the choice needs to be made what solution is the one specific solution to the physical problem. This problem does however not arise when it can be proven that a mathematical problem has at most one solution. If this is the case it can be concluded that all the different methods for solving the problem result in the one and only solution.

2.4.1. Uniqueness for the inertia-excluded model

For the inertia-excluded model the partial differential equation that needs to be solved can be seen in equation (2.4). This partial differential equation does however not form a complete mathematical without initial and boundary conditions. The rails are assumed to be infinite such that boundaries of the system are located at $|x|\to\infty$. The boundary conditions are such that the displacement field and all its spatial derivatives should ten to zero for $|x| \to \infty$. The initial conditions are arbitrary [2] and denoted by

$$\begin{aligned} &w(x,0) = f(x) \\ &\left.\frac{\partial w}{\partial t}\right|_{t=0} = g(x). \end{aligned} \tag{2.12}$$

This mathematical formulation of the problem is now complete. An attempt to solve the problem can be made by making use of different methods such as making use of the Green's function, Fourier transforming, etc. Now assume that there are two different solutions $w_1(x,t)$ and $w_2(x,t)$ and define the difference function $v(x,t)$ as

$$v(x,t) = w_1(x,t) - w_2(x,t). \tag{2.13}$$

Because the components of $v(x,t)$ solve the problem of equation (2.3) with the mentioned boundary conditions initial conditions (2.12) it becomes clear that $v(x,t)$ itself satisfies the same but homogeneous partial differential equation and homogeneous boundary- and initial conditions. The energy balance of equation (2.6) can thus also be used for the difference function resulting in

$$\int_{x_a}^{x_b} \left\{ \frac{1}{2}\rho_b \left(\frac{\partial v}{\partial t}\right)^2 + \frac{1}{2}k_w v^2 + \frac{1}{2}M\kappa \right\} dx = -\int_{x_a}^{x_b}\int_{t_i}^{t} c\left(\frac{\partial v}{\partial t}\right)^2 dx dt. \tag{2.14}$$

The right hand side of the equation is equal or less than zero and the left hand side off this equation is equal or greater than zero. The only way both inequalities can hold is when they are both equal to zero. Because the integrand in the left hand side exists of only quadratic terms it must hold that all these terms equal zero. From this it can be concluded that

$$v(x,t) = 0 \leftrightarrow w_1(x,t) = w_2(x,t) \tag{2.15}$$

This proves that the assumption that was made is incorrect. There do not exist two different solutions for (2.3) in combination with its boundary and initial conditions, which means that there is at most one solution for this problem. So an arbitrary method can be chosen to solve this problem and if a solution is found there is certainty that this is the only solution possible. If one finds another solution in a different form using another method it must be the same solution.

2.4.2. Uniqueness for the inertia-included model

In order to prove uniqueness of the solution for the inertia-included model the steps as in the previous subsection are applied. Both the displacement field of the Euler-Bernoulli and the inertia beam tend to zero for $|x| \to \infty$ and arbitrary initial conditions for both beams are chosen. It is assumed that there are two different solution vectors $\mathbf{w}_1 = [w_1, w_{s1}]^T$ and $\mathbf{w}_2 = [w_2, w_{s2}]^T$ to the problem of equation (2.5). The difference vector is now introduced as $\mathbf{v} = [v, v_s] = \mathbf{w}_1 - \mathbf{w}_2$. The difference vector thus satisfies the same but homogeneous set of partial differential equations and homogeneous boundary- and initial conditions. The energy balance of equation (2.9) can be applied for the difference vector resulting in

$$\begin{aligned} &\int_{x_a}^{x_b} \left\{ \frac{1}{2}\rho_b \left(\frac{\partial w}{\partial t}\right)^2 + \frac{1}{2}EI\kappa^2 + \frac{1}{2}k_p(w_s - w)^2 + \frac{1}{2}\rho_s\left(\frac{\partial w_s}{\partial t}\right)^2 + \frac{1}{2}k_s w_s^2 \right\} dx = \\ &\qquad -\int_{x_a}^{x_b} \left\{ c_p \left(\frac{\partial w_s}{\partial t} + \frac{\partial w}{\partial t}\right)^2 - c_s\left(\frac{\partial w_s}{\partial t}\right)^2 \right\} dx. \end{aligned} \tag{2.16}$$

The right hand side of the equation is equal or less than zero and the left hand side off this equation is equal or greater than zero. The only way both inequalities can hold is when they are both equal to zero. Because the integrand in the left hand side exists of only quadratic terms it must hold that all these terms equal zero. From this the following can be concluded:

$$\mathbf{v} = [0,0]^T \leftrightarrow \mathbf{w}_1 = \mathbf{w}_2. \tag{2.17}$$

This proves the uniqueness of the solution for the inertia-included model.

[2]Note that the initial conditions are not completely arbitrary in the sense that they need to match the boundary conditions.

3

Vavilov-Cherenkov radiation

When a force is applied to a medium it will cause a displacement field that is in line with the laws of physics. In the case of a uniformly moving load with constant magnitude in a homogeneous elastic medium general shapes of the steady state can be distinguished based on the velocity. Two types of such displacement fields that in general occur in one dimensional mechanical systems are the eigenfield and the Vavilov-Cherenkov field. In this chapter it will be shown whether these two displacement fields also occur in the inertia included model and how these fields are related to the load velocity. The steady state of both models will be investigated in this chapter. The steady state displacement fields will be determined according to a geometrical method and a transform method. The steady state behaviour of the inertia-excluded model is extensively investigated in the literature (for example, Wolfert [30] gives a clear investigation into this matter). This will however be repeated in an extensive way to provide the reader with a complete overview and to form a stepping stone towards the inertia-included system.

3.1. Steady state of the inertia-excluded system

3.1.1. Geometrical method

For a uniformly moving constant load in the inertia excluded model the equation of motion is

$$\frac{\partial^4 w}{\partial x^4} + 4\gamma_b^2 \frac{\partial^2 w}{\partial t^2} + 4\alpha_w \frac{\partial w}{\partial t} + 4\beta_w^4 w = \hat{F}\delta(x - vt), \tag{3.1}$$

in which the parameters are defined by

$$4\gamma_b^2 = \frac{\rho_b}{EI}, \quad 4\alpha_w = \frac{c_w}{EI}, \quad 4\beta_w^4 = \frac{k_w}{EI}, \text{ and } \quad \hat{F} = \frac{F}{EI}. \tag{3.2}$$

The load velocity is denoted bt v and δ is the Dirac delta function. As a trial solution a summation of harmonic waves is suggested, which is denoted by

$$w = \sum_j c_j e^{(k_j x - \omega_j t)i}. \tag{3.3}$$

Note that the suggested solution in equation (3.3) can not satisfy the equation of motion in (3.1) due to the Dirac delta function. It is therefore needed to split the spatial domain into two semi-infinite domains, a left domain with respect to the moving load $\Omega^{(1)} = (-\infty, vt^-)$ and a right domain $\Omega^{(1)} = (vt^+, \infty)$. The solutions of these domains are respectively $w^{(1)}$ and $w^{(2)}$ and satisfy

$$\frac{\partial^4 w^{(n)}}{\partial x^4} + 4\gamma_b^2 \frac{\partial^2 w^{(n)}}{\partial t^2} + 4\alpha_w \frac{\partial w^{(n)}}{\partial t} + 4\beta_w^4 w^{(n)} = 0. \tag{3.4}$$

These solutions are related to each other through interface conditions. The interface conditions are a continuity at the forcing point in displacement, slope and bending moment and a discontinuity in shear force. A derivation of the latter interface condition can be found in the work of Faragau [1] and it reads

$$\left.\frac{\partial^3 w}{\partial x^3}\right|_{x=vt^-}^{x=vt^+} = \hat{F}. \tag{3.5}$$

The new formulation of the problem makes it possible to obtain the solution of both domains in the form suggested in equation (3.3). Substitution of this trial solution in one of the two equations of (3.4) yields set of equations

$$k^4 - 4\gamma_b^2\omega^2 - 4\alpha_w i\omega + 4\beta_w^4 = 0 \wedge \omega = kv. \tag{3.6}$$

The first equation in (3.6) relates the wave number k to the frequency ω for a general wave moving in the system. Note that the damping term causes the equation to have complex valued coefficients. This demands additional carefulness of the reader and can lead to a significant increase in difficulty in understanding the subject. The damping is therefore neglected from now on, which results in

$$k^4 - 4\gamma_b^2\omega^2 + 4\beta_w^4 = 0. \tag{3.7}$$

In the case that a frequency is given, the corresponding wave-number can be determined. In order to do so the dispersion equation can be rewritten to

$$k^4 = 4\gamma_b^2\omega^2 - 4\beta_w^4 = z(\omega). \tag{3.8}$$

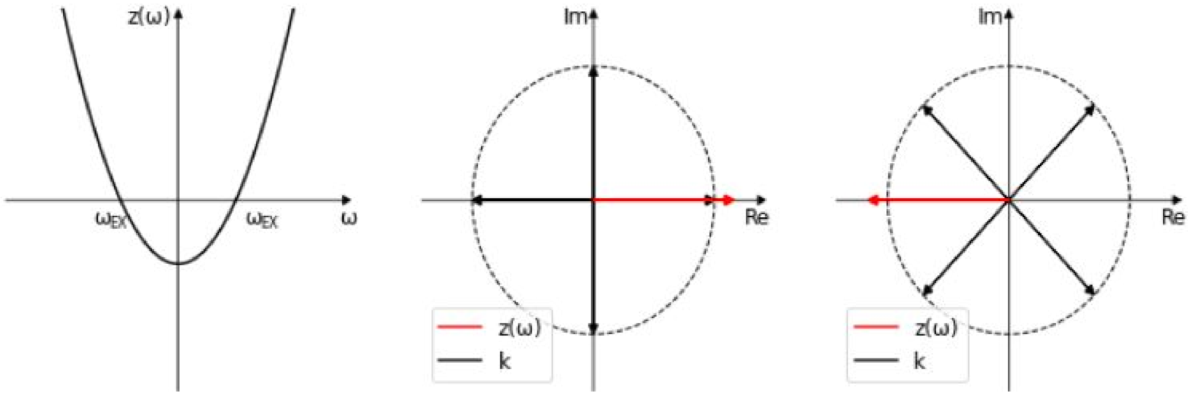

Figure 3.1: The function $z(\omega)$ (left) and its fourth order roots k for $|\omega| > \omega_{EX}$ (middle) and $|\omega| < \omega_{EX}$ (right)

According to equation (3.7) the fourth order roots of the function $z(\omega)$ are the wave-numbers k that correspond to a specific frequency. The properties of these wave-numbers are thus investigated by studying the function $z(\omega)$. Note that the subscript of ω_{EX} denotes that the this is the cut off frequency of the inertia excluded system. It can be seen from Figure 3.1 that the function $z(\omega)$ is negative for $|\omega| < \omega_{EX}$ and positive for $|\omega| > \omega_{EX}$. This frequency ω_{EX} can be obtained by equating $z(\omega)$ to zero and solving the equation which results in

$$\omega_{EX}^2 = \frac{4\beta_w^4}{4\gamma_b^2}. \tag{3.9}$$

This frequency is called the cut off frequency and has a physical interpretation which will become clear. In order to obtain a visual interpretation of the fourth order roots the variable $z(\omega)$ together with its roots have been plotted in the complex plane in Figure 3.1 for the two cases of the argument of $z(\omega)$, either 0 for $|\omega| > \omega_0$ and π for $|\omega| < \omega_0$. It is observed that all four wave-numbers are complex for $|\omega| < \omega_0$, and two are complex and two are real for $|\omega| > \omega_0$. The real wave-numbers have been plotted as a function of the frequency ω, see the left graph in Figure 3.2. These curves are known as the dispersion curves of the system and in general the axes are interchanged such that the vertical axis corresponds with the frequency and the horizontal axis with the wave-numbers, see the right graph in Figure 3.2. One can analyse the behaviour of the system systematically by making use of these dispersion curves. One can conclude from Figure 3.2 that there are no real-valued wave numbers for a frequency of which its absolute value is below the cut off frequency ω_{EX}. This means that all its four wave-numbers are complex as has been shown. Furthermore, it can be concluded that for a frequency of which its absolute value is larger than the cut off frequency ω_{EX} two wave-numbers are complex and two are real valued. This means that in this domain of frequency there are two waves which are purely harmonic and propagate. The cut off frequency ω_{EX} is thus the boundary of frequency at which pure wave propagation is possible in the system.

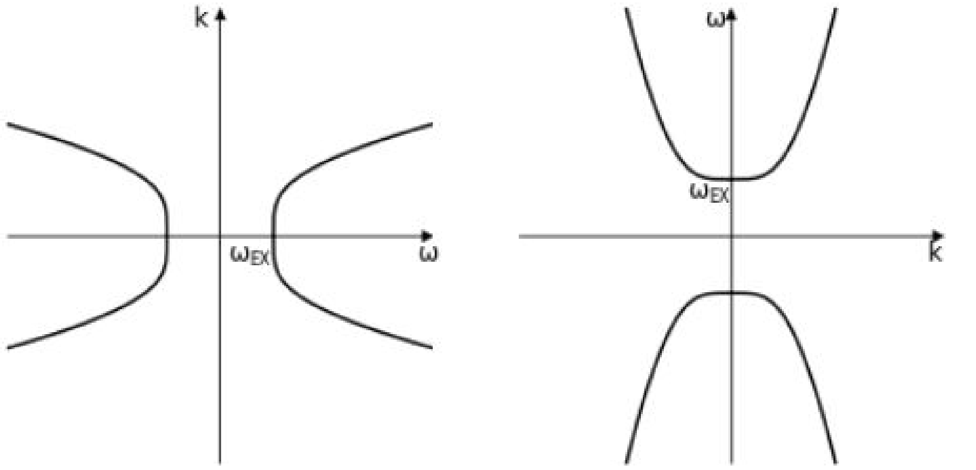

Figure 3.2: Dispersion curves for the inertia-excluded system.

An important property of a wave in mechanical systems is the velocity at which it propagates energy. Rayleigh discussed the velocity of energy propagation $v_{gr}(k)$ in one dimensional systems in 'The theory of sound' [14]. It was found that this velocity of energy propagation equals the group velocity of a wave which is mathematically defined as

$$v_{gr}(k) = \frac{d\omega(k)}{dk}. \tag{3.10}$$

Another important property of a wave is its phase velocity $v_{ph}(k)$ which is defined as the velocity at which the phase of the wave travels and is mathematically defined by

$$v_{ph}(k) = \frac{\omega(k)}{k}. \tag{3.11}$$

In the case that a wave-number k is given, the corresponding frequency $\omega(k)$ can be determined from equation (3.7) after which the phase velocity can be obtained. An arbitrary displacement field at a certain point in time t_a can be described as a summation of harmonic functions with each its own wave-numbers, and thus each its own frequency and finally each its own phase velocity. When time proceeds each of this wave components will travel with its own phase velocity leading to a distortion of the displacement field of time t_a. The reason of this distortion is the fact that the phase velocity is not constant due to the fact that the frequency ω and wave number k are not linearly proportional to each other. Such systems are called dispersive systems and the relation that relates the wave number to the frequency is therefore called the dispersion equation. The first equation in (3.6) is thus called the dispersion equation and its left hand side is from now denoted by $\Delta_{EX}(\omega, k)$, such that

$$\Delta_{EX}(\omega, k) = k^4 - 4\gamma_b^2\omega^2 - 4\alpha_w i\omega + 4\beta_w^4. \tag{3.12}$$

The second equation in (3.6) is called the kinematic invariant and it is an additional relationship between the wave numbers and frequencies but this relationship specifically includes the kinematic characteristics of the moving load, in contrary to the dispersion equation which in general holds for a homogeneous system.

The dispersion and kinematic equation together form a set from which all (k, ω)-pairs of the waves that are present in the steady state can be determined. Solving this set of equations in equivalent to solving

$$\Delta_{EX}(vk, k) = 0, \tag{3.13}$$

which is a quartic equation in k with four solutions. These four wave-numbers k_j are then multiplied by the load velocity to obtain the related frequencies ω_j. The general solution of the semi-infinite domains are then found to be

$$w^{(n)} = \sum_{j=1}^{4} c_j^{(n)} e^{k_j(x-vt)i}. \tag{3.14}$$

What remains in order to complete the solutions are the unknown constants. Before the interface conditions are used it is needed to cancel a number of waves based on the physical behaviour of the system. First of all the displacement field must be bounded for $|x| \to \infty$. This means that constants which relate to waves that have a complex-valued wave number of which its imaginary part is positive should be set to zero in the left semi-infinite domain and those that are negative in the right-semi infinite domain. Second the radiation conditions must hold, which states that energy must propagate away from a source (the load). This means that $v_{gr}(k) > v$ for all waves that propagate (have a real wave-number) in front of the load and $v_{gr}(k) < v$ for waves propagating behind the load, constants corresponding to waves that do not satisfy this condition are set to zero. The remaining unknown constants can then be solved by use of the interface conditions, completing the solution.

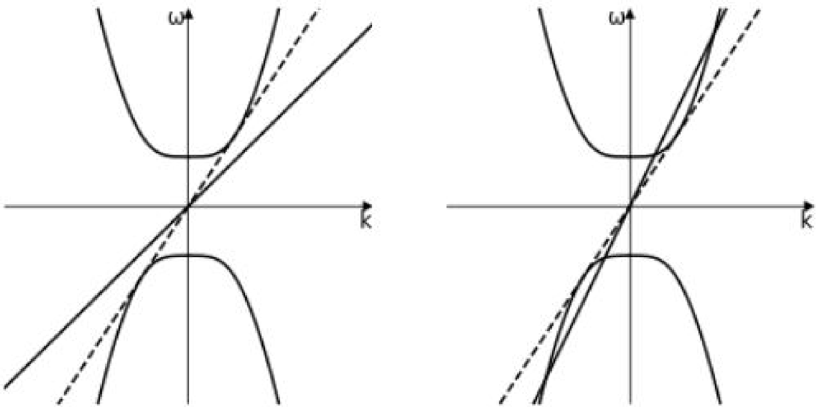

Figure 3.3: Dispersion curves and kinematic invariant for $v < v_{cr}$ (left) and for $v > v_{cr}$ (right).

When solving this problem for different velocities it can be noticed that the different displacement fields do not only show different behaviour quantitatively but also qualitatively. This can be explained by investigation of the dispersion curves and the kinematic invariant. As stated before the wave-numbers present in the steady state are basically the solution to equation (3.13) which is a quartic equation in k. The roots of this expression are basically the intersection points of the dispersion curves and the kinematic invariant. From Figure 3.3 it is observed that for load velocities lower than a certain velocity, which is from now denoted by v_{cr}, no intersection points are present. Equation (3.13) however always has four roots. The explanation for the fact that the roots are not visible as intersection points is because their (k, ω)-pairs are complex valued. The result of this is that the displacement field exists of waves that are not purely harmonic but all decay towards zero for $|x| \to \infty$. In this case, $v < v_{cr}$, the displacement field moves stationary with the load and is known as the eigenfield. For load velocities higher than v_{cr} four intersection points, corresponding to four real valued (k, ω)-pairs, are observed. In this case, $v > v_{cr}$, the displacement fields exist of only harmonic propagating waves and is called the Vavilov-Cherenkov field.

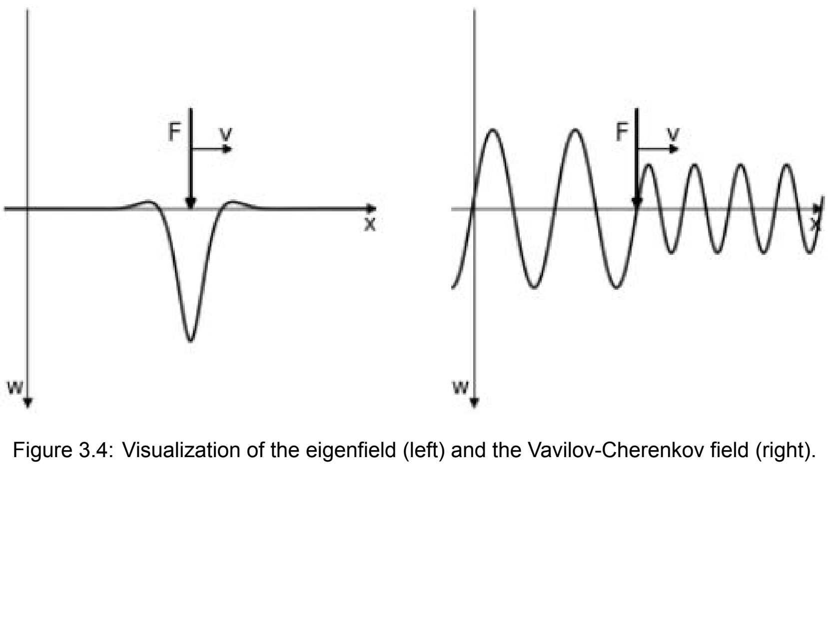

Figure 3.4: Visualization of the eigenfield (left) and the Vavilov-Cherenkov field (right).

The certain velocity v_{cr} is called the critical velocity and it is the minimum velocity of wave propagation from the load. On the previous page it is discussed what happens when the load velocity is lower or greater than this critical velocity. Special attention needs to be given to the case in which the load velocity equals the critical velocity. In that case the kinematic invariant is tangential to the dispersion curve, see the dashed line in Figure 3.3. This means that the load velocity and group velocity are equal. The energy that is inserted in the system by the load can not travel away from the load because the velocity of energy propagation, the group velocity, equals the load velocity. The energy is thus accumulated in the vicinity of the load, causing an infinite displacement to occur[1]. In line with this way of thinking, Metrikine [27] stated in a study: 'It is known that the power of radiation generated by a moving source is higher the closer the source speed to the velocity of wave propagation in the medium' . The importance of determining the critical velocity has been made clear above. Determining the critical velocity for the inertia-excluded system is relatively easy due to the fact that the wave-numbers are solved from a quartic equation (3.13) with even powers. The discriminant of this equation can be set to zero, from which the critical velocity can be determined. The idea behind this is that the solution set of wave-numbers turn from real to complex at the critical velocity, implying a sign change of the discriminant. The expression for the critical velocity for the inertia excluded system is well known and denoted by

$$v_{cr} = \frac{\beta_w}{\gamma_b}. \tag{3.15}$$

Obtaining the critical velocity for the inertia-included system will not be as easy and there will be made use of the relationship that for the steady state the load velocity, which is equivalent to the phase-velocity, should equal the group velocity at the point where the kinematic invariant touches the dispersion curve. From this it can be concluded that the graph for the phase and group velocity should at least touch or intersect for the presence of a critical velocity in the system, which is obviously true for the inertia-excluded system as can be seen from Figure 3.5. This subsection was very elaborated but this choice has been made in order to provide an understanding of the physical processes behind obtaining the mathematical solution and it will be very helpful for the reader in understanding the determination of the steady solution for the inertia-included system.

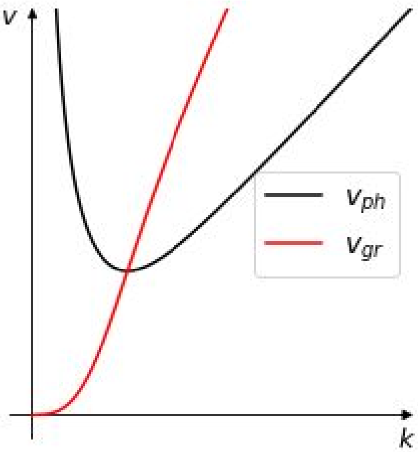

Figure 3.5: Visual representation of the phase velocity $v_{ph}(k)$ and the group $v_{gr}(k)$.

3.1.2. Transform method

This method is more direct than the previous one in the sense that no physical knowledge behind the different steps is needed in order to obtain the steady state solution. Special attention could be given to the physical interpretation behind the steps and one would then see the equivalence between this method and the geometrical method, however in the authors view the previous subsection suffices for this objective. This method serves as relative quick way to obtain the steady state.

The Fourier transforms[2] for the entire thesis are defined as

$$\hat{f}(k,\omega) = \int_{-\infty}^{\infty}\int_{-\infty}^{\infty} f(x,t)e^{-(kx-\omega t)i}dxdt \tag{3.16}$$

and their inversions as

$$f(x,t) = \frac{1}{(2\pi)^2}\int_{-\infty}^{\infty}\int_{-\infty}^{\infty} \hat{f}(k,\omega)e^{(kx-\omega t)i}d\omega dk. \tag{3.17}$$

[1]Note that the displacement is bounded for damped cases.

[2]The plural form is used to indicate a Fourier transform for each variable x and t.

Fourier transforming equation (3.1) for both variables and solving for the transformed steady state solution leads to

$$\hat{w} = \frac{\delta(\omega - kv)}{\Delta_{EX}(\omega, k)} 2\pi\hat{F}. \tag{3.18}$$

Inverse transforming consists of integrating twice of which the first integration is trivial because of the properties of the Dirac delta function, the second integration is more cumbersome and is therefore taken care of in a more elaborated way. After the first integration the expression for the steady state solution is

$$w = \frac{\hat{F}}{2\pi} \int_{-\infty}^{\infty} \frac{1}{\Delta_{EX}(vk, k)} e^{k(x-vt)i} dk. \tag{3.19}$$

This integral can be solved by application of Cauchy's residue Theorem in combination with Jordan's lemma. Two contours are therefore defined. The first contour is denoted by Γ^+ consisting of the segment $[-R, R]$ of the real axis together with the semi-circle $C^+ : k = Re^{i\theta}$, $0 \leq \theta \leq \pi$. Transforming the integral in equation (3.19) to a contour integral over Γ^+ yields

$$\frac{\hat{F}}{2\pi} \int_{\Gamma^+} \frac{1}{\Delta_{EX}(vk, k)} e^{k(x-vt)i} dk = \frac{\hat{F}}{2\pi} \int_{C^+} \frac{1}{\Delta_{EX}(vk, k)} e^{k(x-vt)i} dk + \frac{\hat{F}}{2\pi} \int_{-\infty}^{\infty} \frac{1}{\Delta_{EX}(vk, k)} e^{k(x-vt)i} dk. \tag{3.20}$$

The second contour is denoted by Γ^- consisting of the segment $[-R, R]$ of the real axis together with the semi-circle $C^- : k = Re^{i\theta}$, $-\pi \leq \theta \leq \pi$. Transforming the integral in equation (3.19) to a contour integral over Γ^- yields

$$\frac{\hat{F}}{2\pi} \int_{\Gamma^-} \frac{1}{\Delta_{EX}(vk, k)} e^{k(x-vt)i} dk = \frac{\hat{F}}{2\pi} \int_{C^-} \frac{1}{\Delta_{EX}(vk, k)} e^{k(x-vt)i} dk + \frac{\hat{F}}{2\pi} \int_{\infty}^{-\infty} \frac{1}{\Delta_{EX}(vk, k)} e^{k(x-vt)i} dk. \tag{3.21}$$

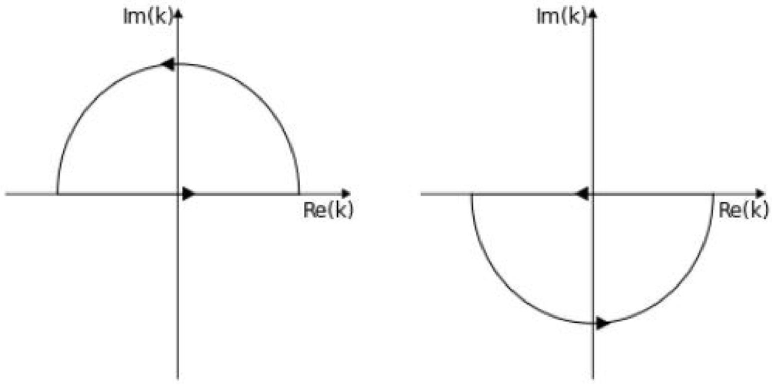

Figure 3.6: Visualization of the contours, Γ^+(left) and Γ^-(right), used for integration.

The next step is to take the limit $R \to \infty$ and applying Jordan's lemma from which it follows that the first term of the right hand side of equation (3.20) vanishes for $x > vt$ and the first term of the right hand side of equation (3.21) vanishes for $x < vt$. Applying Cauchy's residue theorem for the left hand sides of these equations and rearranging terms now yields the steady state solution

$$w = \begin{cases} \sum\limits_{m \in K^+} \dfrac{1}{\prod\limits_{j=1, j\neq m}^{4} (k_m - k_j)} \hat{F} i e^{k_m (x-vt)i} & x > vt \\ \sum\limits_{m \in K^-} \dfrac{-1}{\prod\limits_{j=1, j\neq m}^{4} (k_m - k_j)} \hat{F} i e^{k_m (x-vt)i} & x < vt \end{cases}, \tag{3.22}$$

with k_i being the poles obtained by solving the roots of equation (3.13). Note that two sets are defined, namely K^+ being the set of poles that are located in Γ^+ and K^- being the set of poles that are located in Γ^-. In non-damped cases a problem arises in cases in when poles are located on the segment $[-R, R]$. In those case one should introduce a limit case of damping $\alpha_w \to 0$. The poles will move from the segment and it can be concluded to which subset each individual pole belongs.

3.2. Steady state of the inertia-included system

3.2.1. Geometrical method

For a uniformly moving constant load in the inertia-included system the equation of motion in operator notation is

$$\begin{bmatrix} \left(\frac{\partial^4}{\partial x^4} + 4\gamma_b^2\frac{\partial^2}{\partial t^2} + 4\alpha_p\frac{\partial}{\partial t} + 4\beta_p^4\right) & \left(-4\alpha_p\frac{\partial}{\partial t} - 4\beta_p^4\right) \\ \left(-4\alpha_p\frac{\partial}{\partial t} - 4\beta_p^4\right) & \left(4\gamma_s^2\frac{\partial^2}{\partial t^2} + \left(4\alpha_p + 4\alpha_s\right)\frac{\partial}{\partial t} + \left(4\beta_p^4 + 4\beta_s^4\right)\right) \end{bmatrix} \begin{bmatrix} w \\ w_s \end{bmatrix} = \begin{bmatrix} \hat{F} \\ 0 \end{bmatrix} \delta(x - vt), \tag{3.23}$$

in which the constants are defined by

$$4\gamma_i^2 = \frac{\rho_i}{EI}, \quad 4\alpha_i = \frac{c_i}{EI}, \quad 4\beta_i^4 = \frac{k_i}{EI}, \text{ and } \quad \hat{F} = \frac{F}{EI}. \tag{3.24}$$

The spatial domain is once again split into the two semi-infinite domains $\Omega^{(1)}$ and $\Omega^{(2)}$ with respective solution vector $\mathbf{w}^{(1)} = \begin{bmatrix} w^{(1)} & w_s^{(1)} \end{bmatrix}^T$ and $\mathbf{w}^{(2)} = \begin{bmatrix} w^{(2)} & w_s^{(2)} \end{bmatrix}^T$, such that

$$\begin{bmatrix} \left(\frac{\partial^4}{\partial x^4} + 4\gamma_b^2\frac{\partial^2}{\partial t^2} + 4\alpha_p\frac{\partial}{\partial t} + 4\beta_p^4\right) & \left(-4\alpha_p\frac{\partial}{\partial t} - 4\beta_p^4\right) \\ \left(-4\alpha_p\frac{\partial}{\partial t} - 4\beta_p^4\right) & \left(4\gamma_s^2\frac{\partial^2}{\partial t^2} + \left(4\alpha_p + 4\alpha_s\right)\frac{\partial}{\partial t} + \left(4\beta_p^4 + 4\beta_s^4\right)\right) \end{bmatrix} \begin{bmatrix} w^{(n)} \\ w_s^{(n)} \end{bmatrix} = \begin{bmatrix} 0 \\ 0 \end{bmatrix}. \tag{3.25}$$

As a trial solution a summation of harmonic waves is suggested, which is denoted by

$$\mathbf{w}^{(n)} = \sum_j \mathbf{W}_j^{(n)} e^{(k_j x - \omega_j t)i}. \tag{3.26}$$

The vectors $\mathbf{W}_j^{(n)}$ are the unknown amplitude vectors. Substitution of an arbitrary term of this trial solution in equation (3.25) yields a homogeneous system of linear equations

$$\mathbf{A}(\omega, k)\mathbf{W} = \mathbf{0}. \tag{3.27}$$

The matrix $\mathbf{A}(\omega, k)$ in this system should be singular in order to have non-trivial solution vectors which means that the determinant of this system of equations should be zero. The determinant is denoted by

$$\Delta_{IN}(\omega, k) = \left(k^4 - 4\gamma_b^2\omega^2 - 4\alpha_p\omega i + 4\beta_p^4\right)\left(-4\gamma_s^2\omega^2 - \left(4\alpha_p + 4\alpha_s\right)i\omega + \left(4\beta_p^4 + 4\beta_s^4\right)\right) - \left(4\alpha_p i\omega - 4\beta_p^4\right)^2 \tag{3.28}$$

and equating this determinant to zero results in the dispersion equation. This equation is dependent on two variables, namely the frequency ω and the wave-number k. An additional equation is thus demanded, the kinematic invariant see also equation (3.6). The system for obtaining the (ω, k)-pairs is thus denoted by

$$\Delta_{IN}(\omega, k) = 0 \wedge \omega = kv. \tag{3.29}$$

Solving this system is equivalent to solving

$$\Delta_{IN}(vk, k) = 0, \tag{3.30}$$

which is an equation for the roots of a sixth order polynomial in k in which terms of all order between zero and six occur. Solving such an equation analytically for general parameters is difficult if not impossible. One can however solve this equation numerically by make use of a program such as Maple to obtain the roots. The result of such calculations will be six wave-numbers k_j of which each can be related to their corresponding frequency ω_j through the kinematic invariant. Each of the six (ω_j, k_j)-pairs can be substituted in equation (3.27) to obtain a system from which a relationship between the entries of a solution vector can be obtained, leading to an eigenvector $\hat{\mathbf{W}}_j$ of the system. This is done in successive order for all (ω_j, k_j)-pairs to obtain all eigenvectors of the system. The solution in equation (3.26) can be rewritten as

$$\mathbf{w}^{(n)} = \sum_{j=1}^{6} c_j^{(n)} \hat{\mathbf{W}}_j^{(n)} e^{(k_j x - \omega_j t)i}. \tag{3.31}$$

The constants c_j^n are fully determined from the boundary and interface conditions. A number of constants are canceled based on the radiation condition and on the fact that the solution should be bounded for $|x| \to \infty$. The remaining unknown constants are then solved by making use of interface conditions.

On the previous page the method for obtaining the solution for a uniformly moving constant load in the inertia-included is described. Like with the inertia-excluded system different types of displacement fields for different velocities can be observed when solving the problem. The differences in behaviour for the inertia-excluded system have been explained by investigation of the dispersion curves and the kinematic invariant. A similar investigation is also done in the following for the inertia-included system.

In the case that a frequency ω is given, the corresponding wave-number k can be determined. In order to do so the dispersion equation[3] is first rewritten to

$$k^4 = z(\omega) = \frac{z_1(\omega)}{z_2\omega}, \tag{3.32}$$

with

$$z_1(\omega) = \left(4\gamma_b^2\omega^2 - 4\beta_p^4\right)\left(-4\gamma_s^2\omega^2 + \left(4\beta_p^4 + 4\beta_s^4\right)\right) + \left(4\beta_p^4\right)^2 \tag{3.33}$$

and

$$z_2(\omega) = -4\gamma_s^2\omega^2 + \left(4\beta_p^4 + 4\beta_s^4\right). \tag{3.34}$$

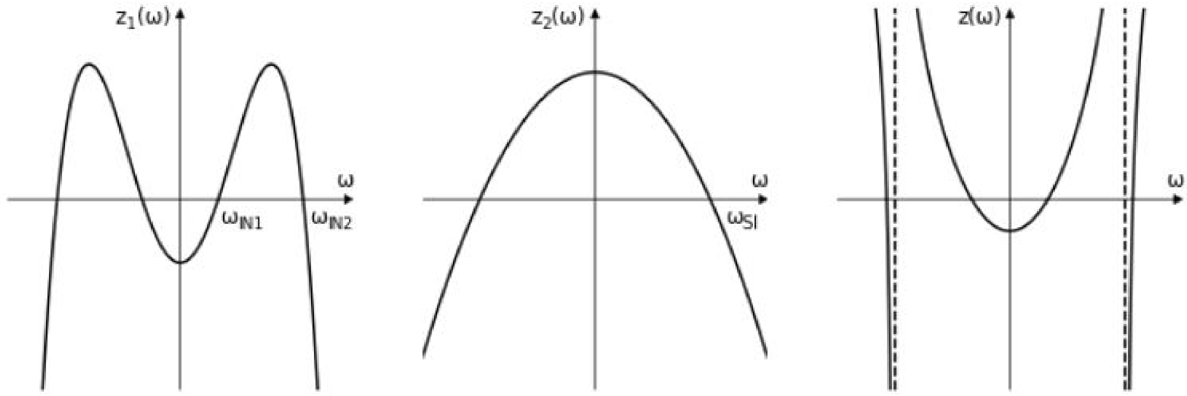

Figure 3.7: Visual representations of the functions $z_1(\omega)$ (left), $z_2(\omega)$ (left) and $z(\omega)$ (right)

The wave numbers k are obtained by taking the fourth order roots of $z(\omega)$. It is thus of importance to know on which intervals of ω the function $z(\omega)$ is positive and on which it is negative. On intervals of ω over which $z(\omega) < 0$ all four wave-numbers are complex-valued and on intervals of ω over which $z(\omega) > 0$ two wave-numbers are real and two wave-numbers are imaginary, see Figure 3.1. The function $z(\omega)$ is a fraction of which its numerator is the fourth order polynomial $z_1(\omega)$ and its denominator the second order polynomial $z_2(\omega)$. The graph of $z_1(\omega)$ is depicted in Figure 3.7 and its positive roots in increasing magnitude are denoted by ω_{IN1} are ω_{IN2}. The graph of $z_2(\omega)$ is depicted in Figure 3.7 and its positive root is denoted by ω_{SI}. Both $z_1(\omega)$ and $z_2(\omega)$ are symmetric polynomials around $\omega = 0$, such that the non-mentioned roots of both polynomials are basically the same as the positive roots with a minus sign. The roots of $z(\omega)$ coincide with the roots of $z_1(\omega)$. The function $z(\omega)$ has singularities at the roots of $z_2(\omega)$ due to the division by zero. At this singularity the sign of $z(\omega)$ changes. The intervals on which $z(\omega)$ is positive is thus dependent on the value of ω_{SI} in comparison with the values of ω_{IN1} and ω_{IN2}. It turns out that the value of ω_{SI} is in between ω_{IN1} and ω_{IN2} for all numerical values of the system parameters that are physically possible, the proof can be found in Appendix A. From this it can be concluded over which intervals $z(\omega)$ is positive and over which it is negative. A proper mathematical expression can be obtained by viewing $z(\omega)$ as a complex number of which its argument is denoted by $\theta_z(\omega)$. It follows that

$$\theta_z(\omega) = \begin{cases} \pi & |\omega| < \omega_{IN1} \\ 0 & \omega_{IN1} < |\omega| < \omega_{SI} \\ \pi & \omega_{SI} < |\omega| < \omega_{IN2} \\ 0 & \omega_{IN2} < |\omega| \end{cases}, \tag{3.35}$$

which is also observed in the graph of $z(\omega)$ shown in Figure 3.7.

[3]Note that the damping is neglected, in line with the reasoning on page 12

The dispersion curves for the inertia-excluded system were obtained by taking the fourth order roots of $z(\omega)$, corresponding to that problem, and plotting the real valued wave-numbers as a function of the frequency ω. This is repeated for the inertia-included system yielding two pairs of dispersion curves which can be explained from the fact that there are four intervals over which $z(\omega)$ is positive, see equation (3.35). The physical explanation for this phenomenon is of course the fact that an additional inertia beam is added to the initial problem. The two pairs of dispersion curves are shown in Figure 3.8 in both a $(\omega, k)-$ and a $(k, \omega)-$coordinate system.

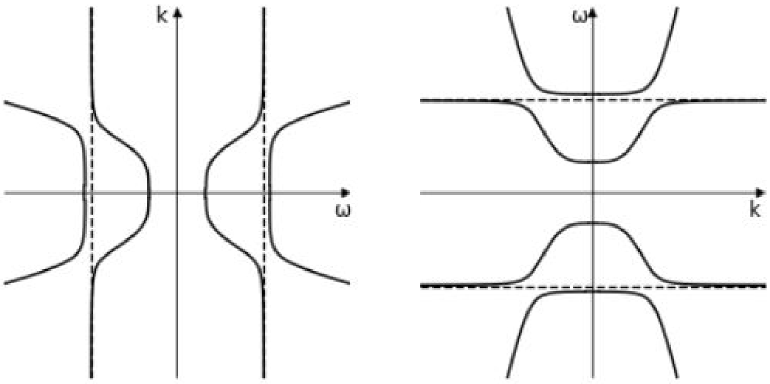

Figure 3.8: Dispersion curves for the inertia-included system.

The dispersion curve corresponding to only positive frequencies of the inner pair of dispersion curves is from now on referenced to as the lower dispersion curve and the dispersion curve corresponding with only positive frequencies of the outer pair of dispersion curves is from now on referenced to as the upper dispersion curve. The lower dispersion curve has a frequency band $(\omega_{IN1}, \omega_{SI})$ and the upper curve has cut-off frequency ω_{IN2}. From this it can be concluded that harmonic propagating waves in the system either have a frequency that is in the frequency band of the lower curve or above the cut-off frequency of the upper curve. The upper dispersion curve shows a strong resemblance with the dispersion curve of the inertia-excluded system and is the curve corresponding to the first equation of (3.25). The lower dispersion curve corresponds to the second equation of (3.25) and tends to the horizontal asymptote ω_{SI} for large value of k. This frequency corresponds to the natural frequency of the inertia beam when the displacement of the Euler-Bernoulli beam is restrained. In that case the equation for the inertia beam reduces to that of a single degree of freedom system with natural frequency ω_{SI}. The natural frequency of a single degree of freedom system is obviously independent of a wave-number, explaining the behaviour of the lower dispersion curve, namely that it tends to a constant value for large values of k. This behaviour is due to the fact that the inertia beam does not have bending stiffness. In the case that it has bending stiffness this is not the case as has been shown in the study of Shamalta [18]. For relatively small values of k however, non-constant behaviour is observed. This can be explained by the coupling between the inertia beam and the Euler-Bernoulli beam.

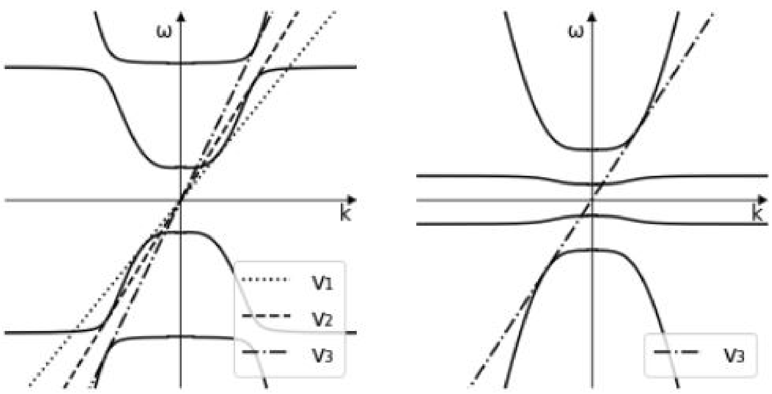

Figure 3.9: Dispersion curves and kinematic invariants corresponding to the tangential velocities v_i for small values of γ_s (left) and large values of γ_s (right).

The dispersion curves for general wave propagation have been studied. The next step is to study the combination of the dispersion curves and the kinematic invariant. The specific interest lays in the critical velocity of the system. For the inertia-excluded system a simple expression could be obtained for the critical velocity, see equation (3.15). It has also been explained that the critical velocity is the minimum velocity of wave propagation from the load and that it is the load velocity for which the kinematic invariant is tangential to the dispersion curve.

When one attempts to draw tangential lines to the dispersion curves that start at the origin, he will find that there are in general two cases that can be distinguished dependent on the value of γ_s, see Figure 3.9. For small values of γ_s three tangential lines can be drawn, corresponding with velocities v_1, v_2 and v_3 in increasing order. For large values of γ_s only one tangential line can be drawn, corresponding with velocity v_3. The choice has been made to denote v_3 by v_3 in both cases because it is the line that is tangential to the upper dispersion curve in both cases. The velocities v_1 and v_2 correspond to the two lines that are tangential to the lower dispersion curve and are only present in the first case.

Obtaining the intersection points between the kinematic invariant and the dispersion curves is equivalent to solving equation (3.29) which has six roots describing the wave-numbers k_j that are present in the steady state. If the number of intersection points is below six, the other wave-numbers are complex. From this conclusions can be made for the steady state behaviour. In the first case, small values of γ_s, it can be observed that there are two propagating waves from the load and thus four non-propagating waves in the system for $v < v_1$ or $v_2 < v < v_3$ and six propagating waves for $v_1 < v < v_2$ or $v > v_3$. In the second case, large values of γ_s, there are two propagating and four non-propagating waves in the system for $v < v_3$ and six propagating waves for $v > v_3$.

Notice that there are always at least two propagating waves in the system. There is now a problem with defining the critical velocities. For all v_i the load velocity equals the group velocity, resulting in an infinite displacement. This is in line with the critical velocity definition for the inertia-excluded system. However, the velocities v_i do not describe minimum velocities of wave propagation because there are already at least two waves propagating in the system for all possible velocities. The velocities v_i do however form boundaries of velocity intervals in which there are either two propagating and four evanescent waves or six propagating waves. The intervals of velocities for which only propagating waves occur are from now on referred to as super-critical velocity intervals and the intervals of velocities for which two propagating and four evanescent waves occur are from now on referred to as sub-critical velocity intervals. It can be summarized that for small values of γ_s the sub-critical velocity intervals are $(0, v_1)$ and (v_2, v_3) and the super-critical velocity intervals are (v_1, v_2) and (v_3, ∞) and that for large values of γ_s the sub-critical velocity interval is $(0, v_3)$ and the super-critical velocity interval is (v_3, ∞).

In order to complete a sound analysis an unambiguous boundary value of γ_s for the two cases needs to be obtained. To obtain this the value the fact that the roots of equation (3.29) correspond to the wave-numbers k_j of the intersection points between the dispersion curves and the kinematic invariant is used. Equation (3.29) is a sixth order polynomial in k in which terms of only even powers[4] are present. This sixth order equation can be simplified to a cubic equation by making the substitution $x = k^2$. This cubic equation is denoted by

$$a(\gamma_s, v)x^3 + b(\gamma_s, v)x^2 + c(\gamma_s, v)x + d = 0, \tag{3.36}$$

with

$$\begin{aligned} a(\gamma_s, v) &= -4\gamma_s^2 v^2 \\ b(\gamma_s, v) &= 16\gamma_b^2\gamma_s^2 v^4 + 4\beta_p^4 + 4\beta_s^4 \\ c(\gamma_s, v) &= \left(-16\gamma_b^2\beta_p^4 - 16\gamma_s^2\beta_p^4 - 16\gamma_b^2\beta_s^4\right) v^2 . \\ d &= 16\beta_p^4\beta_s^4 \end{aligned} \tag{3.37}$$

The nature of the roots of such a cubic equation can be determined by its discriminant D which is defined by

$$D(\gamma_s, v) = 18abcd - 4b^3d + b^2c^2 - 4ac^3 - 27a^2d^2. \tag{3.38}$$

Two cases can be distinguished:

- If $D(\gamma_s, v) > 0$, all three roots x_j are distinct and real.
- If $D(\gamma_s, v) < 0$, one root is real valued and the other two are complex conjugates.

[4] Recall that the damping has been set to zero.

The first possibility for the set of roots coincides with the wave numbers that are obtained from the intersection points between the dispersion curves and a kinematic invariant with a velocity that is in one of the super-critical velocity intervals. The second possibility for the set of roots coincides with the wave numbers that are obtained for a velocity in of the sub-critical velocity intervals. These sub- and super-critical velocity intervals for a set γ_s are thus equivalent with the segments between the roots of the graph for the discriminant $D(\gamma s, v)$. A more convenient map with sub- and super-critical velocity zones can however be obtained by keeping both the velocity v and γ_s variable, setting equation (3.38) to zero and implicit plotting the expression, see Figure 3.10. The obtained curves are the curves on which the discriminant is zero and are thus corresponding to the tangential velocities. The value of $D(\gamma_s, v)$ is either negative or positive in the zones enclosed by these curves and can thus be referred to as sub- or super-critical velocity zones.

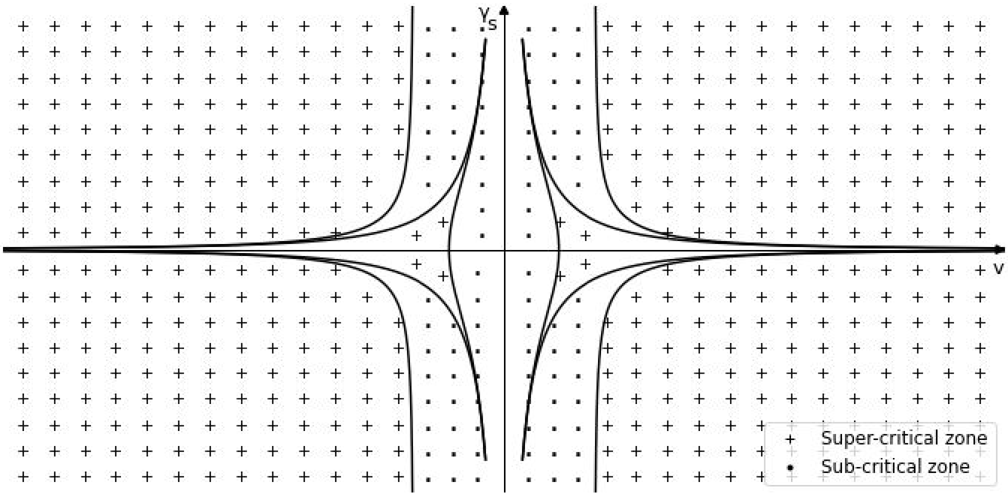

Figure 3.10: A map depicting the critical zones for the inertia-included system.

From Figure 3.10 one can quickly confirm whether a system behaves according to the still not defined small valued γ_s behaviour or large valued γ_s behaviour. In order to well define the difference two values γ_{ss} and γ_{sl} are analysed. These values are therefore plotted in the critical-zone map, see Figure 3.11. Notice that only the first quadrant is depicted due to the fact that the velocity is positive and because negative values of γ_s do not have physical meaning.

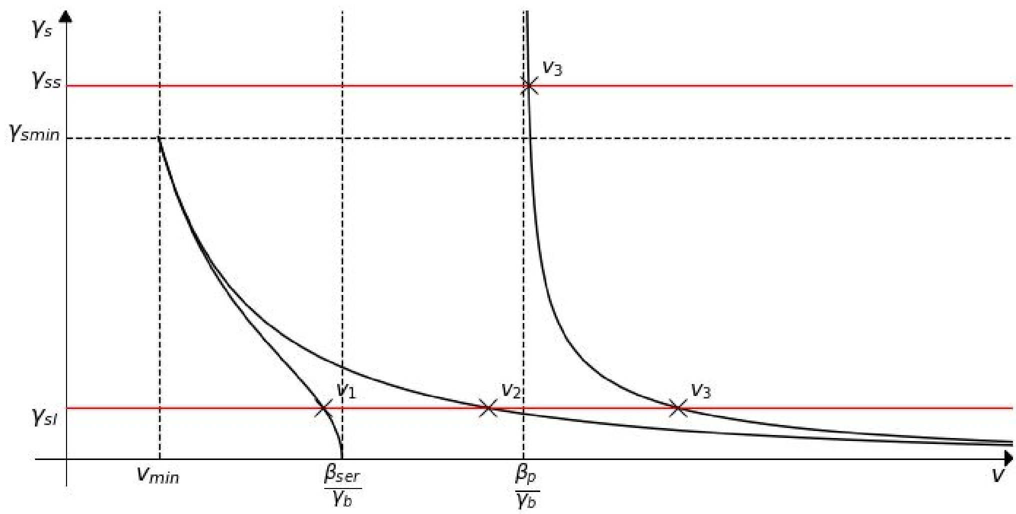

Figure 3.11: Graphical evaluation of the boundary value γ_{smin}.

The horizontal line corresponding to γ_{sl} has three intersection points with the zero curves of the discriminant. The horizontal coordinates of these points correspond to the three tangential velocities that are present in the first type of system behaviour. The horizontal line corresponding to γ_{ss} has only one intersection point with the third zero curve of the discriminant. The horizontal coordinate of this point corresponds to the single tangential velocity that is present in the second type of system behaviour. It can be observed that the difference in system behaviour occurs when γ_s is above a certain minimum value γ_{smin}. This value of γ_{smin} can be obtained numerically by which the task of finding the boundary value between the two cases of system behaviour has been fulfilled. Limit case behaviour can also be analysed from Figure 3.11. For $\gamma_s \to 0$ it is observed that v_1 tends to $\frac{\beta_{ser}}{\gamma_b}$ and that both v_2 and v_3 tend to zero. Note that β_{ser} is defined as

$$\beta_{ser} = \frac{1}{EI}\left(\frac{1}{\frac{1}{k_p}+\frac{1}{k_s}}\right). \tag{3.39}$$

The system thus behaves as if the elastic-layers are in serial connection. This is correct from a physical point of view because the inertial effects of the inertia beam can be neglected when $\gamma_s \to 0$. Notice that this is the same system as the inertia-excluded system, meaning that this limit value of v_1 is basically equal to the critical velocity of the inertia-excluded system. For $\gamma_s \to \infty$ it is observed that v_3 tends to $\frac{\beta_p}{\gamma_b}$ which means that the system acts as if it only exists of the upper elastic layer and the Euler-Bernoulli beam. This can also be explained physically because the velocity of the inertia beam is resisted by the large inertia causing it to have a set displacement in the steady state. In that case the Euler-Bernoulli beam can thus show a behaviour which is independent of the inertia beam and the lower elastic layer. It is furthermore important to notice that $\frac{\beta_p}{\gamma_b}$ is a lower bound value for v_3 and that v_{min} is a lower bound value for both v_1 and v_3. The velocity v_{min} is the velocity that corresponds with the first intersection point of γ_s and the zero-curves. Its value can be computed numerically.

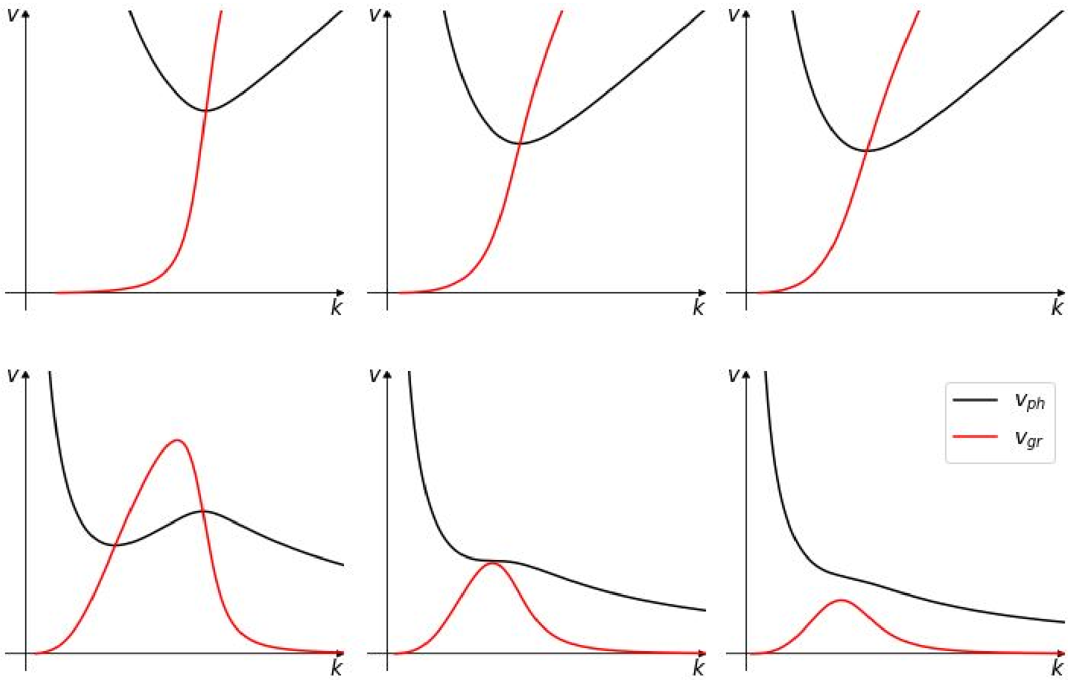

Figure 3.12: The graphs for v_{ph} and v_{gr} for $\gamma_s < \gamma_{smin}$ (left-column), $\gamma_s = \gamma_{smin}$ (middle column) and $\gamma_s > \gamma_{smin}$ (right column). The upper row represents the velocities for the upper dispersion curve and the lower row represents the lower dispersion curve.

Subsection 3.1.1 ended by stating that the graphs of the phase and group velocity should at least touch or intersect for the presence of a critical velocity in the system or, as may be stated now, a tangential velocity. It is thus expected that the total number of intersection points between graphs of the phase and group velocity for the lower and upper curve should equal three for $\gamma_s < \gamma_{smin}$ and two for $\gamma_s > \gamma_{smin}$. This is indeed true as can be seen in Figure 3.12 by which it is once again confirmed that γ_{smin} behaves as a transition point for the two cases of system behaviour.

The situations in which sub- or super-critical behaviour occurs in the system has been elaborated extensively. Usually the term sub-critical is only used for the situation in which only non-propagating waves are present. This is not the case for the inertia-included system because in this system there are always at least two propagating waves as has been discussed. This means that application of this term sub-critical is not completely correct, so the reader should keep in mind that the prefixes sub- and super- are used to indicate the difference between two and six propagating waves. By checking all possibilities of the kinematic invariant for both $\gamma_s < \gamma_{smin}$ and $\gamma_s < \gamma_{smin}$ one can conclude that the two propagating waves that are always present only occur in the left semi-infinite $\Omega^{(1)}$ due to the fact that the group velocity of these two waves is always smaller than the load velocity. This explains the asymmetrical behaviour with respect to the loading point in the eigenfield[5] (sub-critical) and it also explains the occurrence of two distinct wave-numbers to the left of the loading point in the Vavilov-Cherenkov displacement field (super-critical) in Figure 3.13.

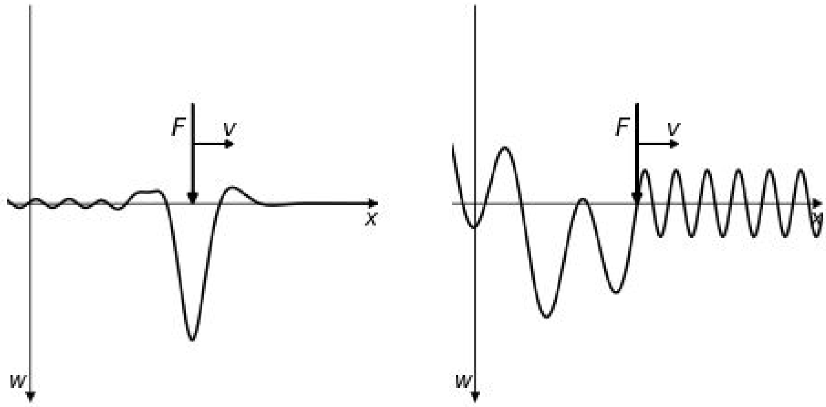

Figure 3.13: Visualization of the eigenfield (left) and the Vavilov-Cherenkov field (right).

One should note that the ripples in Figure 3.13 describing the propagating waves in the eigenfield are relative small compared to the deflection due to the non-propagating waves. This ratio may differ however for different load velocities. It should also be mentioned that the waves propagating in front of the load for the super-critical case are due to the other intersection points between the dispersion curves and kinematic invariant.

3.2.2. Transform method

The steady state for the inertia-included system will also be obtained by making use of the transform method. This is done to have a quick way to determine the steady state solution without paying much attention to the interpretations behind each step. Fourier transforming equation (3.23) leads to

$$\begin{bmatrix} \left(k^4 - 4\gamma_b^2\omega^2 - 4\alpha_p i\omega + 4\beta_p^4\right) & \left(4\alpha_p i\omega - 4\beta_p^4\right) \\ \left(4\alpha_p i\omega - 4\beta_p^4\right) & \left(-4\gamma_s^2\omega^2 - (4\alpha_p + 4\alpha_s)i\omega + (4\beta_p^4 + 4\beta_s^4)\right) \end{bmatrix} \begin{bmatrix} \hat{w} \\ \hat{w}_s \end{bmatrix} = 2\pi \begin{bmatrix} \hat{F} \\ 0 \end{bmatrix} \delta(\omega - kv). \tag{3.40}$$

This linear set of equations can easily be solved multiplying both sides by the inverse of the matrix on the left hand side of the equation. This leads to the transformed steady state solution vector

$$\begin{bmatrix} \hat{w} \\ \hat{w}_s \end{bmatrix} = \begin{bmatrix} \left(-4\gamma_s^2\omega^2 - (4\alpha_p + 4\alpha_s)i\omega + (4\beta_p^4 + 4\beta_s^4)\right) \\ -\left(4\alpha_p i\omega - 4\beta_p^4\right) \end{bmatrix} \frac{\delta(\omega - kv)}{\Delta_{IN}(\omega, k)} 2\pi\hat{F}. \tag{3.41}$$

Inverse transforming the expression and computing the integration over the frequency variable results in

$$\begin{bmatrix} w \\ w_s \end{bmatrix} = \frac{\hat{F}}{2\pi} \int_{-\infty}^{\infty} \begin{bmatrix} \left(-4\gamma_s^2 v^2 k^2 - (4\alpha_p + 4\alpha_s)ivk + (4\beta_p^4 + 4\beta_s^4)\right) \\ -\left(4\alpha_p ivk - 4\beta_p^4\right) \end{bmatrix} \frac{e^{k(x-vt)i}}{\Delta_{IN}(vk, k)} dk. \tag{3.42}$$

[5]The same argumentation for the definition that holds for sub-critical behaviour also holds for the eigenfield.

This final integral can then be computed by by application of Cauchy's residue Theorem in combination with Jordan's lemma. There has been made use of the same contours as in the previous section and the final expression of the steady state solution vector is denoted by

$$\begin{bmatrix} w \\ w_s \end{bmatrix} = \begin{cases} \sum\limits_{m\in K^+} \begin{bmatrix} \left(-4\gamma_s^2 v^2 k_m^2 - (4\alpha_p + 4\alpha_s) ivk_m + (4\beta_p^4 + 4\beta_s^4)\right) \\ -\left(4\alpha_p ivk_m - 4\beta_p^4\right) \end{bmatrix} \dfrac{\hat{F} i e^{k_m (x-vt)i}}{\prod\limits_{j=1, j\neq m}^{6} (k_m - k_j)} & x > vt \\ \sum\limits_{m\in K^-} \begin{bmatrix} \left(-4\gamma_s^2 v^2 k_m^2 - (4\alpha_p + 4\alpha_s) ivk_m + (4\beta_p^4 + 4\beta_s^4)\right) \\ -\left(4\alpha_p ivk_m - 4\beta_p^4\right) \end{bmatrix} \dfrac{-\hat{F} i e^{k_m (x-vt)i}}{\prod\limits_{j=1, j\neq m}^{6} (k_m - k_j)} & x < vt \end{cases} . \tag{3.43}$$

4 Transition radiation

In the introduction of this thesis it was stated that transition radiation is emitted when a source moves through an inhomogeneous medium, such as a boundary between two different media. This phenomenon will be studied in this report for both mechanical models. In both models the constant load is moving uniformly along the infinite beam and the foundation is inhomogeneous in the sense that there is an abrupt jump in the stiffness properties. In his report Wolfert [30] analysed the spectral density of the radiation energy in the direction of the load motion and backward for an elastically supported string. The analyses that are done in this chapter for both models are based on that report.

4.1. Transition radiation in the inertia excluded model

In order to study transition radiation the same model as in equation (3.1) is tackled, once again neglecting the damping. However there has been made a modification to the elastic foundation, in the sense that there is an abrupt jump in the stiffness of the elastic foundation located at $x = 0$, such that

$$k_w(x) = k_w^{(1)} + (k_w^{(2)} - k_w^{(1)})H(x). \tag{4.1}$$

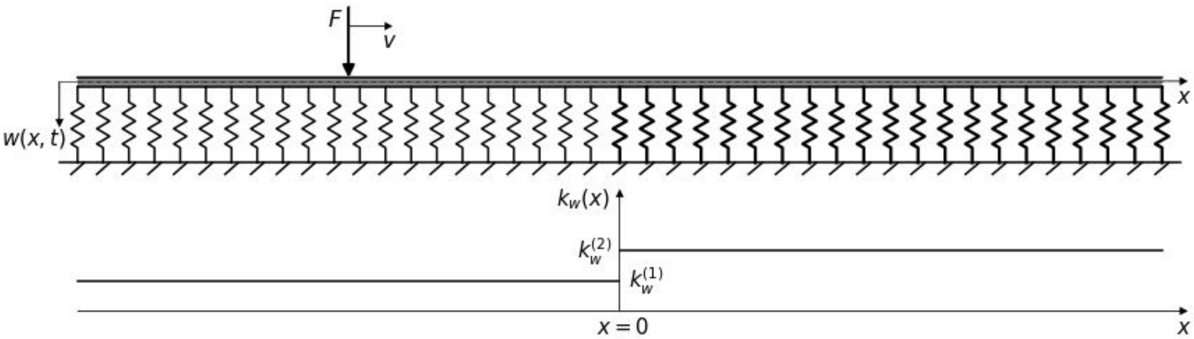

Figure 4.1: Mechanical scheme of a moving load in the inertia-excluded system with an abrupt jump in the foundation stiffness.

Note that $H(x)$ denotes the Heaviside function. The load velocity is furthermore sub-critical in order to prevent Vavilov-Cherenkov radiation because the aim of this chapter is to study transition radiation individually. The governing equation of motion reads

$$\frac{\partial^4 w}{\partial x^4} + 4\gamma_b^2 \frac{\partial^2 w}{\partial t^2} + 4\beta_w^4(x) w = \hat{F}\delta(x - vt). \tag{4.2}$$

Before analysing this problem in the frequency domain, a thought experiment is performed to anticipate the solution. Two situations are discussed first, the situations at $t \to -\infty$ and $t \to \infty$. At both time instances the load is far away from the stiffness transition. From a physical point of view it is expected that the displacement fields at these time instances behave as if the stiffness jump is not there. This implies that the displacement fields at these time instances are the eigenfields $w_e^{(n)}$ corresponding to their respective supporting stiffness $k_w^{(n)}$, see Figure 4.2.

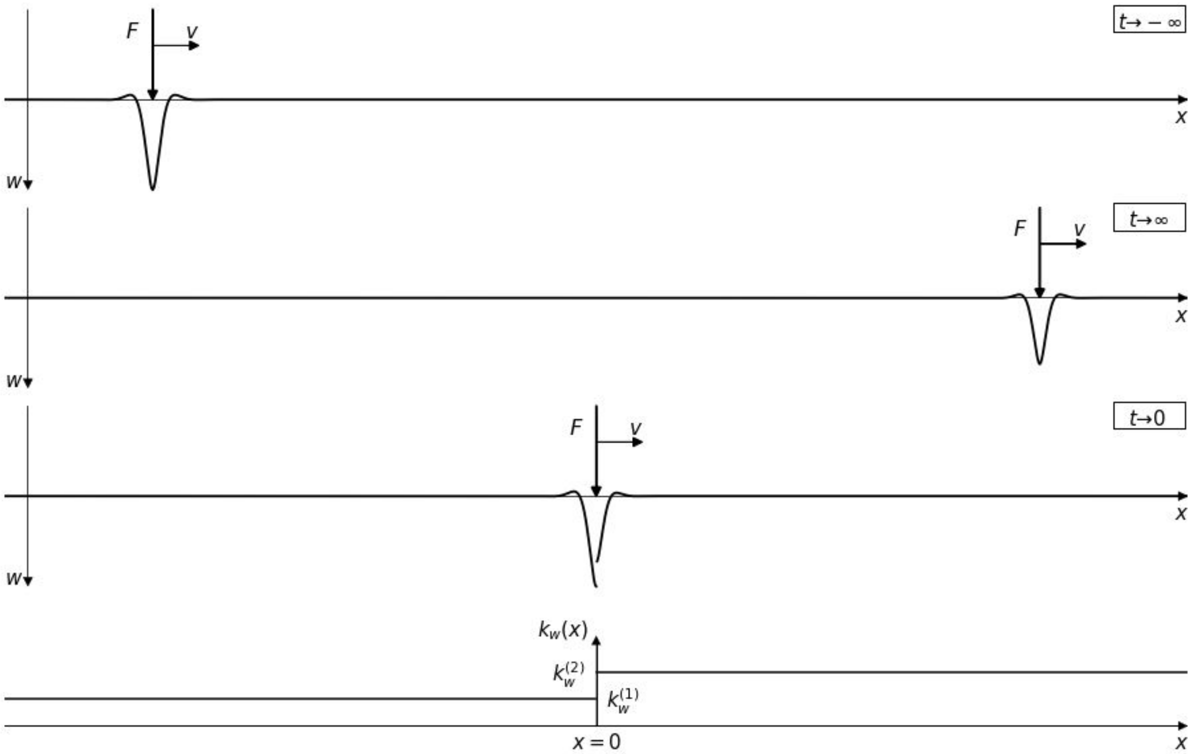

Figure 4.2: The thought experiment for the phenomenon of transition radiation.

Figure 4.2 gives the impression that the solution for $t < 0$, or equivalently $x < 0$, exists of $w_E^{(1)}$ and that the solution for $x > 0$ exists of $w_E^{(2)}$. These solutions do also satisfy equation (4.2) and they also seem to hold for intuitively large $|t|$. However as $|t|$ gets smaller it is noted that the eigenfields on their own would result in a discontinuity in the displacement field at the location of the stiffness jump. This is physically impossible and in order to solve this problem homogeneous solutions can be added in both domains to guaranty the continuity of the solution at $x = 0$. These homogeneous solutions are additional to the eigenfields that occur normally in the case of a homogeneous foundation and are called free fields. Mathematically the eigenfields are thus the particular solutions of both domains and the free fields are the homogeneous solutions that are added to satisfy the interface conditions at the abrupt stiffness jump.

The governing equation of motion will now be analysed in the frequency domain. The forward Fourier transform is applied over time to equation (4.2). This results in

$$\frac{\partial^4 \hat{w}}{\partial x^4} + \left(4\beta_w^4(x) - 4\gamma_b^2\omega^2\right)\hat{w} = \frac{\hat{F}}{v} e^{\frac{\omega}{v}xi}. \tag{4.3}$$

The remaining ordinary differential equation is now split into two semi-infinite domains, a left domain $\Omega^{(1)} = (-\infty, 0)$ and a right domain $\Omega^{(2)} = (0, \infty)$. The solutions of these domains are respectively $w^{(1)}$ and $w^{(2)}$. The Fourier transforms with respect to the time variable t of these solutions satisfy

$$\frac{\partial^4 \hat{w}^{(n)}}{\partial x^4} + \left(4\beta_w^{(n)4} - 4\gamma_b^2\omega^2\right)\hat{w}^{(n)} = \frac{\hat{F}}{v} e^{\frac{\omega}{v}xi}. \tag{4.4}$$

The particular solution can be obtained easily and reads

$$\hat{w}_E^{(n)} = \frac{1}{\Delta_{EX}^{(n)}(\frac{\omega}{v}, \omega)} \frac{\hat{F}}{v} e^{\frac{\omega}{v}xi}. \tag{4.5}$$

This is indeed the Fourier transform with respect to time of the eigenfields. For the homogeneous solution the suggested trial solution is denoted by

$$\hat{w}_F = a(\omega)e^{k(\omega)xi}. \tag{4.6}$$

Substitution of this trial solution in the homogeneous version of equation (4.4) will lead to the fact that the dispersion equation of equation (3.7) needs to be satisfied in order to obtain non-trivial solutions. The four wave-numbers $k_j(\omega)$ corresponding to the different possibilities of ω are visualized in the complex plane in Figure 3.1. The solution for the free fields can thus be denoted as

$$\hat{w}_F^{(n)} = a_1(\omega)e^{k_1^{(n)}(\omega)xi} + a_2(\omega)e^{k_2^{(n)}(\omega)xi} + a_3(\omega)e^{k_3^{(n)}(\omega)xi} + a_4(\omega)e^{k_4^{(n)}(\omega)xi}. \tag{4.7}$$

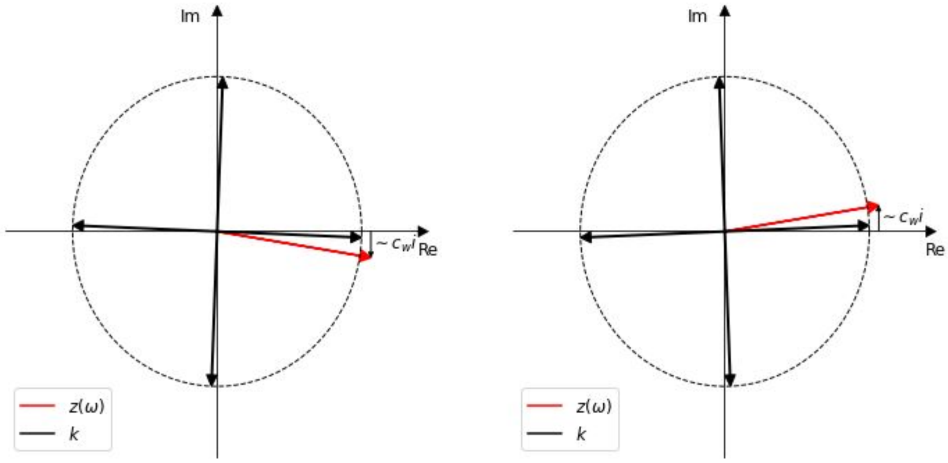

Figure 4.3: Rotation of $z(\omega)$ and its corresponding roots $k_i(\omega)$ due to limit case damping $c_w \to 0$ for $\omega < \omega_{EX}^{n}$ (left) and $\omega > \omega_{EX}^{n}$ (right).

The solution should be bounded for $|x| \to \infty$ which means that for each sub-domain waves with wave numbers k that do not meet this condition should be canceled. For semi-infinite domain $\Omega^{(2)}$ it is required that the $\mathrm{Im}(k) \geq 0$. From Figure 3.1 it is seen that for $|\omega| < \omega_{EX}^{(2)}$ two waves can be canceled immediately because their wave-numbers do not satisfy this condition. For $|\omega| > \omega_{EX}^{(2)}$ only one wave can be canceled immediately. It is however needed to cancel two waves to obtain a system that is solvable with the interface conditions. Two methods can be applied to determine which additional wave should be canceled. The first method is based on the fact that the radiation condition must hold which means that no energy may propagate from $x = \infty$ to the stiffness transition. The group velocity of each wave should thus be larger than zero. The dispersion curve in Figure 3.2 may now be used to determine that for $\omega > \omega_{EX}^{(n)}$ the wave number should be positive and negative for $\omega < \omega_{EX}^{(n)}$. In the second method a limit case of damping $c_w \to 0$ is added to the foundation which causes $z(\omega)$ to make a small rotation in the complex plane, and so do all its roots k_j. From Figure 4.3 it is observed that for $\omega < -\omega_{EX}^{(2)}$ the wave with the wave-number that was positive in Figure 3.1 should be canceled and the wave with the negative wave-number for $\omega > \omega_{EX}^{(2)}$. This result is equivalent with the first method. A similar approach is applied for the left domain. To obtain simple and single valued expressions definitions for two wave numbers are chosen. The first definition is

$$k_1^{(n)}(\omega) = |4\gamma_b^2\omega^2 - 4\beta_b^{(n)4}|^{1/4} \begin{cases} -1 & \omega < -\omega_{EX}^{(n)} \\ e^{\frac{3}{4}\pi i} & |\omega| < \omega_{EX}^{(n)} \\ 1 & \omega > \omega_{EX}^{(n)} \end{cases}, \tag{4.8}$$

and the second definition is

$$k_2^{(n)}(\omega) = |4\gamma_b^2\omega^2 - 4\beta_b^{(n)4}|^{1/4} \begin{cases} i & \omega < -\omega_{EX}^{(n)} \\ e^{\frac{1}{4}\pi i} & |\omega| < \omega_{EX}^{(n)} \\ i & \omega > \omega_{EX}^{(n)} \end{cases}. \tag{4.9}$$

By making use of this expression the homogeneous solution can be denoted as

$$\hat{w}_F^{(n)} = a_1^{(n)}(\omega)e^{(-1)^n k_1^{(n)} xi} + a_2^{(n)}(\omega)e^{(-1)^n k_2^{(n)} xi}. \tag{4.10}$$

Addition of the homogeneous and particular solution results in

$$\hat{w}^n = a_1^{(n)}(\omega)e^{(-1)^n k_1^{(n)} xi} + a_2^{(n)}(\omega)e^{(-1)^n k_2^{(n)} xi} + \frac{1}{\Delta_{EX}^{(n)}(\frac{\omega}{v},\omega)}\frac{\hat{F}}{v}e^{\frac{\omega}{v}xi}. \tag{4.11}$$

The constants $a_1^{(n)}$ and $a_2^{(n)}$ are obtained by application of the interface conditions at the stiffness jump. The expression in equation (4.10) confirms the expectation based on the thought experiment; The solution in both domains is indeed a summation of its eigenfield and a free field to guarantee the continuity at the stiffness transition.

In order to study radiation energy, the energy flux will be investigated. The expression for the energy flux $S^{(n)}(x,t)$ is denoted in equation (2.8). From this expression the outflow of energy from the system at the boundaries of $\Omega^{(1)}$ and $\Omega^{(2)}$ can be computed. For the left domain the interest lays in the energy propagation moving in negative x-direction and for the right domain the interest lays in the energy propagation moving in positive x-direction. The total energy that passes a cross section at $|x| \to \infty$ from $t \to -\infty$ to $t \to \infty$ is denoted by

$$E^{(n)} = (-1)^n EI \int_{-\infty}^{\infty} \lim_{x\to(-1)^n\infty}\left(\frac{\partial^3 w^{(n)}}{\partial x^3}\frac{\partial w^{(n)}}{\partial t} - \frac{\partial^2 w^{(n)}}{\partial x^2}\frac{\partial^2 w^{(n)}}{\partial t \partial x}\right)dt. \tag{4.12}$$

The transition radiation energy $E_r^{(n)}$ is denoted by that part of the total energy caused by the passing of the free field which means that

$$E_r^{(n)} = (-1)^n EI \int_{-\infty}^{\infty} \lim_{x\to(-1)^n\infty}\left(\frac{\partial^3 w_F^{(n)}}{\partial x^3}\frac{\partial w_F^{(n)}}{\partial t} - \frac{\partial^2 w_F^{(n)}}{\partial x^2}\frac{\partial^2 w_F^{(n)}}{\partial t \partial x}\right)dt. \tag{4.13}$$

The first step in computing this expression is to evaluate the inverse transform of to Fourier-domain transformed solution of the free field such that

$$w_f^{(n)} = \frac{1}{2\pi}\int_{-\infty}^{\infty} \hat{w}_f^{(n)} e^{-i\omega t} d\omega \tag{4.14}$$

Before substituting equation (4.14) into equation (4.13) it is important to note what happens with the solution when $|x| \to \infty$. Taking the limit of expression (4.10) yields

$$\lim_{x\to(-1)^n\infty}\left(\hat{w}^{(n)}\right) = \lim_{x\to(-1)^n\infty}\left(\frac{1}{2\pi}\int_{-\infty}^{\infty} a_1^{(n)}(\omega)e^{((-1)^n k_1^{(n)} x - \omega t)i} d\omega\right). \tag{4.15}$$

Note that the second term vanishes due to the definition in equation (4.9). The expression for the transition radiation can now be elaborated. This expression will consist of three integrals of which two can be computed relative easily due to the occurrence of the Fourier transform of a Dirac function. The result after some simplification steps is

$$E_r^{(n)} = \frac{EI}{2\pi}\int_{-\infty}^{\infty} \omega a_1^{(n)}(\omega)a_1^{(n)}(-\omega)\left(k_1^{(n)}(\omega)\right)^2\left(k_1^{(n)}(\omega) - k_1^{(n)}(-\omega)\right)e^{(-1)^n\left(k_1^{(n)}(\omega)-k_1^{(n)}(-\omega)\right)xi}d\omega. \tag{4.16}$$

The final step is to make use of expression (4.9). This results in the final expression for the radiation energy

$$E_r^{(2)} = \left(\frac{2EI}{\pi}\right)\int_{\omega_{EX}^{(n)}}^{\infty} \omega a_1^{(n)}(\omega)a_1^{(n)}(-\omega)\left(k_1^{(n)}(\omega)\right)^3 d\omega = \int_0^{\infty} Q^{(n)}(\omega)d\omega, \tag{4.17}$$

with $Q^{(n)}$ being the spectral density of the transition radiation energy in the direction corresponding to n. The expression for this spectral density for the inertia-excluded system reads

$$Q^{(n)} = \left[\left(\frac{2EI}{\pi}\right)\omega a_1^{(n)}(\omega)a_1^{(n)}(-\omega)\left(k_1^{(n)}(\omega)\right)^3\right]\left[H(\omega - \omega_{EX}^{(n)})\right]. \tag{4.18}$$

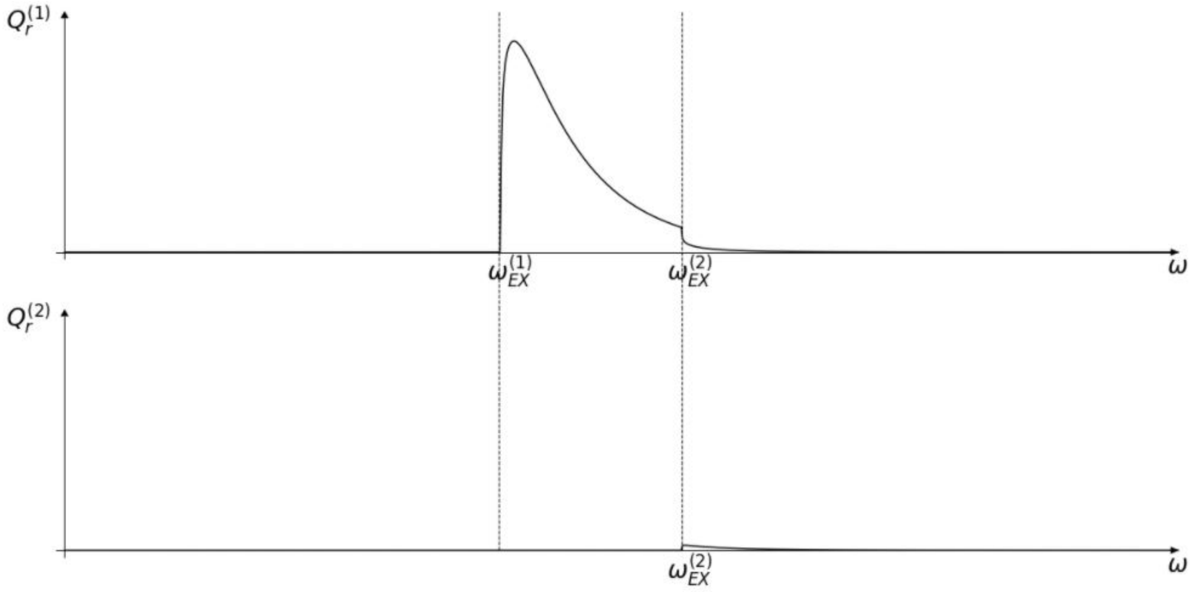

Figure 4.4: Spectra of radiation energy for the inertia-excluded model.

4.2. Transition radiation in the inertia included model

The same model as in equation (3.1) is studied, once again neglecting the damping. The stiffness parameter $k_s(x)$ of the lower elastic layer is however assumed to have a jump discontinuity in analogy with the previous subsection. The expressions for this stiffness parameter is

$$k_s(x) = k_s^{(1)} + \left(k_s^{(2)} - k_s^{(1)}\right) H(x). \tag{4.19}$$

The upper layer represent the pads which are fabricated and are therefore assumed to have constant stiffness properties. Like in the previous subsection the load velocity is assumed to be sub-critical. The governing equation of motion reads

$$\begin{bmatrix} \left(4\gamma_b^2 \frac{\partial^2}{\partial t^2} + 4\beta_p^4(x) + \frac{\partial^4}{\partial x^4}\right) & -\left(4\beta_p^4\right)(x) \\ -\left(4\beta_p^4\right)(x) & \left(4\gamma_s^2 \frac{\partial^2}{\partial t^2} + \left(4\beta_p^4(x) + 4\beta_s^4(x)\right)\right) \end{bmatrix} \begin{bmatrix} w \\ w_s \end{bmatrix} = \begin{bmatrix} \hat{F} \\ 0 \end{bmatrix} \delta(x - vt). \tag{4.20}$$

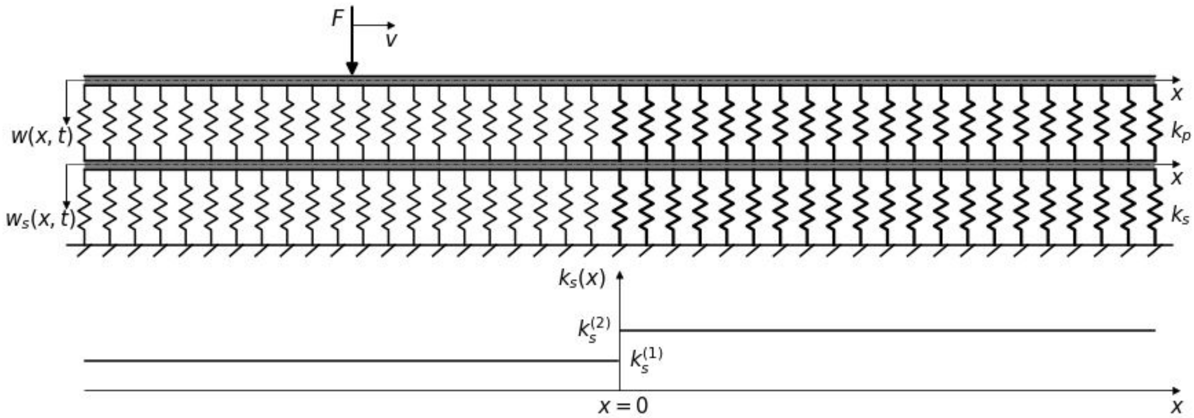

Figure 4.5: Mechanical scheme of a moving load in the inertia-included system with an abrupt jump in the foundation stiffness.

Fourier transforming this equation for the time variable results in

$$\begin{bmatrix} \left(\frac{\partial^4}{\partial x^4} - 4\gamma_b^2\omega^2 + 4\beta_p^4(x)\right) & -\left(4\beta_p^4(x)\right) \\ -\left(4\beta_p^4(x)\right) & \left(-4\gamma_s^2\omega^2 + \left(4\beta_p^4(x) + 4\beta_s^4(x)\right)\right) \end{bmatrix} \begin{bmatrix} \hat{w} \\ \hat{w}_s \end{bmatrix} = \frac{1}{v} \begin{bmatrix} \hat{F} \\ 0 \end{bmatrix} e^{\frac{\omega}{v} x i}. \tag{4.21}$$

The spatial domain is once again split into the two semi-infinite domains $\Omega^{(1)} = (-\infty, 0)$ and $\Omega^{(2)} = (0, \infty)$ with respective solution vectors $\mathbf{w}^{(1)} = \begin{bmatrix} w^{(1)} & w_s^{(1)} \end{bmatrix}^T$ and $\mathbf{w}^{(2)} = \begin{bmatrix} w^{(2)} & w_s^{(2)} \end{bmatrix}^T$. The governing system of differential equations of the Fourier transforms of these solution vectors with respect to the time variable t is

$$\begin{bmatrix} \left(\frac{\partial^4}{\partial x^4} - 4\gamma_b^2\omega^2 + 4\beta_p^{(n)4}\right) & -\left(4\beta_p^{(n)4}\right) \\ -\left(4\beta_p^{(n)4}\right) & \left(-4\gamma_s^2\omega^2 + \left(4\beta_p^{(n)4} + 4\beta_s^{(n)4}\right)\right) \end{bmatrix} \begin{bmatrix} \hat{w}^{(n)} \\ \hat{w}_s^{(n)} \end{bmatrix} = \frac{1}{v} \begin{bmatrix} \hat{F} \\ 0 \end{bmatrix} e^{\frac{\omega}{v}xi}. \tag{4.22}$$

The goal of this section is to obtain the expression for the spectral density of the transition radiation for the inertia-included system. In the previous section it can be seen that these expressions are obtained by making use of the expression for the energy flux. It has been discussed in Chapter 2 that the expression for the energy flux of both the inertia-included and excluded system are only dependent on the displacement of the Euler-Bernoulli beam. Therefore only the displacement of the upper beam is of interest. The particular solution for this beam can be obtained easily and reads

$$\hat{w}_E^{(n)} = \frac{\left(-4\gamma_s^2\omega^2 + 4\beta_p^{(n)4} + 4\beta_s^{(n)4}\right)}{\Delta_{IN}^{(n)}(\frac{\omega}{v}, \omega)} \frac{\hat{F}}{v} e^{\frac{\omega}{v}xi}. \tag{4.23}$$

For the free field the suggested trial solution is

$$\begin{bmatrix} \hat{w}_F^{(n)} \\ \hat{w}_{s\,F}^{(n)} \end{bmatrix} = \begin{bmatrix} a^{(n)}(\omega) \\ b^{(n)}(\omega) \end{bmatrix} e^{k(\omega)xi}. \tag{4.24}$$

Substitution of this trial solution vector in the homogeneous version of equation (4.22) will lead to the fact that the dispersion equation of equation (3.29) needs to be satisfied in order to obtain non-trivial solutions. Like in the case with the inertia-excluded system four distinct wave-numbers $k_j(\omega)$ can be obtained for each frequency ω. The solution for the free field of the Euler-Bernoulli beam is thus of the form

$$\hat{w}_F^{(n)} = a_1^{(n)}(\omega)e^{k_1^{(n)}(\omega)xi} + a_2(\omega)e^{k_2^{(n)}(\omega)xi} + a_3(\omega)e^{k_3^{(n)}(\omega)xi} + a_4(\omega)e^{k_4^{(n)}(\omega)xi}. \tag{4.25}$$

In order to cancel two waves for each sub-domain the same method as in the previous section is applied. One should however pay special attention to the application because there are now two pairs of dispersion curves, see Figure 3.8. By accounting for the different frequency bands of equation (3.35) correctly it is justified to conclude that

$$\hat{w}_F^{(n)} = a_1^{(n)}(\omega)e^{(-1)^n k_1^{(n)}xi} + a_2^{(n)}(\omega)e^{(-1)^n k_2^{(n)}xi}. \tag{4.26}$$

This expression looks similar to that of equation (4.10) but the definitions for the two present wave-numbers have changed because of the frequency bands. The first definition is

$$k_1^{(n)}(\omega) = |z^{(n)}(\omega)|^{1/4} \begin{cases} -1 & \omega < -\omega_{IN2}^{(n)} \\ e^{\frac{3}{4}\pi i} & \omega_{IN2}^{(n)} < \omega < -\omega_{SI}^{(n)} \\ -1 & -\omega_{SI}^{(n)} < \omega < -\omega_{IN1}^{(n)} \\ e^{\frac{3}{4}\pi i} & |\omega| < \omega_{IN1}^{(n)} \\ 1 & \omega_{IN1}^{(n)} < \omega < \omega_{SI}^{(n)} \\ e^{\frac{3}{4}\pi i} & \omega_{SI}^{(n)} < \omega < \omega_{IN2}^{(n)} \\ 1 & \omega > \omega_{IN2}^{(n)} \end{cases}, \tag{4.27}$$

and the second definition is

$$k_2^{(n)}(\omega) = |z^{(n)}(\omega)|^{1/4} \begin{cases} i & \omega < -\omega_{IN2}^{(n)} \\ e^{\frac{1}{4}\pi i} & \omega_{IN2}^{(n)} < \omega < -\omega_{SI}^{(n)} \\ i & -\omega_{SI}^{(n)} < \omega < -\omega_{IN1}^{(n)} \\ e^{\frac{1}{4}\pi i} & |\omega| < \omega_{IN1}^{(n)} \\ i & \omega_{IN1}^{(n)} < \omega < \omega_{SI}^{(n)} \\ e^{\frac{1}{4}\pi i} & \omega_{SI}^{(n)} < \omega < \omega_{IN2}^{(n)} \\ i & \omega > \omega_{IN2}^{(n)} \end{cases}. \tag{4.28}$$

Addition of the homogeneous and particular solutions results in

$$\hat{w}^n = a_1^{(n)}(\omega)e^{(-1)^n k_1^{(n)} xi} + a_2^{(n)}(\omega)e^{(-1)^n k_2^{(n)} xi} + \frac{\left(-4\gamma_s^2\omega^2 + 4\beta_p^{(n)4} + 4\beta_s^{(n)4}\right)}{\Delta_{IN}^{(n)}(\frac{\omega}{v},\omega)}\frac{\hat{F}}{v}e^{\frac{\omega}{v}xi}. \tag{4.29}$$

The unknown constants can be obtained from the continuity of the beam in displacement, slope, bending moment and shear force at the point of the stiffness transition. In order to obtain the expressions for the spectral density of transition radiation energy the same steps as those on page 28 have been followed, resulting in the same expressions. A difference in the derivation is however due to the definitions of the two wave-numbers. The final expression for the spectral density for the inertia-included system reads

$$Q^{(n)}(\omega) = \left[\left(\frac{2EI}{\pi}\right)\omega a_1^{(n)}(\omega)a_1^{(n)}(-\omega)\left(k_1^{(n)}(\omega)\right)^3\right]\left[H(\omega-\omega_{IN1}^{(n)}) - H(\omega-\omega_{SI}^{(n)}) + H(\omega-\omega_{IN2}^{(n)})\right]. \tag{4.30}$$

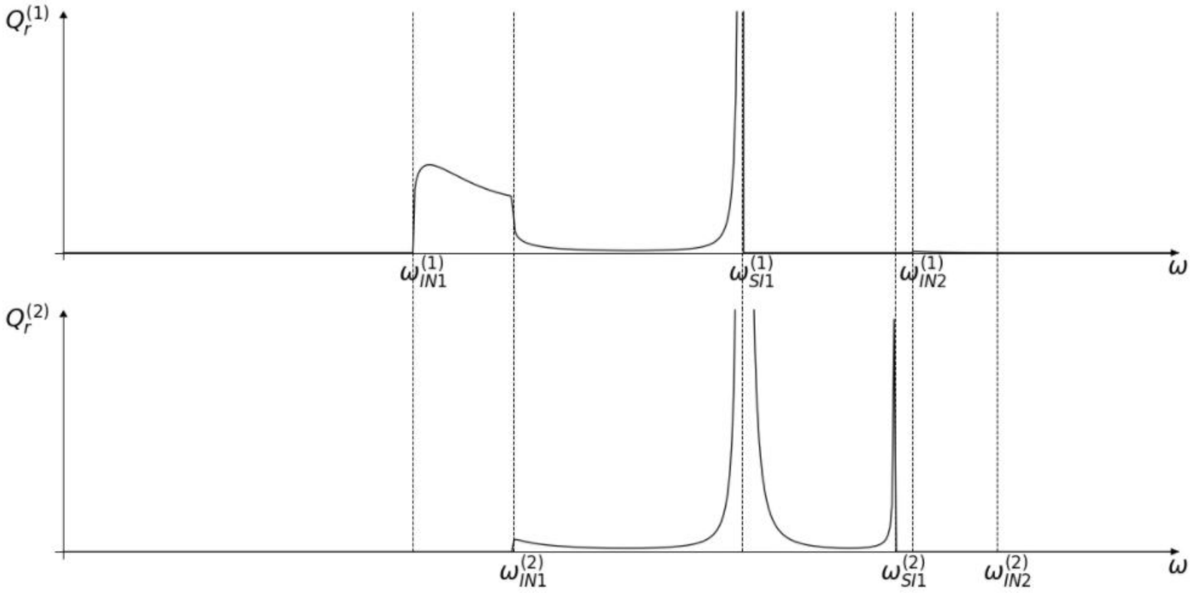

Figure 4.6: Spectra of radiation energy for the inertia-included model.

An important difference between the spectra for the inertia-excluded and included model is the occurrence of infinite peaks. These peaks are located at those frequencies corresponding to the intersection points between the kinematic invariant and dispersion curves. Recall that the kinematic invariant has no intersection points with the dispersion curves of the inertia-excluded system for sub-critical velocities. For the inertia-included model however there are always at least two intersection points between the kinematic invariant and the dispersion curves. The two frequencies have the same value except for their signs, one is negative and one is positive. As mentioned previously, the two waves corresponding to these two frequencies propagate in the eigenfield on the left side of the load. In this case of a transition zone a left and a right eigenfield are present. These eigenfields are not the same which means that there would be a discontinuity at the transition point when the total solution would only exist of the eigenfields. Free fields are therefore added to ensure continuity at the transition point. The expressions for the free fields are substituted into the interface conditions together with the already determined eigenfields. The two propagating waves present in an eigenfield behave as a simple harmonic time function at the transition point. There is thus a left and a right harmonic time function with each its respective frequency, one for each eigenfield. The free fields need to be such that addition of them leads to a total solution which is continuous for all time. This explains the presence of peaks in the spectra of radiation energy for the inertia-included model and the absence of them in the inertia-excluded model. From Fig 4.6 it can be observed that only one peak is present in the spectrum for the left domain. This is because the other frequency happens to be outside the band of wave propagation.

5

Numerical model

A numerical model is formulated to solve the transient solutions of the problems in this thesis. In this model any type of local inhomogeneity can be applied. In the applied technique the spatial dimension is discretized by application of the finite element method This results in a system of ordinary differential equations which can be solved by the Newmark-beta method.

5.1. Finite element method

5.1.1. Spatial discretization for the inertia-excluded model

The general equation of motion for a Winkler supported Euler-Bernoulli beam on a domain $\Omega = (x_a, x_b)$ without damping is denoted by

$$\rho A \frac{\partial^2 w}{\partial t^2} + EI \frac{\partial^4 w}{\partial x^4} + kw = q, \quad x \in \Omega. \tag{5.1}$$

The first step in the finite element method is the derivation of the weak formulation. To do this, multiply equation (5.1) by an arbitrary test function $\eta \in \Sigma$ and integrate over the domain Ω, such that

$$\int_{x_a}^{x_b} \rho A \eta \frac{\partial^2 w}{\partial t^2} + EI \eta \frac{\partial^4 w}{\partial x^4} + k \eta w dx = \int_{x_a}^{x_b} \eta q dx, \quad \forall \eta \in \Sigma. \tag{5.2}$$

Note that Σ is the space of functions that satisfies certain requirements. An important requirement on the space Σ is that if essential boundary conditions are present, functions η satisfy the same but homogeneous essential boundary conditions as w. In that case the function space is denoted by Σ_0. If no essential boundary conditions are present, the function space is just denoted by Σ and the functions η do not need to satisfy any specified boundary conditions. Another important requirement on the functions $\eta \in \Sigma$ is that they should be sufficiently smooth which will be explained further on. The difference between essential and natural boundary conditions of the Euler-Bernoulli equation shall also be explained further on. The second term in the right hand side of equation (5.2) is integrated by parts twice to lower the order of the derivatives that occur in the weak form. This is done so that smoothness requirement for the function space Σ becomes less strict, the result is

$$\int_{x_a}^{x_b} \rho A \eta \frac{\partial^2 w}{\partial t^2} dx + \int_{x_a}^{x_b} \left(EI \frac{d^2 \eta}{dx^2} \frac{d^2 w}{dx^2} + \eta k w \right) dx = \int_{x_a}^{x_b} \eta q dx + \left[\eta V - \frac{d\eta}{dx} M \right]_{x_a}^{x_b}, \quad \forall \eta \in \Sigma. \tag{5.3}$$

From equation (5.3) it becomes clear that the boundary conditions for the moments and shear forces occur naturally in the weak form and are thus automatically taken care of. These boundary conditions are therefore called natural or Neumann boundary conditions. The strong form of the problem in (5.1) however contained a spatial derivative of the fourth order which means that there is a possibility of four different types of boundary conditions. Two of the four types boundary conditions are satisfied naturally in the weak formulation. The other two types of boundary conditions, which are the displacement and slope, need to be demanded and are therefore called essential or Dirichlet boundary conditions.

The solution is now approximated by a linear combination of finite fixed set of basis functions $\Phi_i(x)$. In the Galerkin method the same linear combination is chosen for η, such that

$$\begin{aligned} w(x,t) \approx w^h(x,t) &= \sum_{j=0}^{m} u_j(t)\Phi_j(x), \quad \Phi_j \in \Sigma \\ \eta(x) &= \sum_{i=0}^{m} c_i \Phi_i(x), \quad \Phi_i \in \Sigma_{(0)} \end{aligned} . \tag{5.4}$$

Substitution of equation (5.4) in equation (5.3) leads to

$$\sum_{i=0}^{m}\left[\sum_{j=0}^{m}\left\{\left(\int_{x_a}^{x_b}\rho A\Phi_i\Phi_j dx\right)\frac{d^2u_j}{dt^2}+\left(\int_{x_a}^{x_b}EI\frac{d^2\Phi_i}{dx^2}\frac{d^2\Phi_j}{dx^2}+k\Phi_i\Phi_j dx\right)u_j\right\}\right]c_i=\sum_{i=0}^{m}\left[\left(\int_{x_a}^{x_b}\Phi_i q dx\right)+\left[\Phi_i V-\frac{d\Phi_i}{dx}M\right]_{x_a}^{x_b}\right]c_i. \tag{5.5}$$

Because the number of elements n is arbitrary it can be concluded that

$$\sum_{j=0}^{m}\left\{\left(\int_{x_a}^{x_b}\rho A\Phi_i\Phi_j dx\right)\frac{d^2u_j}{dt^2}+\left(\int_{x_a}^{x_b}EI\frac{d^2\Phi_i}{dx^2}\frac{d^2\Phi_j}{dx^2}+k\Phi_i\Phi_j dx\right)u_j\right\}=\int_{x_a}^{x_b}\Phi_i q dx+\left[\Phi_i V-\frac{d\Phi_i}{dx}M\right]_{x_a}^{x_b}, \quad i=\{0,..,m\}. \tag{5.6}$$

This results in a system of ordinary differential equations which can be solved by a numerical time integration. Before that can be done one first needs to chose the basis functions Φ_i.

5.1.2. Hermite basis functions

In order for the integrals of equation (5.6) to make sense Σ needs to be a subspace of the Sobolev space $H^2(\Omega)$ [29], which contains functions satisfying

$$\int_{x_a}^{x_b} \Phi^2 + \frac{d\Phi}{dx}^2 + \frac{d^2\Phi}{dx^2}^2 \, dx < \infty. \tag{5.7}$$

This is equivalent to be at least C^1 continuous in one dimensional systems. This is the requirement that $\eta \in \Sigma$ should satisfy to be sufficiently smooth. It is thus needed to chose basis functions that ensure this continuity. The first thing to do is subdividing the domain Ω into n elements $e_k = [x_{k-1}, x_k]$. At each node x_i two degrees of freedom are introduced w_i and ϕ_i which are basically the displacement and cross-sectional rotation at the nodes. Hermitian interpolation is applied over the element boundaries to ensure the C^1 continuity. The interpolation per element can be written as

$$w^h(x) = \sum_{j=k-1}^{k} w_j\psi_{j0}(x) + \phi_j\psi_{j1}(x), \quad x \in e_k. \tag{5.8}$$

with $\psi_{i0}(x)$ and $\psi_{i1}(x)$ third degree polynomials, satisfying

$$\psi_{i0}(x_j) = \delta_{ij}, \quad \frac{d\psi_{i0}}{dx}(x_j) = 0, \quad \psi_{i1}(x_j) = 0 \quad \frac{d\psi_{i1}}{dx}(x_j) = -\delta_{ij}. \tag{5.9}$$

These basis functions $\psi_{i0}(x)$ and $\psi_{i1}(x)$ can be expressed in terms of linear basis functions $\lambda_i(x)$

$$\psi_{i0} = \lambda_i^2(3-2\lambda_i) \quad \text{and} \quad \psi_{i1} = \lambda_i^2(1-\lambda_i)\frac{1}{\frac{d\lambda_i}{dx}}. \tag{5.10}$$

The linear basis functions $\lambda_i(x)$ satisfy

$$\lambda_i(x_j) = \delta_{ij}. \tag{5.11}$$

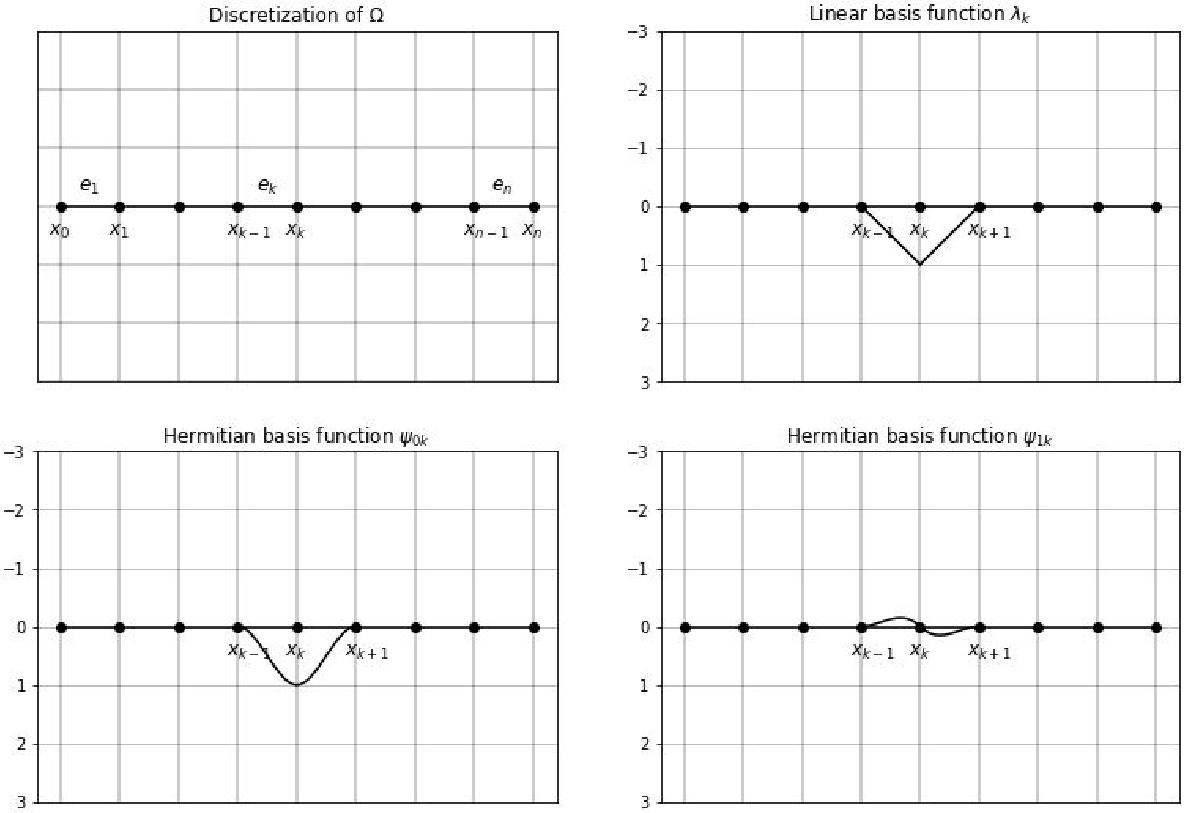

Figure 5.1: Field discretization and the definition of the basis functions.

Note that the parameters u_j in equation (5.4) are either w_j or ϕ_j and the functions Φ_j are either $\psi_{j0}(x)$ and $\psi_{j1}(x)$. Because of this the system of equations in equation (5.6) can be written as

$$
\begin{aligned}
&\sum_{j=0}^{n}\left\{\left(\int_{x_a}^{x_b}\rho A\psi_{i0}\psi_{j0}dx\right)\frac{d^2w_j}{dt^2}+\left(\int_{x_a}^{x_b}EI\frac{d^2\psi_{i0}}{dx^2}\frac{d^2\psi_{j0}}{dx^2}+k\psi_{i0}\psi_{j0}dx\right)w_j\right\}+\\
&\sum_{j=0}^{n}\left\{\left(\int_{x_a}^{x_b}\rho A\psi_{i0}\psi_{j1}dx\right)\frac{d^2\phi_j}{dt^2}+\left(\int_{x_a}^{x_b}EI\frac{d^2\psi_{i0}}{dx^2}\frac{d^2\psi_{j1}}{dx^2}+k\psi_{i0}\psi_{j1}dx\right)\phi_j\right\}=\int_{x_a}^{x_b}\psi_{i0}q\,dx+\Big[\psi_{i0}V\Big]_{x_a}^{x_b},i=\{0,..,n\}\\
&\sum_{j=0}^{n}\left\{\left(\int_{x_a}^{x_b}\rho A\psi_{i1}\psi_{j0}dx\right)\frac{d^2w_j}{dt^2}+\left(\int_{x_a}^{x_b}EI\frac{d^2\psi_{i1}}{dx^2}\frac{d^2\psi_{j0}}{dx^2}+k\psi_{i1}\psi_{j0}dx\right)w_j\right\}+\\
&\sum_{j=0}^{n}\left\{\left(\int_{x_a}^{x_b}\rho A\psi_{i1}\psi_{j1}dx\right)\frac{d^2\phi_j}{dt^2}+\left(\int_{x_a}^{x_b}EI\frac{d^2\psi_{i1}}{dx^2}\frac{d^2\psi_{j1}}{dx^2}+k\psi_{i1}\psi_{j1}dx\right)\phi_j\right\}=\int_{x_a}^{x_b}\psi_{i1}q\,dx-\left[\frac{d\psi_{i1}}{dx}M\right]_{x_a}^{x_b},i=\{0,..,n\}.
\end{aligned}
\tag{5.12}
$$

This system of ordinary differential equations can be written as

$$\mathbf{M}\ddot{\mathbf{w}}+\mathbf{K}\mathbf{w}=\mathbf{f}. \tag{5.13}$$

The matrix $\mathbf{M}$ is called the global mass matrix and it is the discrete representation of the inertia of the beam. The matrix $\mathbf{K}$ is called the global stiffness matrix and it is the discrete representation of the stiffness of the system and it is composed of the bending stiffness and the stiffness of the Winkler foundation. The vector $\mathbf{f}$ is the discrete representation of the load on the beam.

5.1.3. Assembly and definition of element matrices and vectors for the inertia-excluded system

The final system of equations denoted in equation (5.13) that needs to be solved has been determined by making use of the weak form in which a discretized displacement field over all elements has been substituted. The procedure after that existed of straightforward mathematical steps. This procedure included lots of cumbersome summations. The power of the finite element method however lies in the fact that there can be made use of just one element to obtain a system that holds for that element. After this is done an assembly follows which assembles all the element systems to one large system which is the same as that of equation (5.13). This procedure exist of matrices and vectors instead if summations. The displacement field for one element e_1 is denoted by

$$w(x,t) \approx w^m(x,t) = w_0\psi_{00} + \phi_0\psi_{01} + w_1\psi_{10} + \phi_1\psi_{11}. \tag{5.14}$$

This can be put in a matrix vector notation by introducing the $\mathbf{N}$ matrix and the element degree of freedom vector $\mathbf{a}^e$, resulting in

$$w(x,t) \approx w^m(x,t) = \begin{bmatrix}\psi_{00} & \psi_{01} & \psi_{10} & \psi_{11}\end{bmatrix}\begin{bmatrix}w_0\\ \phi_0\\ w_1\\ \phi_1\end{bmatrix} = \mathbf{N}\mathbf{a}^e. \tag{5.15}$$

This is also done for the test function, yielding

$$\eta(x) = \mathbf{N}\mathbf{b}^e. \tag{5.16}$$

Note that the test function is a scalar field such that its inverse is the same as the weight function itself, such that

$$\eta(x) = (\eta(x))^T = (\mathbf{N}\mathbf{b}^e)^T = (\mathbf{b}^e)^T\mathbf{N}^T. \tag{5.17}$$

Substitution of these expressions in the weak form results in

$$(\mathbf{b}^e)^T\left(\left(\int_e \mathbf{N}^T\rho A\mathbf{N}dx\right)\ddot{\mathbf{a}}^e + \left(\int_e \frac{d^2\mathbf{N}^T}{dx^2}EI\frac{d^2\mathbf{N}}{dx^2} + \mathbf{N}^T k\mathbf{N}dx\right)\mathbf{a}^e\right) = (\mathbf{b}^e)^T\left(\int_e \mathbf{N}^T q dx + \left[\mathbf{N}^T - \frac{d\mathbf{N}}{dx}M\right]_{x_a}^{x_b}\right), \tag{5.18}$$

from which it can be concluded that

$$\left(\int_e \mathbf{N}^T\rho A\mathbf{N}dx\right)\ddot{\mathbf{a}}^e + \left(\int_e \frac{d^2\mathbf{N}^T}{dx^2}EI\frac{d^2\mathbf{N}}{dx^2} + \mathbf{N}^T k\mathbf{N}dx\right)\mathbf{a}^e = \int_e \mathbf{N}^T q dx + \left[\mathbf{N}^T - \frac{d\mathbf{N}}{dx}M\right]_{x_a}^{x_b}. \tag{5.19}$$

This system can be written at element level, such that

$$\mathbf{M}^e\ddot{\mathbf{a}}^e + \mathbf{K}^e\mathbf{a}^e = \mathbf{f}^e. \tag{5.20}$$

The matrices and vectors in this expression are called element matrices and vectors. The element matrices and vectors for all elements in the system are assembled afterwards in order to obtain the global matrices and vectors. The first step is to design the degree of freedom vector $\mathbf{w}$ which is simply a vector filled with all nodal degree of freedom. In the case of a system that exists of two element this is simply

$$\mathbf{w} = \begin{bmatrix}w_0 & \phi_0 & w_1 & \phi_1 & w_2 & \phi_2\end{bmatrix}^T. \tag{5.21}$$

The second step is to obtain the force vector which contains the total nodal forces due to the external load along the beam and due to the boundary conditions. The two element force vectors which contain the nodal forces due to the contributions of the concerned elements only are then defined as

$$\begin{aligned}\mathbf{f}^{e_1} &= \begin{bmatrix}F_{01} & T_{01} & F_{11} & T_{11}\end{bmatrix}^T\\ \mathbf{f}^{e_2} &= \begin{bmatrix}F_{12} & T_{12} & F_{22} & T_{22}\end{bmatrix}^T.\end{aligned} \tag{5.22}$$

The force vector can then be assembled by adding the nodal forces of the element force vectors at those location where there is overlap such that

$$\mathbf{f} = \begin{bmatrix}F_0 & T_0 & F_1 & T_1 & F_2 & T_2\end{bmatrix}^T = \begin{bmatrix}F_{01} & T_{01} & (F_{11}+F_{12}) & (T_{11}+T_{12}) & F_{22} & T_{22}\end{bmatrix}^T. \tag{5.23}$$

The final system has the form

$$\mathbf{M}\ddot{\mathbf{a}} + \mathbf{K}\mathbf{w} = \mathbf{f}. \tag{5.24}$$

In order for this system to make sense the dimensions of both the mass and stiffness matrices need to be six by six in the case of two elements. Because the nodal forces of the zeroth node are independent of the degrees of freedom of the second node one easily sees that the first two rows of the mass matrix exist of the first two of the first mass element matrix, the remaining terms are zero. A similar reasoning can be applied to the last two rows and the second element matrix. For the middle two rows it holds that both element matrices have a contribution and that overlapping terms are used twice. This results in the global mass matrix

$$\mathbf{M} = \begin{bmatrix} M_{11}^{e_1} & M_{12}^{e_1} & M_{13}^{e_1} & M_{14}^{e_1} & 0 & 0 \\ M_{21}^{e_1} & M_{22}^{e_1} & M_{23}^{e_1} & M_{24}^{e_1} & 0 & 0 \\ M_{31}^{e_1} & M_{32}^{e_1} & (M_{33}^{e_1} + M_{11}^{e_2}) & (M_{34}^{e_1} + M_{12}^{e_2}) & M_{13}^{e_2} & M_{14}^{e_2} \\ M_{41}^{e_1} & M_{42}^{e_1} & (M_{43}^{e_1} + M_{21}^{e_2}) & (M_{44}^{e_1} + M_{22}^{e_2}) & M_{23}^{e_2} & M_{24}^{e_2} \\ 0 & 0 & M_{31}^{e_2} & M_{32}^{e_2} & M_{33}^{e_2} & M_{34}^{e_2} \\ 0 & 0 & M_{41}^{e_2} & M_{42}^{e_2} & M_{43}^{e_2} & M_{44}^{e_2} \end{bmatrix}. \tag{5.25}$$

The same rules can be applied to the stiffness matrix. This process of combining element matrices and vector into the global system is called assembly and can be extended to an arbitrary number of elements.

5.1.4. Application to the inertia-included model

The finite element method or more specifically the Galerkin method [24] will now be applied for the inertia-included model. This involves: find $w^h \in \Sigma_w^h$ and $u^h \in \Sigma_u^h$ such that

$$\begin{gathered} \int_e \overline{w}^h \rho_b \frac{\partial^2 w^h}{\partial t^2} dx + \int_e \frac{\partial^2 \overline{w}^h}{\partial x^2} EI \frac{\partial^2 w^h}{\partial x^2} + \overline{w}^h k_p w^h dx - \int_e \overline{w}^h k_p w_s^h dx = \int_e \overline{w}^h q dx + \left[\overline{w}^h V - \frac{\partial \overline{w}^h}{\partial x} M \right]_{x_a}^{x_b} \\ \int_e \overline{w_s}^h \rho_s \frac{\partial^2 w_s^h}{\partial t^2} dx - \int_e \overline{w_s}^h k_p w_s^h dx + \int_e \overline{w_s}^h (k_p + k_s) w_s^h dx = 0 \end{gathered} \tag{5.26}$$

The discretized fields read

$$w^h = \mathbf{N}_w \mathbf{a}_w^e, \quad \overline{w}^h = \mathbf{N}_w \mathbf{b}_w^e, \quad w_s^h = \mathbf{N}_{w_s} \mathbf{a}_{w_s}^e \quad \text{and} \quad \overline{w_s}^h = \mathbf{N}_{w_s} \mathbf{b}_{w_s}^e. \tag{5.27}$$

Substitution of these expressions in equation (5.26) results in the set of equations

$$\begin{gathered} \left(\int_e \mathbf{N}_w^T \rho_b \mathbf{N}_w dx \right) \ddot{\mathbf{a}}_w^e + \left(\int_e \frac{\partial^2 \mathbf{N}_w^T}{\partial x^2} EI \frac{\partial^2 \mathbf{N}_w}{\partial x^2} + \mathbf{N}_w^T k_p \mathbf{N}_w dx \right) \mathbf{a}_w^e - \left(\int_e \mathbf{N}_w^T k_p \mathbf{N}_{w_s} dx \right) \mathbf{a}_{w_s}^e = \left(\int_e \mathbf{N}_w^T q dx \right) + \left[\mathbf{N}_w^T V - \frac{\partial \mathbf{N}_w}{\partial x} M \right]_{x_a}^{x_b} \\ \left(\int_e \mathbf{N}_{w_s}^T \rho_s \mathbf{N}_{w_s} dx \right) \ddot{\mathbf{a}}_{w_s}^e - \left(\int_e \mathbf{N}_{w_s}^T k_p \mathbf{N}_w dx \right) \mathbf{a}_w^e + \left(\int_e \mathbf{N}_{w_s}^T (k_p + k_s) \mathbf{N}_{w_s} dx \right) \mathbf{a}_{w_s}^e = 0, \end{gathered} \tag{5.28}$$

which can be written as

$$\begin{bmatrix} \mathbf{M}_{ww} & \emptyset \\ \emptyset & \mathbf{M}_{w_s w_s} \end{bmatrix} \begin{bmatrix} \ddot{\mathbf{a}}_w^e \\ \ddot{\mathbf{a}}_{w_s}^e \end{bmatrix} + \begin{bmatrix} \mathbf{K}_{ww} & \mathbf{K}_{w w_s} \\ \mathbf{K}_{w_s w} & \mathbf{K}_{w_s w_s} \end{bmatrix} \begin{bmatrix} \mathbf{a}_w^e \\ \mathbf{a}_{w_s}^e \end{bmatrix} = \begin{bmatrix} \mathbf{f}_q^e \\ \emptyset \end{bmatrix} + \begin{bmatrix} \mathbf{f}_{nc}^e \\ \emptyset \end{bmatrix}. \tag{5.29}$$

This expression denotes a system of linear differential equations for one element. In order to obtain a system for the entire beam there needs to be assembly of all element matrices and vectors. The current order of the element matrices and vectors is not optimal for this assembly.

To obtain an optimal orientation a re-ordering needs to take place. This re-ordering is shown for the stiffness matrix, the degree of freedom vector and the force vector. The element stiffness matrix multiplication with the degree of freedom vector initially has the form

$$\begin{bmatrix} \mathbf{K}_{ww} & \mathbf{K}_{ww_s} \\ \mathbf{K}_{w_sw} & \mathbf{K}_{w_sw_s} \end{bmatrix} \begin{bmatrix} \mathbf{a}_w^e \\ \mathbf{a}_{w_s}^e \end{bmatrix} = \begin{bmatrix} (K_{ww})_{11} & (K_{ww})_{12} & (K_{ww})_{13} & (K_{ww})_{14} & (K_{ww_s})_{11} & (K_{ww_s})_{12} \\ (K_{ww})_{21} & (K_{ww})_{22} & (K_{ww})_{23} & (K_{ww})_{24} & (K_{ww_s})_{21} & (K_{ww_s})_{22} \\ (K_{ww})_{31} & (K_{ww})_{32} & (K_{ww})_{33} & (K_{ww})_{34} & (K_{ww_s})_{31} & (K_{ww_s})_{32} \\ (K_{ww})_{41} & (K_{ww})_{42} & (K_{ww})_{43} & (K_{ww})_{44} & (K_{ww_s})_{41} & (K_{ww_s})_{42} \\ (K_{w_sw})_{11} & (K_{w_sw})_{12} & (K_{w_sw})_{13} & (K_{w_sw})_{14} & (K_{w_sw_s})_{11} & (K_{w_sw_s})_{12} \\ (K_{w_sw})_{21} & (K_{w_sw})_{22} & (K_{w_sw})_{23} & (K_{w_sw})_{24} & (K_{w_sw_s})_{21} & (K_{w_sw_s})_{22} \end{bmatrix} \begin{bmatrix} w_{k-1} \\ \phi_{k-1} \\ w_k \\ \phi_k \\ (w_s)_{k-1} \\ (w_s)_k \end{bmatrix}. \tag{5.30}$$

The degree of freedom vector is re-ordered such that

$$\mathbf{a}^e = \begin{bmatrix} w_{k-1} & \phi_{k-1} & (w_s)_{k-1} & w_k & \phi_k & (w_s)_k \end{bmatrix}^T. \tag{5.31}$$

The order of the elements in the degree of freedom vector has changed but the multiplication of the element stiffness matrix and the degree of freedom vector needs to be unchanged. In order to do that the element stiffness matrix also needs to be re-ordered, such that

$$\begin{bmatrix} \mathbf{K}_{ww} & \mathbf{K}_{ww_s} \\ \mathbf{K}_{w_sw} & \mathbf{K}_{w_sw_s} \end{bmatrix} \begin{bmatrix} \mathbf{a}_w^e \\ \mathbf{a}_{w_s}^e \end{bmatrix} = \begin{bmatrix} (K_{ww})_{11} & (K_{ww})_{12} & (K_{ww_s})_{11} & (K_{ww})_{13} & (K_{ww})_{14} & (K_{ww_s})_{12} \\ (K_{ww})_{21} & (K_{ww})_{22} & (K_{ww_s})_{21} & (K_{ww})_{23} & (K_{ww})_{24} & (K_{ww_s})_{22} \\ (K_{ww})_{31} & (K_{ww})_{32} & (K_{ww_s})_{31} & (K_{ww})_{33} & (K_{ww})_{34} & (K_{ww_s})_{32} \\ (K_{ww})_{41} & (K_{ww})_{42} & (K_{ww_s})_{41} & (K_{ww})_{43} & (K_{ww})_{44} & (K_{ww_s})_{42} \\ (K_{w_sw})_{11} & (K_{w_sw})_{12} & (K_{w_sw_s})_{11} & (K_{w_sw})_{13} & (K_{w_sw})_{14} & (K_{w_sw_s})_{12} \\ (K_{w_sw})_{21} & (K_{w_sw})_{22} & (K_{w_sw_s})_{21} & (K_{w_sw})_{23} & (K_{w_sw})_{24} & (K_{w_sw_s})_{22} \end{bmatrix} \begin{bmatrix} w_{k-1} \\ \phi_{k-1} \\ (w_s)_{k-1} \\ w_k \\ \phi_k \\ (w_s)_k \end{bmatrix}. \tag{5.32}$$

The matrix and vector in the left hand side of the equation are not the same as that of the right hand side. The vector that follows from the multiplication of the two objects are however the same in both sides of the equation which justifies the equal sign. The main goal of this re-ordering is to simplify the assembly of the element vectors and matrices. The degree of freedom vector is already re-ordered but the force vector not yet. The re-ordering of the force-vector is denoted as

$$\begin{bmatrix} \mathbf{f} \\ \emptyset \end{bmatrix} = \begin{bmatrix} f_1 \\ f_2 \\ f_3 \\ f_4 \\ 0 \\ 0 \end{bmatrix} \rightarrow \mathbf{f}^e = \begin{bmatrix} f_1 \\ f_2 \\ 0 \\ f_3 \\ f_4 \\ 0 \end{bmatrix}. \tag{5.33}$$

This re-ordering imposes an additional change to the element stiffness matrix which results in

$$\begin{bmatrix} \mathbf{K}_{ww} & \mathbf{K}_{ww_s} \\ \mathbf{K}_{w_sw} & \mathbf{K}_{w_sw_s} \end{bmatrix} \rightarrow \mathbf{K}^e = \begin{bmatrix} (K_{ww})_{11} & (K_{ww})_{12} & (K_{ww_s})_{11} & (K_{ww})_{13} & (K_{ww})_{14} & (K_{ww_s})_{12} \\ (K_{ww})_{21} & (K_{ww})_{22} & (K_{ww_s})_{21} & (K_{ww})_{23} & (K_{ww})_{24} & (K_{ww_s})_{22} \\ (K_{w_sw})_{11} & (K_{w_sw})_{12} & (K_{w_sw_s})_{11} & (K_{w_sw})_{13} & (K_{w_sw})_{14} & (K_{w_sw_s})_{12} \\ (K_{ww})_{31} & (K_{ww})_{32} & (K_{ww_s})_{31} & (K_{ww})_{33} & (K_{ww})_{34} & (K_{ww_s})_{32} \\ (K_{ww})_{41} & (K_{ww})_{42} & (K_{ww_s})_{41} & (K_{ww})_{43} & (K_{ww})_{44} & (K_{ww_s})_{42} \\ (K_{w_sw})_{21} & (K_{w_sw})_{22} & (K_{w_sw_s})_{21} & (K_{w_sw})_{23} & (K_{w_sw})_{24} & (K_{w_sw_s})_{22} \end{bmatrix}. \tag{5.34}$$

The transformation of the element stiffness matrix is completed and that of the element mass matrix is similar. The element matrices and vectors can now be assembled according to the same systematic approach that has been used for the inertia-excluded model.

5.1.5. Gauss integration

In the cases that the physical quantities are not constant over the length of the beam it is needed to approximate the integrals in the element matrices and vector. One could argue that these could also be computed analytically which is true in some cases but in order to make the process as efficient as possible it is favourable to have a type of quadrature that computes these integrals for each element according to a set rule. This especially holds for a system that exist of a large number of elements. The quadrature that will be used is the Gauss integration technique. The integrals that occur in the finite element method are integrals over an arbitrary element $e_k = [x_{k-1}, x_k]$ and thus have the following form

$$I = \int_{x_{k-1}}^{x_k} f(x)dx \tag{5.35}$$

In models that deal with multi-dimensional elements it is cumbersome to compute the integrals over each element individually. Isoparametric mapping is a method in which a base element is introduced with useful properties. This base element is then used to compute the integrals over an arbitrary element by making use of the Jacobian of the transformation that maps the base element into an arbitrary element. Applying this method to a one dimensional problem is the same as applying a substituion. The base element is a one-dimensional element in the ξ-space that spans from -1 to 1 such that $e_b = [-1, 1]$. The transformation that maps this base element e_b from the ξ-space into an arbitrary element e_k in the x-space is

$$x = \frac{1}{2}(1-\xi)x_{k-1} + \frac{1}{2}(1+\xi)x_k \tag{5.36}$$

The Jacobian of this transformation is given by

$$J = \frac{1}{2}(x_k - x_{k-1}) = \frac{1}{2}h_k \tag{5.37}$$

The integral over an arbitrary element can thus be computed by an integral over the base element by making use of the introduced transformation such that

$$I = \frac{1}{2}h_k \int_{-1}^{1} f(\xi)d\xi \tag{5.38}$$

The remaining integral is now approximated by making use of integration points ξ_i. The function value f_i at the these integration points are determined, then multiplied by their weights W_i after which all these products are summed for the total number of integration points n such that

$$I \approx \frac{1}{2}h_k \left(\sum_{i=1}^{n} f_i W_i \right) \tag{5.39}$$

In the Gauss quadrature the integration points and the weights are chosen such that a scheme with n integration points integrates a polynomial of degree $2n-1$ exactly.

5.2. Non reflective boundary conditions

In this subsection non-reflective boundary conditions will be derived in order to model the infinite system behaviour by a finite model. The first step is to divide the infinite system into a left semi-infinite system for $x < x_a$, a computational zone for $x \in (x_a, x_b)$ and a right semi-infinite system for $x > x_b$.

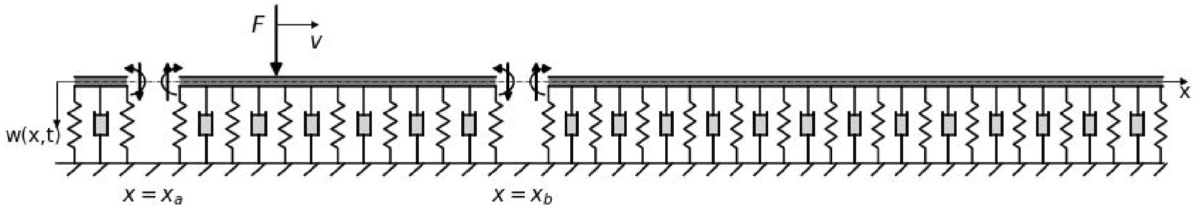

Figure 5.2: Subdivision of the infinite system in the formulation of the numerical model.

The numerical model consists out of the computational zone. The boundary conditions of this model must be such that they match the continuity in interface conditions of the actual infinite system. In order to define these non-reflective boundary conditions the general solutions for the semi-infinite systems are derived. These general solutions can be used to find a relationship between the cross-sectional forces and degree of freedoms at the interfaces. These relationships are then forced on the finite element model as Robin boundary conditions, completing the derivation and application of the non-reflective boundary conditions. This derivation will be shown for the right non-reflective boundary condition of the inertia-excluded model. The derivation of the left condition for the inertia-excluded model and both conditions for the inertia-included model are left out of the thesis. This is because the steps followed are very similar and the single derivation should be enough to make the concept clear for the reader.

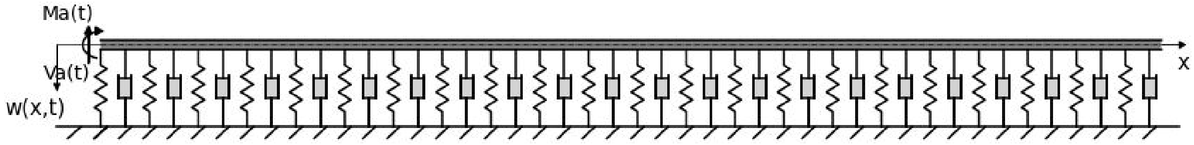

Figure 5.3: The right semi-infinite sub-system.

The equation of motion for this sub-system reads

$$\rho_b \frac{\partial^2 w}{\partial t^2} + c_w \frac{\partial w}{\partial t} + k_w w + EI \frac{\partial^4 w}{\partial x^4} = 0. \tag{5.40}$$

The Laplace transform method will be used in order to solve this problem. The Laplace transform of a function $f(t)$ is

$$\hat{f}(s) = \int_0^\infty f(t) e^{-st} dt \tag{5.41}$$

and the complex inversion formula is

$$f(t) = \lim_{y \to \infty} \left(\frac{1}{2\pi i} \int_{\sigma - yi}^{\sigma + yi} \hat{f}(s) e^{ts} ds \right). \tag{5.42}$$

Laplace transforming the equation of motion, substituting the initial conditions $w|_{t=0} = f(x)$ and $w_t|_{t=0} = g(x)$ and rearranging terms leads to

$$\frac{\partial^4 \hat{w}}{\partial x^4} + \left(4\gamma_b^2 s^2 + 4\alpha_w s + 4\beta_w^4\right) \hat{w} = \left(4\gamma_b^2 s + 4\alpha_w\right) f(x) + \left(4\gamma_b^2\right) g(x) \tag{5.43}$$

The particular solution of equation (5.43) is dependent on the initial conditions which are general. The particular solution is therefore just denoted by $\hat{w}_{ic}$. For the homogeneous solution the trial solution is

$$\hat{w}_{hom} = a(s)e^{\lambda(s)x}. \tag{5.44}$$

Substitution of the trial solution into equation (5.43) leads to the characteristic equation

$$\lambda(s)^4 = -(4\gamma_b^2 s^2 + 4\alpha_w s + 4\beta_w^4) = -z(s). \tag{5.45}$$

The eigenvalues $\lambda(s)$ can now be obtained from taking a fourth order root of a complex variable. In the previous chapters it has been shown that this causes reduction and rotation of the polar representation in the complex plane. In order to have a systematic procedure it is of importance to think a few steps ahead. Notice that for all values of s that are of interest it holds that $\arg(s) \in (-\frac{1}{2}\pi, \frac{1}{2}\pi)$. This can be concluded from the fact that there will be integrated over the Bromwich line which is a vertical line located at a positive real value σ, see equation (5.43). This can in turn be used to deduce that $\arg(z(s)) \in (-\pi, \pi)$. Now that this is clear the derivation will continue. Taking the fourth order roots of equation (5.45) results in

$$\lambda_n(s) = e^{(\frac{1}{2}n-\frac{1}{4})\pi i} z^{\frac{1}{4}}(s). \tag{5.46}$$

From the previous argumentation it follows that $\arg(z^{\frac{1}{4}}(s)) \in (-\frac{1}{4}\pi, \frac{1}{4}\pi)$. This can be used in combination with equation (5.46) to conclude that $\arg(\lambda_n(s)) \in (\frac{1}{2}(n-1)\pi, \frac{1}{2}n\pi)$. These conclusions can also be observed from the plots in Figure 5.4.

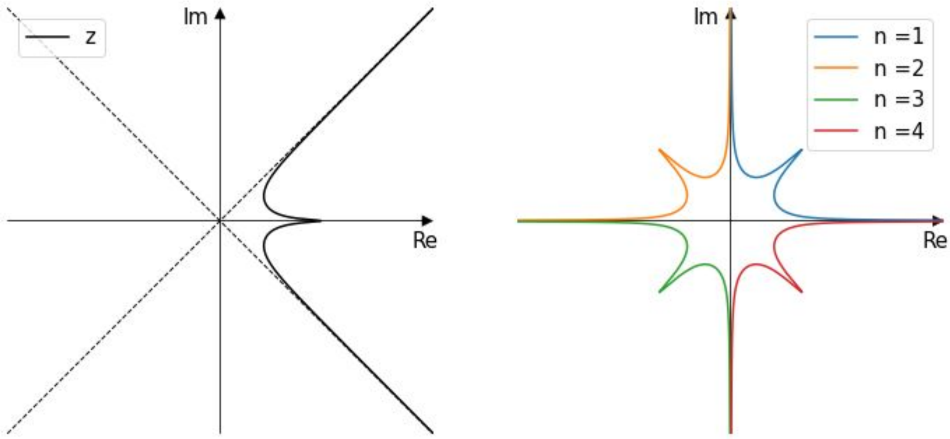

Figure 5.4: Plots of $z^{\frac{1}{4}}(s)$ (left) and $\lambda_n(s)$ (right) for varying values of y along the Bromwich line.

The homogeneous solution can thus denoted as

$$\hat{w}_{hom} = a_1(s)e^{\lambda_1(s)x} + a_2(s)e^{\lambda_2(s)x} + a_3(s)e^{\lambda_3(s)x} + a_4(s)e^{\lambda_4(s)x}. \tag{5.47}$$

The solution should be bounded for $x \to \infty$ meaning that solution terms corresponding to eigenvalues with real part larger than zero should be canceled. From Figure 5.4 it can be concluded that eigenvalues corresponding to n equals 1 and 2 should be canceled. The homogeneous solution then becomes

$$\hat{w}_{hom} = a_3(s)e^{\lambda(s)\,(x)} + a_4(s)e^{\lambda(s)i\,x}, \tag{5.48}$$

in which $\lambda(s) = \lambda_3(s)$. The total solution can then be obtained by addition of the homogeneous and particular solution. This solution can be used to obtain the expressions for the cross-sectional rotation and the cross-section forces. These can then be related to each other which leads to the flexibility relationship in the Laplace domain. This flexibility relationship reads

$$\begin{bmatrix} \hat{w} - \hat{w}_{ic} \\ \hat{\phi} - \hat{\phi}_{ic} \end{bmatrix} = \frac{1}{EI} \begin{bmatrix} -\frac{(i+1)}{\lambda^3} & \frac{i}{\lambda^2} \\ \frac{i}{\lambda^2} & \frac{(1-i)}{\lambda} \end{bmatrix} \begin{bmatrix} \hat{V} - \hat{V}_{ic} \\ \hat{M} - \hat{M}_{ic} \end{bmatrix}. \tag{5.49}$$

The flexibility relationship needs to be inverse transformed to obtain the relationship in the time domain. It is now mentioned that in this thesis the model will only be used for sub-critical load cases as also specified in Section 4.1. The length of the computational zone is then chosen such that the initial conditions in the semi-infinite system are approximately zero, meaning that $\hat{w}_{ic}$ and all its derivatives are also zero. The inverse transform of equation (5.49) is then denoted by

$$\begin{bmatrix} w \\ \phi \end{bmatrix} = \int_0^t \begin{bmatrix} c_{11}(t-\tau) & c_{12}(t-\tau) \\ c_{21}(t-\tau) & c_{22}(t-\tau) \end{bmatrix} \begin{bmatrix} V(\tau) \\ M(\tau) \end{bmatrix} d\tau. \tag{5.50}$$

The terms c_{11} are the inverse transforms of the indices $\hat{c}_{11}$ of the flexibility matrix in the Laplace domain. The integrals in equation (5.50) will be approximated numerically[1] at a time t_{n+1} which leads to

$$\begin{bmatrix} w(t_{n+1}) \\ \phi(t_{n+1}) \end{bmatrix} = \begin{bmatrix} \mathbf{GK} \end{bmatrix} \begin{bmatrix} V(t_{n+1}) \\ M(t_{n+1}) \end{bmatrix} + \begin{bmatrix} w_{his}(t_{n+1}) \\ \phi_{his}(t_{n+1}) \end{bmatrix}. \tag{5.51}$$

The last vector in equation (5.51) is called the history displacement vector and at a time t_{n+1} it is dependent on the cross-sectional forces at time t_n and smaller. The matrix $\mathbf{GK}$ is the time-domain dynamic flexibility matrix. Equation (5.51) is inverted to a stiffness relationship in order to implement it in the finite element model. This relationship reads

$$\begin{bmatrix} V(t_{n+1}) \\ M(t_{n+1}) \end{bmatrix} = \begin{bmatrix} \mathbf{KG} \end{bmatrix} \begin{bmatrix} w(t_{n+1}) \\ \phi(t_{n+1}) \end{bmatrix} + \begin{bmatrix} V_{his}(t_{n+1}) \\ M_{his}(t_{n+1}) \end{bmatrix}, \tag{5.52}$$

with

$$\begin{bmatrix} V_{his}(t_{n+1}) \\ M_{his}(t_{n+1}) \end{bmatrix} = -\begin{bmatrix} \mathbf{KG} \end{bmatrix} \begin{bmatrix} w_{his}(t_{n+1}) \\ \phi_{his}(t_{n+1}) \end{bmatrix}. \tag{5.53}$$

It should be mentioned that $\mathbf{KG}$ is the inverse matrix of $\mathbf{GK}$. The obtained expression in equation (5.52) can be now be implemented in the finite element model. The system of N ordinary differential equations obtained by the finite element model has the following form

$$\begin{bmatrix} m_{1,1} & \cdots & \cdots & m_{1,N} \\ \vdots & \ddots & \cdots & \vdots \\ \vdots & \cdots & m_{N-1,N-1} & m_{N,N-1} \\ m_{N,1} & \cdots & m_{N-1,N} & m_{N,N} \end{bmatrix} \begin{bmatrix} \vdots \\ \vdots \\ \ddot{w}(t_{n+1}) \\ \ddot{\phi}(t_{n+1}) \end{bmatrix} + \begin{bmatrix} k_{1,1} & \cdots & \cdots & k_{1,N} \\ \vdots & \ddots & \cdots & \vdots \\ \vdots & \cdots & k_{N-1,N-1} & k_{N,N-1} \\ k_{N,1} & \cdots & k_{N-1,N} & k_{N,N} \end{bmatrix} \begin{bmatrix} \vdots \\ \vdots \\ w(t_{n+1}) \\ \phi(t_{n+1}) \end{bmatrix} = \begin{bmatrix} \vdots \\ \vdots \\ V(t_{n+1}) \\ M(t_{n+1}) \end{bmatrix}. \tag{5.54}$$

Substitution of the non-reflective boundary conditions of equation (5.52) into equation (5.54) and rearranging terms yields

$$\mathbf{M\ddot{a}} + \begin{bmatrix} k_{1,1} & \cdots & \cdots & k_{1,N} \\ \vdots & \ddots & \cdots & \vdots \\ \vdots & \cdots & (k_{N-1,N-1} - KG_{11}) & (k_{N,N-1} - KG_{12}) \\ k_{N,1} & \cdots & (k_{N-1,N} - KG_{21}) & (k_{N,N} - KG_{22}) \end{bmatrix} \begin{bmatrix} \vdots \\ \vdots \\ w(t_{n+1}) \\ \phi(t_{n+1}) \end{bmatrix} = \begin{bmatrix} \vdots \\ \vdots \\ V_{his}(t_{n+1}) \\ M_{his}(t_{n+1}) \end{bmatrix}. \tag{5.55}$$

This system can then be solved by making use of a quadrature by choice. At each time step the nodal degrees of freedom can be determined. One then has to substitute the obtained values of the degrees of freedom for the node at the non-reflective boundary into equation (5.52) which results in the cross-sectional forces at the boundary. These cross-sectional forces are then used to determine the history force vector for the next time step. The nodal degrees of freedom can then be determined for the following step and the algorithm is repeated. This completes the derivation and application of the non-reflective boundary conditions.

[1] See Appendix B for a full derivation.

5.3. Time integration

After application of the finite element method and inclusion of the non-reflective boundary conditions the system of ordinary differential equations that is left solve is

$$\mathbf{M}\ddot{\mathbf{w}} + \mathbf{K}\mathbf{w} = \mathbf{f}. \tag{5.56}$$

This system of ordinary differential equations will be solved by making use of a generalised Newmark-beta scheme. In order to do so, one first increments the time in discrete time steps $t_n = n\Delta t$. A discrete system at t_{n+1} is then denoted by

$$\mathbf{M}\ddot{\mathbf{w}}_{n+1} + \mathbf{K}\mathbf{w}_{n+1} = \mathbf{f}_{n+1}. \tag{5.57}$$

The Newmark-beta algorithm defines $\mathbf{w}_{n+1}$ and $\dot{\mathbf{w}}_{n+1}$ as

$$\begin{aligned} \mathbf{w}_{n+1} &= \mathbf{w}_n + \Delta t\dot{\mathbf{w}}_n + \frac{\Delta t^2}{2}((1-2\beta)\ddot{\mathbf{w}}_n + 2\beta\ddot{\mathbf{w}}_{n+1}) \\ \dot{\mathbf{w}}_{n+1} &= \dot{\mathbf{w}}_n + \Delta t((1-\gamma)\ddot{\mathbf{w}}_n + \gamma\ddot{\mathbf{w}}_{n+1}) \end{aligned}. \tag{5.58}$$

The Newmark-beta method is unconditionally stable for

$$\frac{1}{2} \leq \gamma \leq 2\beta. \tag{5.59}$$

The initial conditions of the problem are given and are known as $w(x,0)$ and $\frac{\partial w}{\partial t}\big|_{t=0}$. These fields are also discretized in order to obtain the vectors that represent these initial conditions $\mathbf{w}_0$ and $\dot{\mathbf{w}}_0$. The initial acceleration vector is then determined from equation (5.56) and reads

$$\ddot{\mathbf{w}}_0 = \mathbf{M}^{-1}\left(\mathbf{f}_0 - \mathbf{K}\mathbf{w}_0\right). \tag{5.60}$$

All quantities at the initial time are now known. The algorithm can now be started in order to obtain the quantities at future time steps. The Newmark expressions are therefore substituted in (5.57) which results in

$$\left(\mathbf{M} + \beta\Delta t^2\mathbf{K}\right)\ddot{\mathbf{w}}_{n+1} = \mathbf{f}_{n+1} - \mathbf{K}\tilde{\mathbf{w}}_{n+1}. \tag{5.61}$$

Note that the $\tilde{\mathbf{w}}_{n+1}$ is called a predictor. The two predictors in the Newmark-beta scheme have the expressions

$$\begin{aligned} \tilde{\mathbf{w}}_{n+1} &= \mathbf{w}_n + \Delta t\dot{\mathbf{w}}_n + \frac{\Delta t^2}{2}(1-2\beta)\ddot{\mathbf{w}}_n \\ \dot{\tilde{\mathbf{w}}}_{n+1} &= \dot{\mathbf{w}}_n + \Delta t(1-\gamma)\ddot{\mathbf{w}}_n \end{aligned}. \tag{5.62}$$

Equation (5.61) forms a system from which $\ddot{\mathbf{w}}_{n+1}$ can be solved at any time step. This term can then be used to correct the predictor in order to obtain the displacement and velocity vector at each time step. The correctors are defined by the expressions

$$\begin{aligned} \mathbf{w}_{n+1} &= \tilde{\mathbf{w}}_{n+1} + \beta\Delta t^2\ddot{\mathbf{w}}_{n+1} \\ \dot{\mathbf{w}}_{n+1} &= \dot{\tilde{\mathbf{w}}}_{n+1} + \gamma\Delta t\ddot{\mathbf{w}}_{n+1} \end{aligned}. \tag{5.63}$$

The degree of freedom vector can be obtained at each time step by making use of this method. The coefficients in the degree of freedom vector are each multiplied with their corresponding shape function and summed to obtained the solution of the problem.

6

Results and discussion

6.1. Steady state behaviour

The steady state displacement field of both systems are presented for different load velocities. The first step in order to do so is setting the value of γ_s. This value is set to have a corresponding velocity v_1 of 120 m/s which is a common value for the critical velocity in railway tracks. This velocity is the lowest critical velocity of the inertia-included system. The critical velocity for the inertia-excluded system is approximately 480 m/s. Note that this value and all other calculations in the chapter are based on the parameters in Table 2.1. The velocities that are studied for both systems are chosen such that

$$\Delta v = \frac{v_{in}}{v_{cr}} = \frac{v_{ex}}{v_1}. \tag{6.1}$$

The reader should notice that the load velocity for the inertia-included system v_{in} and the load velocity for the inertia-excluded system v_{ex} are not equal. The ratios between these velocities and the critical velocity of their respective system are however the same. This choice has been made to obtain just means of comparison for the dynamical effects of the moving load. The results for different values of Δv are shown in Figure 6.1. The results show that the steady state displacement fields coincide very much for different values of Δv. It can be noticed that the difference between the displacement fields increases with increasing values of Δv. This difference however remains very small as can be observed for the results.

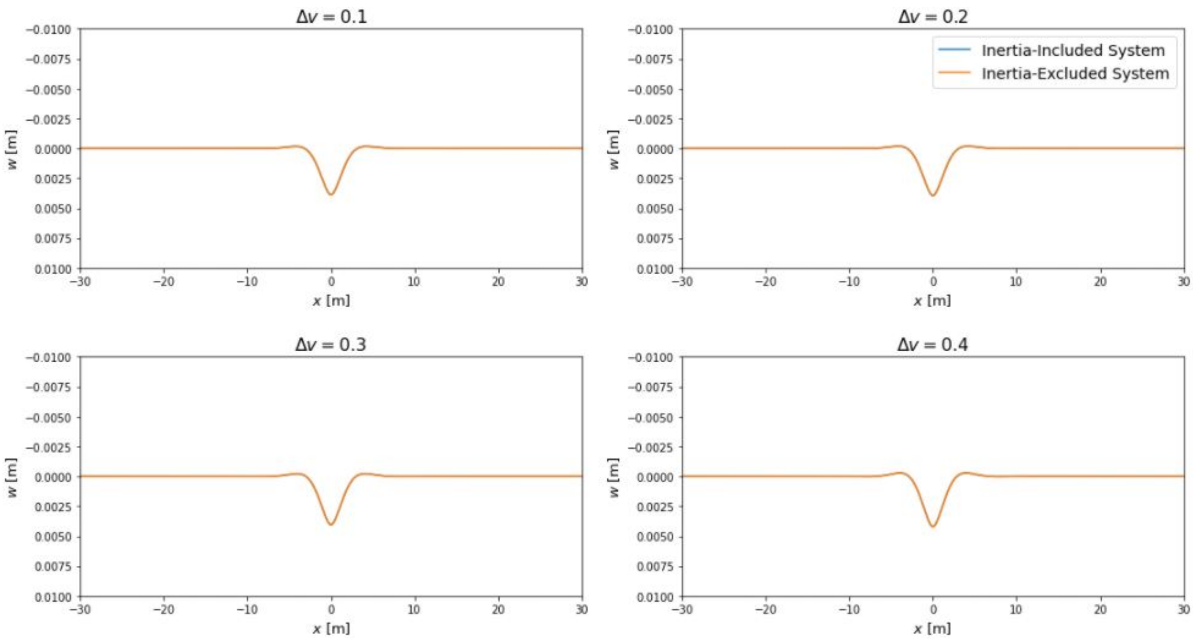

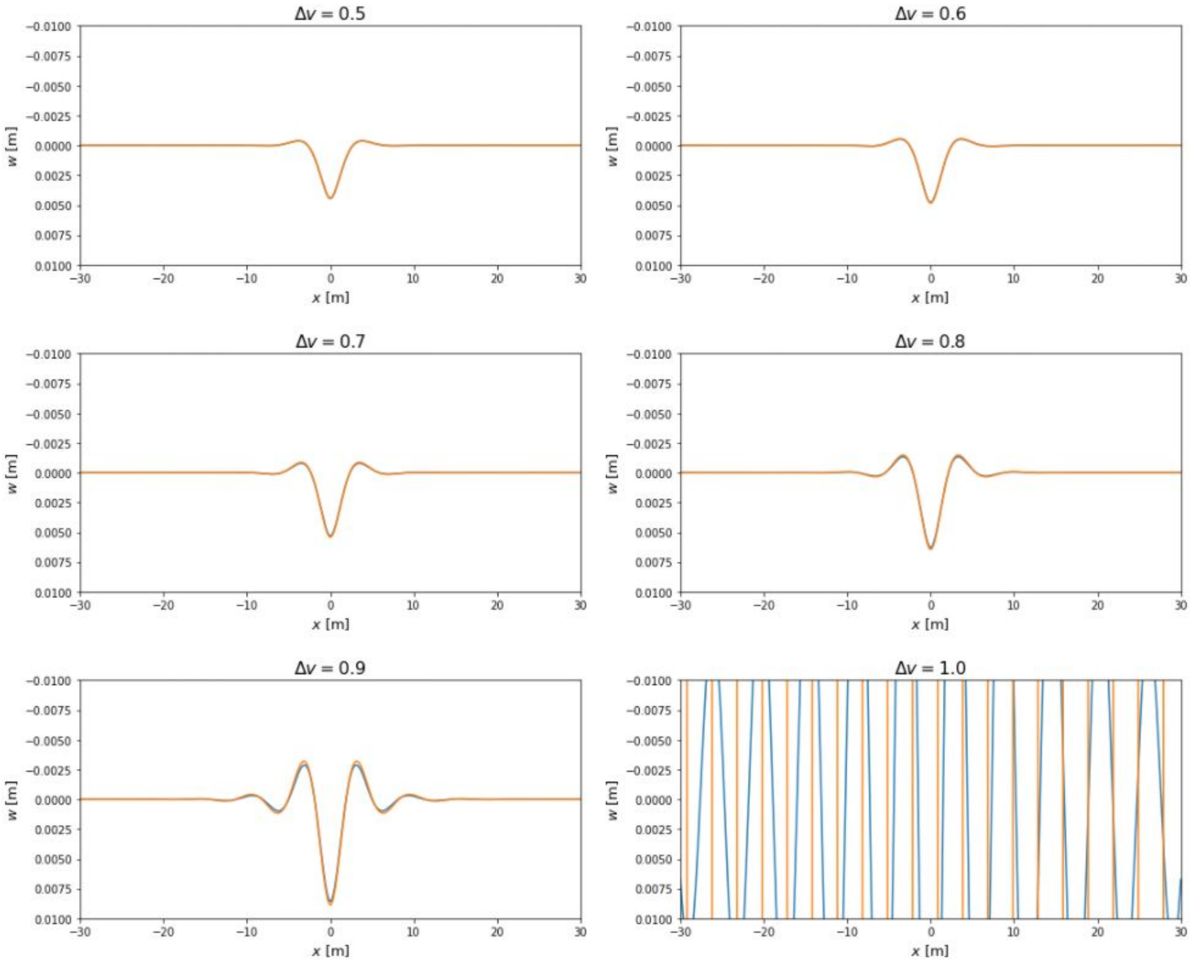

Figure 6.1: Steady state displacement fields at $t = 0$ corresponding to increasing values of Δv.

6.2. Transition radiation

The interest of this thesis lies in the effect of the addition of the inertia-beam on the transition radiation. The spectral density of transition radiation energy $Q^{(n)}$ is therefore presented and integrated resulting in the radiation energy $E_r^{(n)}$. The properties of the rails, pads, sleepers and ballast can be tested extensively in fabrication before construction of the railway track. Their properties are therefore assumed to be constant. The transition of properties in the model are thus only caused by an inhomogeneity in the subgrade. A transition zone in the inertia-included model is therefore modeled by an abrupt jump in the lower elastic layer, such that

$$k_s^{(2)} = nk_s^{(1)}. \tag{6.2}$$

For the inertia-excluded model one should make sure that the Winkler foundation has the same stiffness as the serial combination of the inertia-included system, such that

$$\frac{1}{k_w^{(2)}} = \frac{1}{nk_s^{(1)}} + \frac{1}{k_p}. \tag{6.3}$$

All parameters in the system are set except for the load velocity and the ratio n between the stiffness of the lower elastic layer before and after the transition. Two different cases will therefore be studied:

- The first case with varying values of Δv and a set $n = 2$. The spectral densities of transition radiation energy are shown in Figure 6.2 and the numerical values of the integrated radiation energy in Table 6.1.
- The second case with a set value of $\Delta v = 0.5$ and a varying n. The spectral densities of transition radiation energy are shown in Figure 6.4 and the numerical values of the integrated radiation energy in Table 6.2.

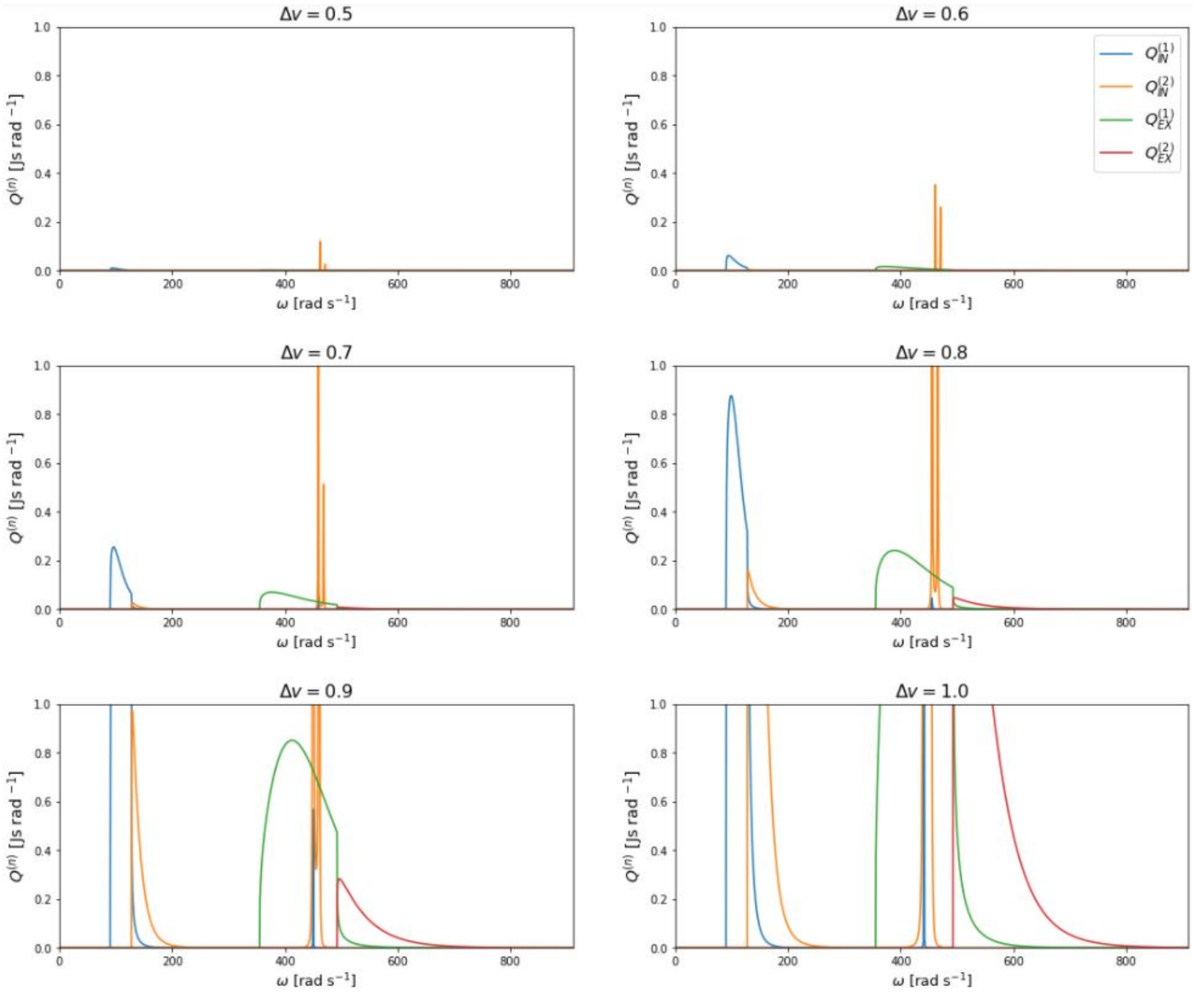

Figure 6.2: Spectral densities of transition radiation energy for the first case.

It can be observed from Figure 6.3 that the spectral densities of radiation energy obtain greater values for increasing values of Δv. This means that the transition radiation energy becomes larger as the load velocity approaches the critical velocity of the respective model. It is furthermore noticed that the the frequencies at which the spectral densities of transition radiation energy becomes non zero are different for both models. This can be explained from the fact that the frequency intervals of wave propagation differ for both models as has been explained in Chapter 3 and it can also be observed from the dispersion curves shown in Figure 6.3. For increasing values of n the spectral densities for the transition radiation in the positive x-direction shift to the right as can be observed from Figure 6.4. This can be explained by the fact that the values of the cut off frequency $\omega_{EX}^{(2)}$ and the lower bound of the first frequency band $\omega_{IN1}^{(1)}$ increase for an increasing value of k_s.

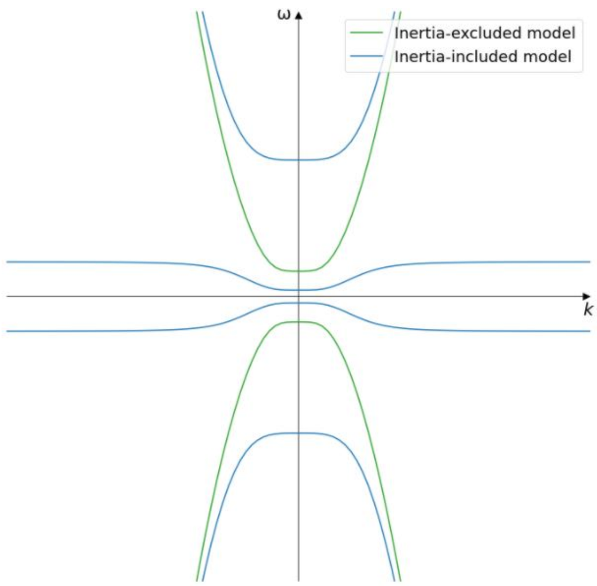

Figure 6.3: Dispersion curves for both models.

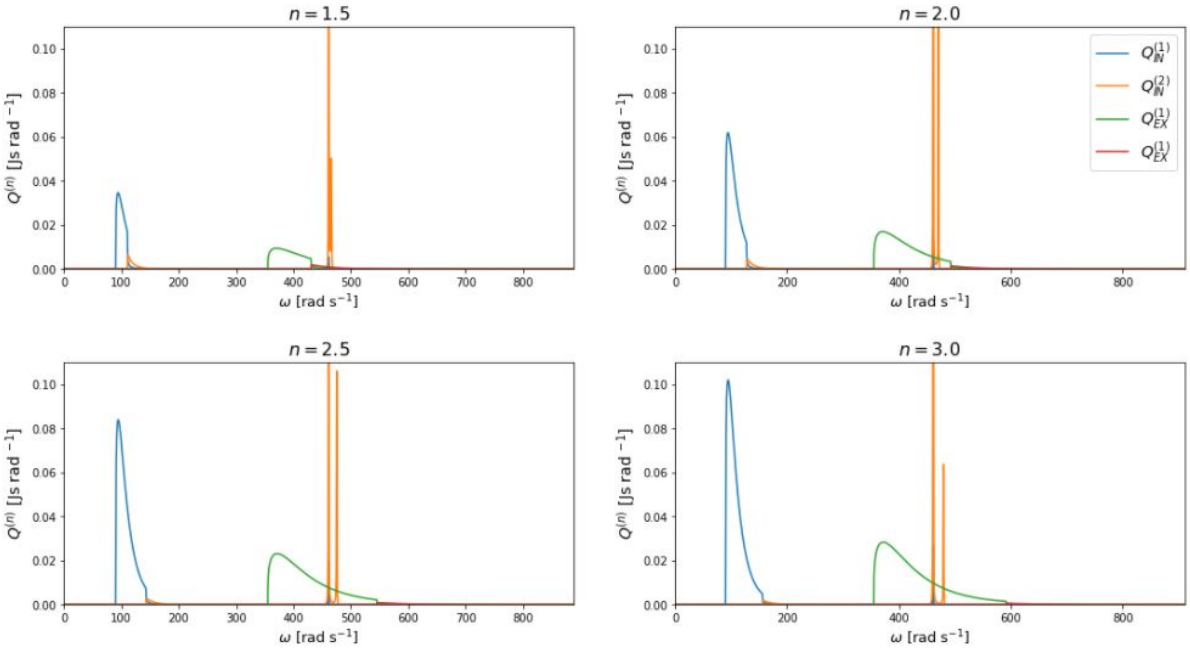

Figure 6.4: Spectral densities of transition radiation energy for the second case.

Δv	$E_{R,ex}^{(1)}$	$E_{R,in}^{(1)}$	$\Delta E_R^{(1)}$	$E_{R,ex}^{(2)}$	$E_{R,in}^{(2)}$	$\Delta E_R^{(2)}$	$E_{R,ex}$	$E_{R,in}$	ΔE_R
0.00	$0.00\,10^{0}$	$0.00\,10^{0}$	−−	$0.00\,10^{0}$	$0.00\,10^{0}$	−−	$0.00\,10^{0}$	$0.00\,10^{0}$	−−
0.10	$3.11\,10^{-6}$	$3.05\,10^{-6}$	0.98	$5.46\,10^{-8}$	$2.86\,10^{-7}$	5.24	$3.17\,10^{-6}$	$3.34\,10^{-6}$	1.06
0.20	$8.11\,10^{-4}$	$7.96\,10^{-4}$	0.98	$1.74\,10^{-5}$	$7.38\,10^{-5}$	4.25	$8.29\,10^{-4}$	$8.70\,10^{-4}$	1.05
0.30	$2.14\,10^{-2}$	$2.11\,10^{-2}$	0.98	$5.68\,10^{-4}$	$2.06\,10^{-3}$	3.62	$2.20\,10^{-2}$	$2.31\,10^{-2}$	1.05
0.40	$2.22\,10^{-1}$	$2.30\,10^{-1}$	1.03	$7.51\,10^{-3}$	$1.63\,10^{-1}$	21.7	$2.30\,10^{-1}$	$3.93\,10^{-1}$	1.71
0.50	$1.39\,10^{0}$	$1.38\,10^{0}$	0.99	$6.28\,10^{-2}$	$7.55\,10^{1}$	12.0	$1.45\,10^{0}$	$2.13\,10^{0}$	1.47
0.60	$6.40\,10^{0}$	$6.32\,10^{0}$	0.99	$4.16\,10^{-1}$	$3.67\,10^{0}$	8.83	$6.82\,10^{0}$	$9.99\,10^{0}$	1.46
0.70	$2.51\,10^{1}$	$2.46\,10^{1}$	0.98	$2.54\,10^{0}$	$1.47\,10^{1}$	5.78	$2.76\,10^{1}$	$3.93\,10^{1}$	1.42
0.80	$9.68\,10^{1}$	$9.54\,10^{1}$	0.99	$1.71\,10^{1}$	$1.55\,10^{2}$	9.06	$1.14\,10^{2}$	$2.50\,10^{2}$	2.20
0.90	$4.99\,10^{2}$	$4.96\,10^{2}$	0.99	$1.82\,10^{2}$	$2.53\,10^{3}$	13.9	$6.81\,10^{2}$	$3.02\,10^{3}$	4.44
1.00	$0.00\,10^{0}$	$0.00\,10^{0}$	−−	$0.00\,10^{0}$	$0.00\,10^{0}$	−−	$0.00\,10^{0}$	$0.00\,10^{0}$	−−

Table 6.1: Numerical values of transition radiation energy $E_R^{(n)}$ for the first case. The superscript (n) denotes which field is observed, (1) for the left field and (2) for the right field. The superscript is emitted when the total transition radiation energy is denoted. A subscript ex or in is used when referred to either the inertia-excluded or included system. Lastly, The ratio between the transition radiation energy for the inertia-included and excluded model is denoted by $\Delta E_R^{(n)}$.

n	$E_{R,ex}^{(1)}$	$E_{R,in}^{(1)}$	$\Delta E_R^{(1)}$	$E_{R,ex}^{(2)}$	$E_{R,in}^{(2)}$	$\Delta E_R^{(2)}$	$E_{R,ex}$	$E_{R,in}$	ΔE_R
1.00	$0.00\,10^{0}$	$0.00\,10^{0}$	−−	$0.00\,10^{0}$	$0.00\,10^{0}$	−−	$0.00\,10^{0}$	$0.00\,10^{0}$	−−
1.50	$5.82\,10^{-1}$	$5.78\,10^{-1}$	0.99	$7.18\,10^{-2}$	$4.38\,10^{-1}$	6.09	$6.54\,10^{-1}$	$1.02\,10^{0}$	1.55
2.00	$1.39\,10^{0}$	$1.37\,10^{0}$	0.99	$6.29\,10^{-2}$	$8.14\,10^{-1}$	12.9	$1.45\,10^{0}$	$2.18\,10^{0}$	1.51
2.50	$2.09\,10^{0}$	$2.05\,10^{0}$	0.98	$4.52\,10^{-2}$	$5.13\,10^{-1}$	11.3	$2.13\,10^{0}$	$2.56\,10^{0}$	1.20
3.00	$2.68\,10^{0}$	$2.62\,10^{0}$	0.98	$3.23\,10^{-2}$	$4.82\,10^{-1}$	14.9	$2.71\,10^{0}$	$3.10\,10^{0}$	1.14

Table 6.2: Numerical values of transition radiation energy for the second case.

It is observed from both Table 6.1 and Table 6.2 that the difference between the radiation energy for the inertia-included and excluded model in the negative x-direction is very small. This results in a ratio $\Delta E_R^{(1)}$ that is very close to 1.0 for all cases. This is however not the case for the transition radiation energy in the positive x-direction. As mentioned in the end of Chapter 5 there is an important difference between the spectral densities for the inertia-excluded and included system which was the occurrence of the peaks. These peaks occur due to the fact that there are always two intersection points between the kinematic invariant and dispersion curves for the inertia-included system. This is because the lower dispersion curve tends to a horizontal asymptote $\omega = \omega_{SI}$ which in turn is a result of the absence of any internal stiffness in the inertia beam. This means that wave propagation from the load occurs as soon as the load velocity is non-zero which is an artifact of the model. These peaks are now removed because they are physically irrelevant and the amount of transition energy without their contributions is quantified. Figure 6.5 shows the way a peak is removed and Table 6.3 and 6.4 show the numerical values of the transition radiation energy for the two cases based on the spectral densities with removed peaks.

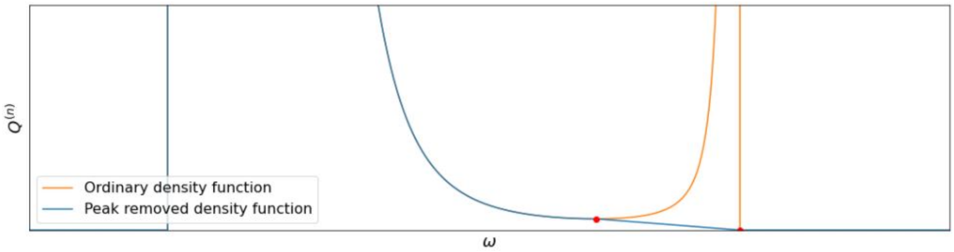

Figure 6.5: Removal of a peak in a spectral energy density function.

Δv	$E_{R,ex}^{(1)}$	$E_{R,in}^{(1)}$	$\Delta E_R^{(1)}$	$E_{R,ex}^{(2)}$	$E_{R,in}^{(2)}$	$\Delta E_R^{(2)}$	$E_{R,ex}$	$E_{R,in}$	ΔE_R
0.00	$0.00\,10^{0}$	$0.00\,10^{0}$	$--$	$0.00\,10^{0}$	$0.00\,10^{0}$	$--$	$0.00\,10^{0}$	$0.00\,10^{0}$	$--$
0.10	$3.11\,10^{-6}$	$3.00\,10^{-6}$	0.98	$5.46\,10^{-8}$	$5.33\,10^{-8}$	0.98	$3.17\,10^{-6}$	$3.00\,10^{-6}$	0.98
0.20	$8.11\,10^{-4}$	$7.93\,10^{-4}$	0.98	$1.74\,10^{-5}$	$1.69\,10^{-5}$	0.97	$8.29\,10^{-4}$	$8.10\,10^{-4}$	0.98
0.30	$2.14\,10^{-2}$	$2.09\,10^{-2}$	0.98	$5.68\,10^{-4}$	$5.52\,10^{-4}$	0.97	$2.20\,10^{-2}$	$2.15\,10^{-2}$	0.98
0.40	$2.22\,10^{-1}$	$2.17\,10^{-1}$	0.98	$7.51\,10^{-3}$	$7.28\,10^{-3}$	0.97	$2.30\,10^{-1}$	$2.24\,10^{-1}$	0.98
0.50	$1.39\,10^{0}$	$1.36\,10^{0}$	0.98	$6.28\,10^{-2}$	$6.09\,10^{-2}$	0.97	$1.45\,10^{0}$	$1.42\,10^{0}$	0.98
0.60	$6.40\,10^{0}$	$6.26\,10^{0}$	0.98	$4.16\,10^{-1}$	$4.02\,10^{-1}$	0.97	$6.82\,10^{0}$	$6.66\,10^{0}$	0.98
0.70	$2.51\,10^{1}$	$2.45\,10^{1}$	0.98	$2.54\,10^{0}$	$2.45\,10^{0}$	0.97	$2.76\,10^{1}$	$2.70\,10^{1}$	0.98
0.80	$9.68\,10^{1}$	$9.47\,10^{1}$	0.98	$1.71\,10^{1}$	$1.65\,10^{1}$	0.96	$1.14\,10^{2}$	$1.11\,10^{2}$	0.98
0.90	$4.99\,10^{2}$	$4.89\,10^{2}$	0.98	$1.82\,10^{2}$	$1.76\,10^{2}$	0.96	$6.81\,10^{2}$	$6.66\,10^{2}$	0.98
1.00	$0.00\,10^{0}$	$0.00\,10^{0}$	$--$	$0.00\,10^{0}$	$0.00\,10^{0}$	$--$	$0.00\,10^{0}$	$0.00\,10^{0}$	$--$

Table 6.3: Numerical values of transition radiation energy for the first case. The peaks have been removed from the spectral energy density functions corresponding to the inertia-included system.

n	$E_{R,ex}^{(1)}$	$E_{R,in}^{(1)}$	$\Delta E_R^{(1)}$	$E_{R,ex}^{(2)}$	$E_{R,in}^{(2)}$	$\Delta E_R^{(2)}$	$E_{R,ex}$	$E_{R,in}$	ΔE_R
1.00	$0.00\,10^{0}$	$0.00\,10^{0}$	$--$	$0.00\,10^{0}$	$0.00\,10^{0}$	$--$	$0.00\,10^{0}$	$0.00\,10^{0}$	$--$
1.50	$5.82\,10^{-1}$	$5.71\,10^{-1}$	0.98	$7.18\,10^{-2}$	$6.96\,10^{-2}$	0.97	$6.54\,10^{-1}$	$6.41\,10^{-1}$	0.98
2.00	$1.39\,10^{0}$	$1.36\,10^{0}$	0.98	$6.29\,10^{-2}$	$6.08\,10^{-2}$	0.97	$1.45\,10^{0}$	$1.42\,10^{0}$	0.98
2.50	$2.09\,10^{0}$	$2.03\,10^{0}$	0.97	$4.52\,10^{-2}$	$4.39\,10^{-2}$	0.97	$2.13\,10^{0}$	$2.07\,10^{0}$	0.97
3.00	$2.68\,10^{0}$	$2.58\,10^{0}$	0.96	$3.23\,10^{-2}$	$3.26\,10^{-2}$	1.01	$2.71\,10^{0}$	$2.62\,10^{0}$	0.96

Table 6.4: Numerical values of transition radiation energy for the second case. The peaks have been removed from the spectral energy density functions corresponding to the inertia-included system.

It is observed from Table 6.3 and Table 6.4 that removal of the peaks leads to the situation in which the ratios $\Delta E_R^{(1)}$, $\Delta E_R^{(2)}$ and ΔE_R are approximately 0.98. This means that both models lead to similar amounts of total transition radiation energy after removal of the peaks. This result is very interesting when one keeps in mind that the spectral density functions are not similar as can be seen from the previous figures. It can furthermore be observed from Table 6.3 that the transition radiation energy increases for increasing values of Δv as has been mentioned before. Moreover, it can be observed that the transition radiation energy in negative x-direction keeps increasing for increasing values of n. This follows physical expectations because when the elastic layer in right field would be rigid there would be no possibility for displacements in the right field and thus also no energy propagation. All transition radiation energy is then transmitted in the left field. In line with this it would thus be expected that the transition radiation in the negative x-direction increases with increasing value of n which is confirmed. Lastly, it can be observed from Table 6.4 that the transition radiation energy in the positive $x-$direction starts of from zero for $n = 1$, increases and keeps decreasing afterwards. This means that there is a certain value of n for which the transition radiation energy in the positive x-direction is maximum. This can also be explained physically because there is no transition radiation energy when there is no transition in the stiffness parameters and the transition radiation energy tends to zero when the right elastic foundation becomes rigid as has also been sated above. Furthermore the amount of energy is always positive which means that there should be a maximum value of transition radiation energy in the positive x-direction for increasing values of n.

6.3. Transient behaviour

The transient behaviour will be visualized to analyse the differences in transition radiation processes between the two models in the time domain. One should recall that the load velocities in the two models are different. It is therefore chosen to plot the displacement fields for different values of the location of the load x_F. The numerical models defined in Chapter 6 are therefore used. The value of n equals 2 and the value of $\Delta v = 0.5$. The results are shown in Figure 6.6.

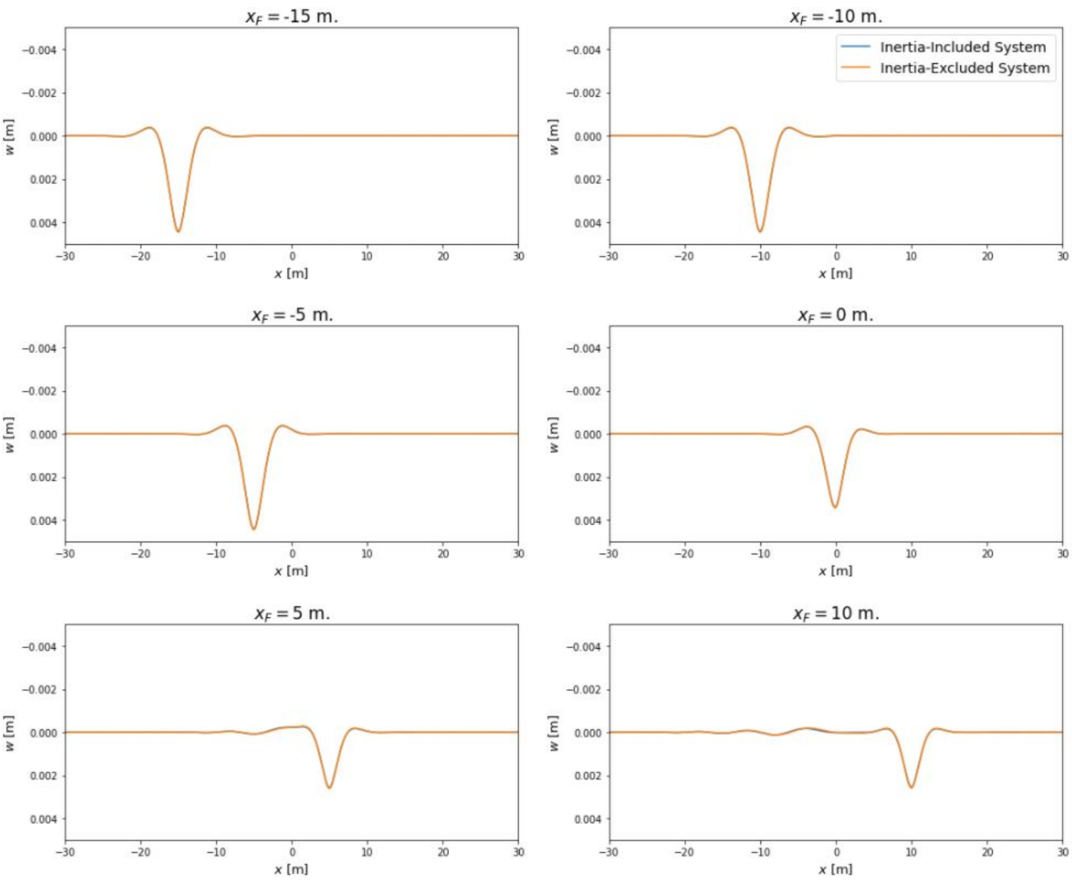

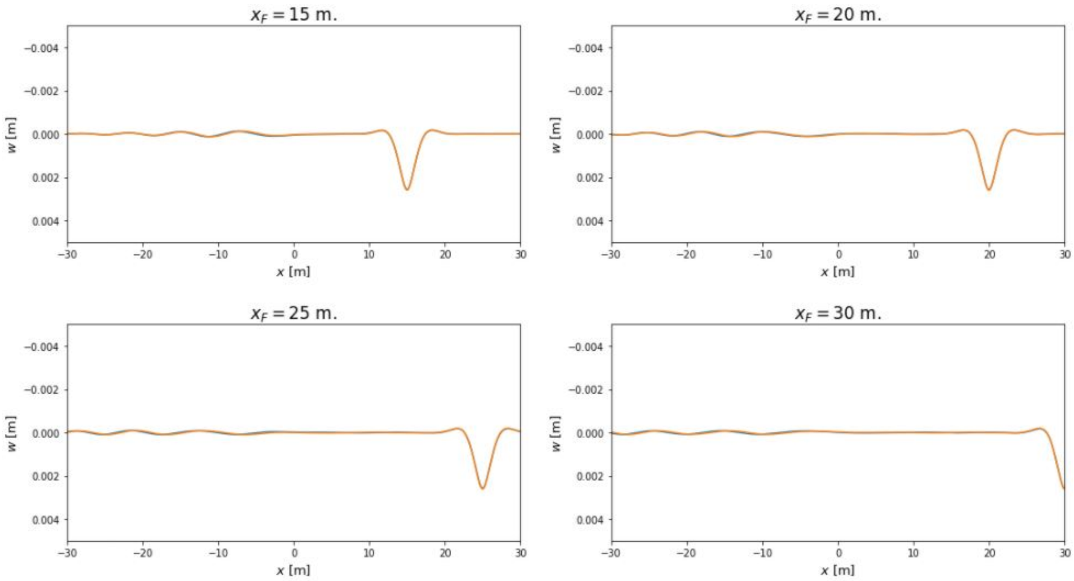

Figure 6.6: The transient behaviour of a transition zone for both models.

The total solution for both models consists of a set of an eigenfield and a free field for the semi-infinite system to the left of the transition point and a set of an eigenfield and a free field for the semi-infinite system to the right of the transition point. The eigenfield for the inertia-excluded model consist of only evanescent waves. The eigenfield for the the inertia-included model consists of four evanescent waves and two propagating waves which occur as ripples to the left of the moving loads as has been stated in Subsection 3.2.1. These ripples however happen to be relatively so small in the studied case that one can hardly make a distinction between the eigenfield of the inertia-excluded and included system. This has been observed in the first section of this chapter. This means that for both the eigenfields one can observe a significant displacement at the vicinity of the load which rapidly tends to zero as the spatial distance from the load increases. The waves that are observed when the load passes the transition point in Figure 6.6 are thus caused by the free field. The transient behaviour of both models coincide very well which means that the free fields of both models are also very similar. This is an interesting result because the Fourier transformed free fields are different as has been show in Chapter 4. This means that despite the Fourier transformed free fields are different they are still such that their representations in the time domain are very similar, which is worth noting.

7
Conclusion

This thesis has focused on the influence of including the inertia of the supporting structure that is activated by the moving load. This has been included by adding a secondary beam with no bending stiffness, the inertia beam. This inertia-included model has in turn been compared to the inertia-excluded model throughout the chapters of this thesis. The inertia-excluded model represented the well known system which exists of an infinitely long Winkler supported Euler-Bernoulli beam. This model is known to have an important constraint which is its inability to result in a critical velocity that makes sense for railway-tracks. The obtained critical velocity by such a model is in general far larger than the measured velocity of Rayleigh waves.

This problem raised the question whether it was possible to lower the critical velocity by the addition of the inertia beam. The influence of the addition of the inertia beam on the critical velocity has been studied extensively in Chapter 3. It has been shown that two types of system behaviour can be observed. The first type in which three critical velocities can be distinguished and the second type in which there is only one critical velocity. It has been shown that it can be determined which one of the two types of system behaviour occur by checking whether the density of the inertia beam is smaller or larger then γ_{smin}. It turned out that the first of the three critical velocities in the first type of system behaviour is always smaller than the default critical velocity obtained by calculation based on the Winkler supported Euler-Bernoulli beam. Application of this insight obtained by this study led to the reduction of a critical velocity from 480 to 120 m/s, answering the first research question.

The problem of the critical velocity has been tackled but as stated in the introduction this leads to new questions. This is because it was expected that modification of the system would not only lead to a difference in the obtained critical velocity but also to changes in other output such as the steady state behaviour, emitted transition radiation energy and the transient behaviour at a transition zone.

For the inertia-excluded model a strict difference between sub- and super-critical steady state behaviour can be made. For that model the sub-critical steady state behaviour consists of only evanescent waves and the super-critical steady state behaviour of only propagating waves. Such a strict difference in definition could not be made for the inertia-included model because there are always at least two waves propagating for all possible velocities. This is due to the absence of any internal stiffness for the inertia beam. It was thus chosen to define the sub-critical steady state behaviour as the situation for which only two of the six waves propagate and the super-critical behaviour as the situation for which all six waves propagate. This has as a result that additional ripples to the left of the load are present for the eigenfield (sub-critical steady state displacement field). The eigenfields for both models have been plotted for different velocities and compared with each other. In order to make a comparison the velocities for both systems have been chosen such that ratios Δv between their own respective critical velocity were equal. From the results it could be observed that the steady state displacement fields for both models were almost identical, answering the second research question. This suggests that the relative velocity is of main importance when one aims to model a railway track by a Winkler supported Euler-Bernoulli beam and not the absolute value. This may render the investigations of those researchers that overestimate the critical velocity of the track and then use a realistic absolute value of the load velocity questionable.

Spectral energy densities for the transition radiation energy have been determined. Integration of these densities leads to the emitted transition radiation energy. The main differences between the density functions for both models will be restated briefly. The spectral density for the inertia-excluded model is non-zero for frequencies higher than the cut off frequency. The spectral density for the inertia-included model however is non-zero for two frequency intervals. The cut off frequency is also larger than the lower bound of the first frequency interval of wave propagation for the inertia-included system. All of this can be explained by comparison of the dispersion curves for both systems. Another important difference is the occurrence of peaks in the density functions for the inertia-included model. These peaks occur due to the fact that there are always two waves present in the inertia-included system. This is mentioned before and can also be explained by the dispersion curves in combination with the kinematic invariant. With regards to the emitted transition radiation, it has been shown that there are quite remarkable differences between both models for the transition radiation energy in positive x-direction. However, removal of the peaks leads to almost equivalent results for both directions for both models, answering the third research question.

A numerical model has been formulated in which the finite element method has been applied for the spatial discretization and the Newmark-beta method for the time discretization. This model can take care of non-constant system properties and general loads. Non-reflecctive boundary conditions have also been implemented in the model. This model has been used to obtain the transient behaviour of a uniformly moving load of constant magnitude passing by an abrupt transition in the stiffness properties for both models. The results have been shown and also this transient behaviour showed great similarity for both systems, answering the last research question.

In this thesis much attention has been paid to the physical meaning and interpretation of the results obtained from the introduced model. The differences between this model and the ordinary Winkler supported Euler-Bernoulli beam have been addressed. Also a numerical model has been formulated which can be used for those who wish to investigate other load cases or other non-constant system properties. This model can be extended further by future researchers with extensions such as the inclusion of non-linear behaviour, more complex vehicle models and many more. An interesting study that could be done next is to modify the stiffness of the pads at the transition zone in order to decrease the amount of transition radiation. This is the study that should performed next from the authors point of view.

A

The dispersion equation for the inertia included system is denoted by

$$\left(k^4 - 4\gamma_b^2\omega^2 + 4\beta_p^4\right)\left(-4\gamma_s^2\omega^2 + \left(4\beta_p^4 + 4\beta_s^4\right)\right) - \left(4\beta_p^4\right)^2 = 0. \tag{A.1}$$

The lower bound frequencies of the frequency bands of wave propagation are those frequencies of which their corresponding wave-number equal zero. To find this frequencies one has to solve

$$\left(4\gamma_b^2\omega^2 - 4\beta_p^4\right)\left(-4\gamma_s^2\omega^2 + \left(4\beta_p^4 + 4\beta_s^4\right)\right) + \left(4\beta_p^4\right)^2 = 0. \tag{A.2}$$

Rewriting this expression yields

$$-(4\gamma_b^2)(4\gamma_s^2)\omega^4 + \left((4\beta_p^4)(4\gamma_b^2 + 4\gamma_s^2) + (4\beta_s^4)(4\gamma_b^2)\right)\omega^2 - (4\beta_p^4)(4\beta_s^4) = 0. \tag{A.3}$$

Make the substitution $\omega = x^2$ in order to obtain the quadratic equation

$$-(4\gamma_b^2)(4\gamma_s^2)x^2 + \left((4\beta_p^4)(4\gamma_b^2 + 4\gamma_s^2) + (4\beta_s^4)(4\gamma_b^2)\right)x - (4\beta_p^4)(4\beta_s^4) = 0, \tag{A.4}$$

in short notation

$$ax^2 + bx + c = 0, \tag{A.5}$$

which in turn has the following solutions

$$x_{1,2} = \frac{-b \pm \sqrt{D}}{2a}. \tag{A.6}$$

The discriminant is now elaborated in order to study the roots:

$$\begin{aligned}
D &= \left((4\beta_b^4)(4\gamma_b^2 + 4\gamma_s^2) + (4\beta_s^4)(4\gamma_b^2)\right)^2 - 4(4\gamma_b^2)(4\gamma_s^2)(4\beta_p^4)(4\beta_s^4) \\
&= (4\beta_b^4)^2(4\gamma_b^2 + 4\gamma_s^2)^2 + (4\beta_s^4)^2(4\gamma_b^2)^2 + 2(4\gamma_b^2)(4\gamma_b^2 + 4\gamma_s^2)(4\beta_p^4)(4\beta_s^4) \\
&- 4(4\gamma_b^2)(4\gamma_s^2)(4\beta_p^4)(4\beta_s^4) \\
&= (4\beta_p^4)^2(4\gamma_b^2 + 4\gamma_s^2)^2 + (4\beta_s^4)^2(4\gamma_b^2)^2 - 2(4\gamma_b^2)(4\gamma_s^2)(4\beta_p^4)(4\beta_s^4) \\
&+ 2(4\gamma_b^2)^2(4\beta_p^4)(4\beta_s^4) \\
&= (4\beta_p^4)^2((4\gamma_b^2)^2 + 2(4\gamma_b^2)(4\gamma_s^2) + (4\gamma_s^2)^2) + (4\beta_s^4)^2(4\gamma_b^2)^2 \\
&- 2(4\gamma_b^2)(4\gamma_s^2)(4\beta_p^4)(4\beta_s^4) + 2(4\gamma_b^2)^2(4\beta_p^4)(4\beta_s^4) \\
&= (4\beta_p^4)^2(4\gamma_b^2)^2 - 2(4\gamma_b^2)(4\gamma_s^2)(4\beta_p^4)(4\beta_s^4) + (4\beta_s^4)^2(4\gamma_b^2)^2 \\
&(4\beta_p^4)^2(2(4\gamma_b^2)(4\gamma_s^2) + (4\gamma_s^2)^2) + 2(4\gamma_b^2)^2(4\beta_p^4)(4\beta_s^4) \\
&= ((4\beta_b^4)(4\gamma_b^2) - (4\beta_s^4)(4\gamma_b^2))^2 + (4\beta_p^4)^2(2(4\gamma_b^2)(4\gamma_s^2) + (4\gamma_s^2)^2) + 2(4\gamma_b^2)^2(4\beta_p^4)(4\beta_s^4) > 0
\end{aligned} \tag{A.7}$$

The previous result can be used to conclude properties of the roots $x_{1,2}$. From the definition of the discriminant it thus follows that

$$D = b^2 - 4ac > 0. \tag{A.8}$$

And it is also known that $4ac > 0$. Using these two results it can be conclude that

$$\begin{aligned} &0 < D < b^2 \\ &0 < \sqrt{D} < b \end{aligned} \tag{A.9}$$

At last one can use the fact that $a < 0$ and equation (A.6) to make the conclusion that

$$x_{1,2} > 0 \quad \text{and} \quad x_1 < x_2. \tag{A.10}$$

Another interesting frequency is that frequency for which the dispersion equation does not hold such that

$$\omega_{IN}^2 = \frac{4\beta_p^4}{4\gamma_s^2} + \frac{4\beta_s^4}{4\gamma_s^2} = \omega_{IN1}^2 + \omega_{IN2}^2. \tag{A.11}$$

Recall that the cut off frequency for the inertia-excluded system is denoted by

$$\omega_{EX}^2 = \frac{4\beta_w^4}{4\gamma_b^2}. \tag{A.12}$$

We we are interested in whether ω_{IN}^2 is between x_1 and x_2 or not. In order to do that we start by rewriting the expressions for $x_{1,2}$, such that

$$\begin{aligned} x_{1,2} &= \frac{-b \pm \sqrt{b^2 - 4ac}}{2a} \\ &= \left(\frac{-b}{2a}\right) \pm \sqrt{\left(\frac{-b}{2a}\right)^2 - \frac{c}{2a}}. \end{aligned} \tag{A.13}$$

We now study this first term in the expression such that

$$\begin{aligned} \left(\frac{-b}{2a}\right) &= \frac{(4\beta_p^4)(4\gamma_b^2 + 4\gamma_s^2) + (4\beta_s^4)(4\gamma_b^2)}{2(4\gamma_b^2)(4\gamma_s^2)} \\ &= \frac{(4\gamma_b^2)(4\beta_p^4 + 4\beta_s^4) + (4\gamma_s^2)(4\beta_p^4)}{2(4\gamma_b^2)(4\gamma_s^2)} \\ &= \frac{1}{2}\frac{4\beta_p^4 + 4\beta_s^4}{4\gamma_s^2} + \frac{1}{2}\frac{4\beta_p^4}{4\gamma_b^2} \\ &= \frac{1}{2}\omega_{IN}^2 + \frac{1}{2}\omega_{BP}^2 \end{aligned}. \tag{A.14}$$

The other term beneath the squared root is defined as

$$\begin{aligned} \frac{c}{2a} &= \frac{1}{2}\frac{4\beta_p^4}{4\gamma_b^2}\frac{4\beta_s^4}{4\gamma_s^2} \\ &= \frac{1}{2}\omega_{EP}^2\left(\omega_{IN}^2 - \omega_{IN1}^2\right) \end{aligned}. \tag{A.15}$$

Using these expressions we can rewrite the expression for $x_{1,2}$ into

$$x_{1,2} = \frac{1}{2}\omega_{IN}^2 + \frac{1}{2}\omega_{EP}^2 \pm \sqrt{\left(\frac{1}{2}\omega_{IN}^2 + \frac{1}{2}\omega_{EP}^2\right)^2 - \frac{1}{2}\omega_{EP}^2\left(\omega_{IN}^2 - \omega_{IN1}^2\right)}. \tag{A.16}$$

In order to find the location of ω_{IN}^2 with respect to x_1 and x_2 we first assume that $\omega_{IN}^2 \geq x_2$ and see whether this is correct:

$$\begin{aligned} \frac{1}{2}\omega_{IN}^2 + \frac{1}{2}\omega_{EP}^2 + \sqrt{\left(\frac{1}{2}\omega_{IN}^2 + \frac{1}{2}\omega_{EP}^2\right)^2 - \frac{1}{2}\omega_{EP}^2\left(\omega_{IN}^2 - \omega_{IN1}^2\right)} &\leq \omega_{IN}^2 \\ \sqrt{\left(\frac{1}{2}\omega_{IN}^2 + \frac{1}{2}\omega_{EP}^2\right)^2 - \frac{1}{2}\omega_{EP}^2\left(\omega_{IN}^2 - \omega_{IN1}^2\right)} &\leq \left(\frac{1}{2}\omega_{IN}^2 - \frac{1}{2}\omega_{EP}^2\right) \end{aligned}. \tag{A.17}$$

We have already proven that the left hand side is positive which means that the inequality can only hold when the right hand side is at least positive ($\omega_{IN} > \omega_{EB}$). Proceeding with this assumption one can elaborate the inequality yielding

$$\begin{aligned} \left(\frac{1}{2}\omega_{IN}^2 + \frac{1}{2}\omega_{EP}^2\right)^2 - \left(\frac{1}{2}\omega_{IN}^2 - \frac{1}{2}\omega_{EP}^2\right)^2 &\leq \frac{1}{2}\omega_{EP}^2\left(\omega_{IN}^2 - \omega_{IN1}^2\right) \\ \omega_{IN}^2\omega_{EP}^2 &< \frac{1}{2}\omega_{EP}^2\left(\omega_{IN}^2 - \omega_{IN1}^2\right) \\ \omega_{IN}^2 &\leq \frac{1}{2}\left(\omega_{IN}^2 - \omega_{IN1}^2\right) \end{aligned} \tag{A.18}$$

This inequality is obviously incorrect, which means that the assumption that $\omega_{IN}^2 \geq x_2$ was incorrect and that $\omega_{IN}^2 < x_2$. We have thus now found an upper boundary for ω_{IN}^2. In order to obtain a lower boundary we now assume that $\omega_{IN}^2 \leq x_1$ and see whether this assumption is correct:

$$\begin{aligned} \frac{1}{2}\omega_{IN}^2 + \frac{1}{2}\omega_{EP}^2 - \sqrt{\left(\frac{1}{2}\omega_{IN}^2 + \frac{1}{2}\omega_{EP}^2\right)^2 - \frac{1}{2}\omega_{EP}^2\left(\omega_{IN}^2 - \omega_{IN1}^2\right)} &\geq \omega_{IN}^2 \\ -\sqrt{\left(\frac{1}{2}\omega_{IN}^2 + \frac{1}{2}\omega_{EP}^2\right)^2 - \frac{1}{2}\omega_{EP}^2\left(\omega_{IN}^2 - \omega_{IN1}^2\right)} &\geq \left(\frac{1}{2}\omega_{IN}^2 - \frac{1}{2}\omega_{EP}^2\right) \end{aligned}. \tag{A.19}$$

We have already proven that the left hand side is negative which means that the inequality can only hold when the right hand side is at least negative ($\omega_{IN} < \omega_{EB}$). Proceeding with this assumption one can elaborate the inequality yielding

$$\begin{aligned} \left(\frac{1}{2}\omega_{IN}^2 + \frac{1}{2}\omega_{EP}^2\right)^2 - \left(\frac{1}{2}\omega_{IN}^2 - \frac{1}{2}\omega_{EP}^2\right)^2 &\leq \frac{1}{2}\omega_{EP}^2\left(\omega_{IN}^2 - \omega_{IN1}^2\right) \\ \omega_{IN}^2\omega_{EP}^2 &< \frac{1}{2}\omega_{EP}^2\left(\omega_{IN}^2 - \omega_{IN1}^2\right) \\ \omega_{IN}^2 &\leq \frac{1}{2}\left(\omega_{IN}^2 - \omega_{IN1}^2\right) \end{aligned} \tag{A.20}$$

This inequality is the same as previously found and thus incorrect, which means that the assumption that $\omega_{IN}^2 \leq x_1$ was incorrect and that $\omega_{IN}^2 > x_1$. We have thus now found an lower boundary for ω_{IN}^2, which results in the wanted boundaries for ω_{IN}^2, such that

$$x_1 < \omega_{IN}^2 < x_2. \tag{A.21}$$

B

The choice has been made to approximate the integrals in equation (5.50) at a certain time step t_{n+1} by

$$\int_0^{t_{n+1}} c_{ij}(t_{n+1}-\tau)f(\tau)d\tau \approx \sum_{m=1}^{n+1}\left[\frac{f(t_m)+f(t_{m-1})}{2}\right]\int_{t_{m-1}}^{t_m} c_{ij}(t_{n+1}-\tau)d\tau. \tag{B.1}$$

It can be shown that the following holds

$$\int_{t_{m-1}}^{t_m} c_{ij}(t_{n+1}-\tau)d\tau = \int_0^{t_{n-(m-2)}} c_{ij}(t_{n-(m-2)}-\tau)d\tau - \int_0^{t_{n-(m-1)}} c_{ij}(t_{n-(m-1)}-\tau)d\tau. \tag{B.2}$$

New functions $G_{ij}(t)$ are now defined as

$$G_{ij}(t) = \int_0^t c_{ij}(t-\tau)d\tau = \int_0^t c_{ij}(t-\tau)H(\tau)d\tau \tag{B.3}$$

Note that $G_{ij}(t)$ is the response of the i^{th} degree of freedom due to the j^{th} cross-sectional force that behaves as a unit time step function. The functions can thus be interpreted as some kind of Green's functions. In order to denote the coming results in compact forms a new notation is introduced, namely

$$G_{ij}(t_a;t_b) = G_{ij}(t_a) - G_{ij}(t_b). \tag{B.4}$$

The previous steps make it possible to rewrite equation (B.1) into the form

$$\int_0^{t_{n+1}} c_{ij}(t_{n+1}-\tau)f(\tau)d\tau \approx \frac{1}{2}G_{ij}(t_{n+1};t_n)f(t_0) + \sum_{m=1}^{n}\frac{1}{2}G_{ij}(t_{n-(m-2)};t_{n-m})f(t_m) + \frac{1}{2}G_{ij}(t_1;t_0)f(t_{n+1}). \tag{B.5}$$

Application of this equation makes it possible to approximate equation (5.50) at a discrete time step t_{n+1} by

$$\begin{bmatrix} w(t_{n+1}) \\ \phi(t_{n+1}) \end{bmatrix} = \frac{1}{2}\begin{bmatrix} G_{11}(t_{n+1};t_n) & G_{12}(t_{n+1};t_n) \\ G_{21}(t_{n+1};t_n) & G_{22}(t_{n+1};t_n) \end{bmatrix}\begin{bmatrix} V(t_0) \\ M(t_0) \end{bmatrix} + \sum_{m=1}^{n}\frac{1}{2}\begin{bmatrix} G_{11}(t_{n-(m-2)};t_{n-m}) & G_{12}(t_{n-(m-2)};t_{n-m}) \\ G_{21}(t_{n-(m-2)};t_{n-m}) & G_{22}(t_{n-(m-2)};t_{n-m}) \end{bmatrix}\begin{bmatrix} V(t_m) \\ M(t_m) \end{bmatrix}$$
$$+\frac{1}{2}\begin{bmatrix} G_{11}(t_1;t_0) & G_{12}(t_1;t_0) \\ G_{21}(t_1;t_0) & G_{22}(t_1;t_0) \end{bmatrix}\begin{bmatrix} V(t_{n+1}) \\ M(t_{n+1}) \end{bmatrix}, \tag{B.6}$$

or in a more short form

$$\begin{bmatrix} w(t_{n+1}) \\ \phi(t_{n+1}) \end{bmatrix} = \begin{bmatrix} w_{his}(t_{n+1}) \\ \phi_{his}(t_{n+1}) \end{bmatrix} + \begin{bmatrix} \mathbf{GK} \end{bmatrix}\begin{bmatrix} V(t_{n+1}) \\ M(t_{n+1}) \end{bmatrix}. \tag{B.7}$$

The last step to fully define all terms is to determine the functions $G_{ij}(t)$. By application of the complex inversion formula, a table of Laplace transformations of one choice like that in the book of Schiff [23] and equation (B.3) one can obtain

$$G_{ij}(t) = \lim_{y\to\infty}\left(\frac{1}{2\pi i}\int_{\sigma-yi}^{\sigma+yi}\frac{\hat{c}_{ij}}{s}e^{ts}ds\right). \tag{B.8}$$

This integral has is computed by a quadrature. In order to do so the integrand is first split into two functions. One function of which the integrals can be computed analytically and the other function vanishes for large value of y such that it is justified to truncate the integral to finite boundaries $\sigma \pm \bar{y}$. The steps are

$$\begin{aligned}
G_{ij}(t) &= \lim_{y\to\infty}\left(\frac{1}{2\pi i}\int_{\sigma-yi}^{\sigma+yi}\frac{\Delta\hat{c}_{ij}}{s}e^{ts}ds\right) + \lim_{y\to\infty}\left(\frac{1}{2\pi i}\int_{\sigma-yi}^{\sigma+yi}\frac{\hat{c}_{app,ij}}{s}e^{ts}ds\right)\\
G_{ij}(t) &\approx \frac{1}{2\pi i}\int_{\sigma-\bar{y}i}^{\sigma+\bar{y}i}\frac{\Delta\hat{c}_{ij}}{s}e^{ts}ds + \lim_{y\to\infty}\left(\frac{1}{2\pi i}\int_{\sigma-yi}^{\sigma+yi}\frac{\hat{c}_{app,ij}}{s}e^{ts}ds\right) \quad .\\
G_{ij}(t) &\approx \Delta G_{ij}(t) + G_{app,ij}(t)
\end{aligned} \tag{B.9}$$

For the terms $\hat{c}_{app,ij}$ it is chosen to approximate $\lambda(s)$ by

$$\lambda_{app}(s) = e^{\frac{3}{4}\pi i}\sqrt{2\gamma_b s}, \tag{B.10}$$

which approximates the behaviour of the original $\lambda(s)$ for large values of $|y|$ well. The accompanied approximated flexibility matrix is

$$\hat{C}_{app} = -\frac{1}{EI}\begin{bmatrix} \frac{1}{2}\frac{1}{\gamma_b\sqrt{\gamma_b}}\frac{1}{s\sqrt{s}} & \frac{1}{2\gamma_b s} \\ \frac{1}{2\gamma_b s} & \frac{1}{\sqrt{\gamma_b s}} \end{bmatrix}. \tag{B.11}$$

The indices can be substituted in equation (B.9) and their corresponding integrals can be computed analytically, resulting in

$$\begin{bmatrix} G_{11}(t) & G_{12}(t) \\ G_{21}(t) & G_{22}(t) \end{bmatrix} = \begin{bmatrix} \Delta G_{11}(t) & \Delta G_{12}(t) \\ \Delta G_{21}(t) & \Delta G_{22}(t) \end{bmatrix} - \frac{1}{EI}\begin{bmatrix} \frac{2}{3}\frac{1}{\gamma_b\sqrt{\gamma_b}}t\sqrt{\frac{t}{\pi}} & \frac{1}{2}\frac{1}{\gamma_b}t \\ \frac{1}{2}\frac{1}{\gamma_b}t & 2\frac{1}{\sqrt{\gamma_b}}\sqrt{\frac{t}{\pi}}. \end{bmatrix} \tag{B.12}$$

The functions $\Delta G_{ij}(t)$ are approximated by applying a quadrature of choice to their respective integrals denoted in equation (B.9). At last the definition of the terms $\Delta\hat{c}_{ij}$ are provided which are

$$\Delta\hat{c}_{ij} = \hat{c}_{ij} - \hat{c}_{app,ij}. \tag{B.13}$$

Bibliography

[1] Faragau A.B., Keijdener C., Oliveira de Barbosa J.M., Metrikine A.V., and van Dalen K.N. Transition radiation in a nonlinear and infinite one-dimensional structure: a comparison of solution methods. *Nonlinear Dynamics*, 2021.

[2] Bouma A.L. *Mechanica van constructies: Elasto-statica van slanke structuren*, chapter 11, page 123. Delftse Uitgevers Maatschappij, 1993.

[3] Dipanjan Basu and NSV Kameswara Rao. Analytical solutions for euler-bernoulli beam on visco-elastic foundation subjected to moving load. *International Journal for Numerical and Analytical Methods in Geomechanics*, 37(8):945–960, 2013.

[4] Esveld C. *Geometrisch en constructief ontwerp van wegen en spoorwegen*, page 131. 2005.

[5] P.A. Cherenkov. Visible emission of clean liquids by action of γ radiation. *Doklady Akademii Nauk SSSR*, 2:451–454, 1934.

[6] João Manuel de Oliveira Barbosa and Karel N van Dalen. Dynamic response of an infinite beam periodically supported by sleepers resting on a regular and infinite lattice: semi-analytical solution. *Journal of Sound and Vibration*, 458:276–302, 2019.

[7] Metrikine A.V. Dieterman H.A. The equivalent stiffness of a half-space interacting with a beam. critical velocities of a moving load along the beam. *European Journal of Mechanics Series A Solids*, 15:67–90, 1996.

[8] Zuzana Dimitrovová. A general procedure for the dynamic analysis of finite and infinite beams on piece-wise homogeneous foundation under moving loads. *Journal of Sound and Vibration*, 329 (13):2635–2653, 2010.

[9] Matthias Germonpré, Geert Degrande, and Geert Lombaert. A track model for railway-induced ground vibration resulting from a transition zone. *Proceedings of the Institution of Mechanical Engineers, Part F: Journal of Rail and Rapid Transit*, 232(6):1703–1717, 2018.

[10] V.L. Ginzburg and I.M. Frank. Radiation of a uniformly moving electron crossing a boundary between two media. *Journal of Experimental and Theoretical Physics*, 16:15–30, 1946.

[11] Tien Hoang, Denis Duhamel, Gilles Foret, Hai-Ping Yin, and Gwendal Cumunel. Response of a periodically supported beam on a nonlinear foundation subjected to moving loads. *Nonlinear Dynamics*, 86(2):953–961, 2016.

[12] L Jezequel. Response of periodic systems to a moving load. 1981.

[13] P Castro Jorge, FMF Simões, and A Pinto Da Costa. Dynamics of beams on non-uniform nonlinear foundations subjected to moving loads. *Computers & Structures*, 148:26–34, 2015.

[14] Rayleigh J.W.S. *Rayleigh, The theory of sound*. Dover Publications, New-York, 1945.

[15] Amir M Kaynia, Joonsang Park, and Karin Norén-Cosgriff. Effect of track defects on vibration from high speed train. *Procedia engineering*, 199:2681–2686, 2017.

[16] Van Dalen K.N., Metrikine A.V, and Tsouvalas A. Transition radiation excited by a load moving over the interface of two elastic layers. *International Journal of Solids and Structures*, 2015.

[17] Xiaoyan Lei and Lijun Mao. Dynamic response analyses of vehicle and track coupled system on track transition of conventional high speed railway. *Journal of Sound and Vibration*, 3(271): 1133–1146, 2004.

[18] Shamalta M and Metrikine AV. Analytical study of the dynamic response of an embedded railway track to a moving load. *Archive of Applied Mechanics*, 73(1):131–146, 2003.

[19] Denys J Mead. Free wave propagation in periodically supported, infinite beams. *Journal of Sound and Vibration*, 11(2):181–197, 1970.

[20] André Paixão, Eduardo Fortunato, and Rui Calçada. Transition zones to railway bridges: track measurements and numerical modelling. *Engineering structures*, 80:435–443, 2014.

[21] André Filipe da Silva Rodrigues. *Viability and Applicability of Simplified Models for the Dynamic Analysis of Ballasted Railway Tracks*. PhD thesis, 'Universidade Nova de Lisboa', 2017.

[22] Mehran Sadri, Tao Lu, and Michaël Steenbergen. Railway track degradation: The contribution of a spatially variant support stiffness-local variation. *Journal of Sound and Vibration*, 455:203–220, 2019.

[23] Joel L. Schiff. *The Laplace Transform: Theory and Applications*. Springer, 1988.

[24] A Segal and Fred Vermolen. *Numerical methods in scientific computing*. VSSD, 2008.

[25] JN Varandas, P Hölscher, and MAG Silva. Three-dimensional track-ballast interaction model for the study of a culvert transition. *Soil Dynamics and Earthquake Engineering*, 89:116–127, 2016.

[26] José N Varandas, Paul Hölscher, and Manuel AG Silva. Dynamic behaviour of railway tracks on transitions zones. *Computers & structures*, 89(13-14):1468–1479, 2011.

[27] A.I. Vesnitskii and A.V. Metrikin. Transition radiation in mechanics. *Physics-Uspekhi*, 39(10):983, 1996.

[28] Metrikine A.V. Vostroukhov A.V. Periodically supported beam on a visco-elastic layer as a model for dynamic analysis of a high-speed railway track. *International journal of solids and structures*, 40(21):5723–5752, 2003.

[29] Garth N. Wells. *The Finite Element Method: An Introduction*. 2011.

[30] A.R.M. Wolfert. *Wave-Effects in One-Dimensional Elastic Systems Interacting with Moving Objects*. PhD thesis, 'University of Technology Delft', 1999.